CANADA
DEPARTMENT OF MINES AND TECHNICAL SURVEYS
Dominion Observatories

PUBLICATIONS

of the

DOMINION OBSERVATORY

OTTAWA

Volume XXIV • No. 10

A SYMPOSIUM ON EARTHQUAKE MECHANISM

John H. Hodgson, *Editor*

International Union of Geodesy and Geophysics
Association of Seismology and Physics of the Earth's Interior
Twelfth General Assembly, Helsinki, Finland

1960

Price $5.00

ROGER DUHAMEL, F.R.S.C.
QUEEN'S PRINTER AND CONTROLLER OF STATIONERY
OTTAWA, 1961

96705-9—1

TABLE OF CONTENTS

96705-9—1½

TABLE OF CONTENTS—*Concluded*

A Symposium on Earthquake Mechanism

Foreword

A symposium on the mechanism of faulting was held in 1957 at the Toronto meetings of the Association of Seismology and Physics of the Earth's Interior, and the papers presented there were printed in these Publications. Among those people working on earthquake mechanism there was a general feeling that the published symposium had been a helpful contribution, and the hope was widely expressed that a similar symposium might be held at the Helsinki meetings. A request that this be arranged was made to Sir Harold Jeffreys, President of the Association, and he appointed Dr. V. I. Keylis-Borok to convene the symposium. At the same time, with the approval of the President, an attempt was made to find a publisher for the papers to be presented. When no one else could be found to do it, the Department of Mines and Technical Surveys, Canada, agreed to print the papers in these Publications. We are very much indebted to Sir Harold Jeffreys, who concurred in this arrangement on behalf of the Association, and to Dr. Marc Boyer, Deputy Minister, who agreed on behalf of the Department.

The symposium was arranged by Dr. Keylis-Borok, but unfortunately he was not able to attend the meetings. At his request I acted as Chairman. He and I had hoped to cooperate in the editing of the papers, and to complete the editorial work in Helsinki; this was impossible owing to his absence, and I have had to undertake the editorial work without his help.

The papers have been arranged in this symposium in the same order as in the previous one, that is, papers dealing with theory or fundamentals of method first, then those giving the summary of results and, finally, papers dealing with the interpretation of results. In the case of the Toronto symposium I wrote a summary paper, attempting to define the position of the fault-plane work as it then stood. I have not attempted to do so in this case. At the time of the previous symposium the outstanding problem was that of selecting the appropriate mechanism and, since the theory had been established, this seemed to be simply a matter of further careful observations. Since that time much more theoretical work has been done, which has complicated rather than clarified the problem, and the observational results show little consistency. An attempt to select between the theoretical models, or to seek out the reasons for the variation in the observational results, would be a major research effort, quite beyond the scope of a review paper. It is better that each investigator should speak for himself.

JOHN H. HODGSON,
Editor

Release of Energy at the Source of an Earthquake

PERRY BYERLY

University of California, Berkeley, California, U.S.A.

We are all agreed here that for many earthquakes the direction of the first motion of P waves and the relations among the amplitudes of SH, SV, and P give a pattern on the earth's surface which indicates that a source composed of a force system (or displacement) suddenly applied at the focus would have been sufficient to explain the pattern.

It is true that all investigators have not reached the same conclusions regarding the force systems which are most common. Although several earthquakes have recently been explained by STAUDER as due to single forces, the great majority of solutions have been interpreted as due to a single couple or a double couple of forces (without moment) acting at the source.

At the start of this type of investigation in America, we assumed, perhaps naively, that the single couple was obvious. The 1906 earthquake in California with the accompanying magnificent fault break, left no doubt in our minds that the cause of the shaking was the fault break. By cause and effect I mean here that the faulting preceded, not followed, the shaking. We extended the idea so that we considered almost all earthquakes to be caused by faulting, our argument being that we have this 1906 shock and a few others where the cause seems obvious so why bring in a multiplicity of causes on theoretical grounds.

A foreign colleague, on the other hand, told me a few years ago that the 1906 phenomenon should be disregarded in the formation of theories of earthquake source. It was a "freak" to him, but the "type" earthquake to us. Our early solutions made little use of S waves. Thorough use of S waves should solve the ambiguity. However, a P solution using many observations should be followed by the use of many S observations, not just a few.

KEYLIS-BOROK has had great success in explaining the source as a single couple using S waves. HONDA on the other hand is a strong advocate of the double couple. He thinks in terms of the principal strains—not fault planes.

As for the double couple without moment it seems to follow as necessary theoretically from that peculiarity of elastic theory that a state of strain may be specified by the gradient of a scalar plus the curl of a vector—by a dilatation plus a rotation. We note that this is qualified by LOVE—"if the dilatation exists". In a recent series of lectures on elasticity at Harvard University, CARL E. PEARSON states that although we can so specify the strain it is profitless to try to attach further physical significance to the statement.

There is the concept of "pure shear" in which the dilatation and rotation both vanish.

As KEYLIS-BOROK has pointed out, the static stress field may have been produced in different ways and may be released in different ways—that its release or partial release need not necessarily involve a double couple in which the forces are of equal magnitude in which both couples are released at the same time.

We can agree that the continued careful analyses of many seismograms should indicate whether or not certain systems of forces are more common than others. I would like to ask our Japanese colleagues to make use of seismograms from round the earth in their studies rather than confine themselves to Japanese records.

HODGSON has pointed out that about 12 per cent of the observations on which his solutions are based are inconsistent. At the University of California we have a short-period Benoiff vertical seismometer, free period one second, with galvanometer of period 0.5 second, Wood-Anderson horizontals of period 0.8 second, three component Galitzins with periods of 12 seconds for both seismometers and galvanometers, three components of Press-Ewings, pendulums at 30 seconds, galvanometers at 90 seconds. The short-period instruments of course select a different range of frequencies to record than do the long-period instruments. WILLIAM BAKER has recently studied the records for a five-year period. He found 226 earthquakes for which there were good beginnings of P and both long- and short-period seismograms. These began at the same time. On 198 of these the sign of P was the same on the short and long periods, on 28 they were of opposite sign. Note that this is about 12 per cent—the figure HODGSON found for the observations inconsistent with his solutions. Again BAKER found that for some of our stations, particularly at Fresno located on deep alluvium, only the first few waves of P enter on great circle paths from the epicenters. Later waves in P enter from other directions affected by the immediate underground as well as more distant surface irregularities.

So much for the problem of deciding from seismograms what sort of a set of arrows to draw at the focus. Our

more serious problem is the mechanism which struck the impulsive blows or produced these sudden displacements. We have heard about pockets of magma which became suddenly discontented and either migrated or applied sudden pressure or sudden torques on the cavities in which they had previously been content to live. We have heard of spherical bodies of rock which decided to crush themselves suddenly—their volumes have been computed. The same idea has been applied to bodies of rock of other shapes.

Now our problem is not primarily the small earthquakes associated with volcanic phenomena. We are trying to get sharp blows in regions where other geological processes are slow.

It was to meet this problem after the 1906 California earthquake that HARRY FIELDING REID proposed the 'elastic rebound theory'. It was based on geodetic triangulation observations by the United States Coast and Geodetic Survey over a fifty-year period. (Later observations have amply and frighteningly confirmed it.) Forces acting presumably from below cause coastal California to drift slowly northerly relative to inland California. Over a zone about 10 miles wide the differential movement is at least 2 inches a year; this produces a strain which is eventually relieved in faulting.

There still remains the problem of just how the slowly accumulated potential energy of strain which occupies a considerable volume of rock is converted into the kinetic energy of vibrations. We think of the motion of the rock in two parts—one is the mass movement of the large body of rock and is called the "fling"—the other is the vibration very near the fault surface due to grating.

When one observes the beautiful quadrant distribution of the first motion of P in many earthquakes, one is inclined to think of the fling as its generator, and yet few if any of us feel that the fault overshoots its position of no strain and that the whole mass previously under strain vibrates back and forth. SEZAWA came to the conclusion from thermodynamic reasoning that such a release of strain could not send out waves.

REID was very insistent that the seismic radiation originates in the fault surface and not directly in the mass movement. BENIOFF and HOUSNER have each discussed simplified models of the jerking effect of frictional failure at the fault surface. Is the idea of the waves originating in the fault surface as consistent with the quadrant distribution of the first motion in P as the idea of this motion being due to fling?

Of course we have the added problem of the great inhomogeneity of the earth's crust.

When theoreticians do not agree it is because experimentalists have not given them conclusive observations. We must continue to study P and S and surface waves on seismograms. We may find one or two or more types of sources. When observations point the way, theory will follow.

Generalized Focal Mechanism

R. E. INGRAM, S.J.

Rathfarnham Castle, Dublin, Ireland

ABSTRACT

It is shown that a system of forces consisting of three couples without moment introduces a cone of the second degree as the surface separating the compressions and dilatations as recorded at extended distances. This cone is the generalization of the pair of planes associated with a single couple with moment or with two couples without moment. The corresponding surfaces for SH and for SV are also given. The projection of these surfaces on the central plane is examined and some of the geometrical properties noted. In particular, it is seen that the projected S direction passes through a fixed point if two of the couples are equal. An example of the separation of the compressions and dilatations by a hyperbola is given.

INTRODUCTION

The success of the fault-plane method of investigating the mechanism of earthquakes (BYERLY 1938, HODGSON 1957, HONDA 1952, 1957, KEILIS-BOROK 1957, RITSEMA 1957 and others) is not lessened by the small number of earthquakes which do not admit a solution. There is evidence that for some of these shocks a more complicated system of forces may be appropriate. The choice of a more general system may be made in many ways. Here one such system is considered. It is an obvious generalisation of the two equal and oppositely signed couples without moment as considered by HONDA (1957). If successful in its applications to the exceptional cases, it may in turn be evidence of the two couples without moment rather than the single couple with moment as the usual model.

GENERALIZED MECHANISM AND DISPLACEMENTS

The displacements in an infinite elastic medium due to a couple, X, without moment acting at the origin of rectangular coordinate axes (x, y, z) and in the x direction are (LOVE, 1906, 292–294)

$$\mathrm{P} = (x, y, z)\, x^2 X\, f'(\alpha t - r)/r^4$$

$$\mathrm{S} = (r^2 - x^2, -xy, -xz)\, xX\, g'(\beta_t - r)/r^4$$

where $r^2 = x^2 + y^2 + z^2$ and f' and g' are functions of propagation for the longitudinal displacement, P, and the transverse displacement, S, with velocities α and β.

The generalized focal mechanism is considered as due to three such couples, X, Y, Z, along the x, y, z directions at the origin (Figure 1). They are supposed to represent the changes in stress before and after the earthquake. For the mathematical treatment it is convenient to use the positive sign for each couple. In actual fact it will appear most often that one or two of the couples is negative, or that one is zero and the other two of opposite sign. HONDA (1957) considered $Z=0$, $X=-Y$.

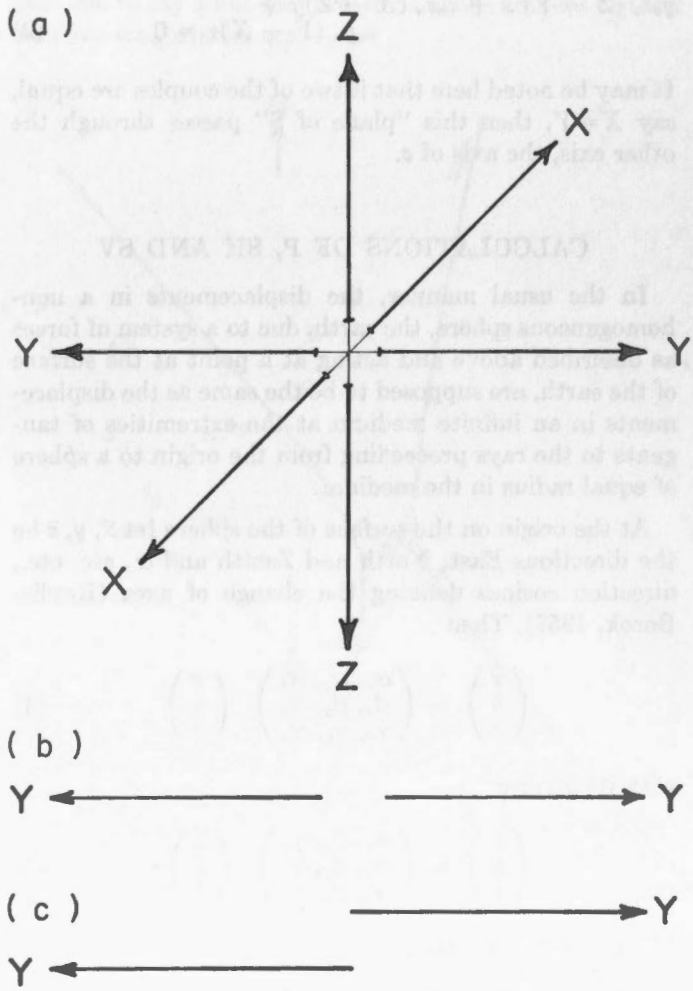

Figure 1. (a) Three couples without moment along mutually perpendicular directions. The couples are shown as acting outwards; a change of sign in X, Y, Z gives an inward acting couple. (b) A couple without moment. (c) A couple with moment.

The displacements due to the three couples are

$$\begin{aligned} P &= (x, y, z)\,(x^2X + y^2Y + z^2Z)\,f'\,(\alpha t - r)/r^4 \\ S &= [(xX, yY, zZ)\,r^2 - (x, y, z)\,(x^2X + y^2Y + z^2Z)]\,g'(\beta t - r)/r^4 \end{aligned} \tag{1}$$

THE PLANE OF S

The direction perpendicular to P and S is

$$yz\,(Z - Y),\ zx\,(X - Z),\ xy\,(Y - X)$$

Hence a plane through the origin and the point (x_o, y_o, z_o) and containing the S motion at (x_o, y_o, z_o) has the equation

$$y_oz_o\,(Z - Y)\,x + z_ox_o\,(X - Z)y + x_oy_o\,(Y - X)z = 0 \tag{2}$$

It may be noted here that if two of the couples are equal, say $X = Y$, then this "plane of S" passes through the other axis, the axis of z.

CALCULATIONS OF P, SH AND SV

In the usual manner, the displacements in a non-homogeneous sphere, the earth, due to a system of forces as described above and acting at a point at the surface of the earth, are supposed to be the same as the displacements in an infinite medium at the extremities of tangents to the rays proceeding from the origin to a sphere of equal radius in the medium.

At the origin on the surface of the sphere let $\bar{x}, \bar{y}, \bar{z}$ be the directions East, North and Zenith and α_x etc. etc., direction cosines defining the change of axes (Keylis-Borok, 1957). Then

$$\begin{pmatrix} \bar{x} \\ \bar{y} \\ \bar{z} \end{pmatrix} = \begin{pmatrix} \alpha_x, \alpha_y, \alpha_z \\ \beta_x, \beta_y, \beta_z \\ \gamma_x, \gamma_y, \gamma_z \end{pmatrix} \begin{pmatrix} x \\ y \\ z \end{pmatrix} \tag{3}$$

with its inverse

$$\begin{pmatrix} x \\ y \\ z \end{pmatrix} = \begin{pmatrix} \alpha_x, \beta_x, \gamma_x \\ \alpha_y, \beta_y, \gamma_y \\ \alpha_z, \beta_z, \gamma_z \end{pmatrix} \begin{pmatrix} \bar{x} \\ \bar{y} \\ \bar{z} \end{pmatrix}. \tag{4}$$

Using a vector notation,

SH = $(r \times \bar{z})\cdot$S, where $(r \times \bar{z})$ is a unit vector perpendicular to P and z.

SV = $(r \times (r \times \bar{z}))\cdot$S, where $(r \times (r \times \bar{z}))$ is a unit vector perpendicular to P and SH.

We then have the following quantities

$$P = (x^2X + y^2Y + z^2Z)\,f'\,(\alpha t - r)/r^3 \tag{5}$$

$$SH = [yz\gamma_x\,(Y - Z) + z\,x\gamma_y\,(Z - X) + xy\gamma_z\,(X - Y)]\,g'\,(\beta t - r)/r^2(r^2 - \bar{z}^2)^{\frac{1}{2}}$$

$$SV = [\bar{z}(x^2X + y^2Y + z^2Z) - r^2(x\gamma_xX + y\gamma_yY + z\gamma_zZ)]\,g'\,(\beta t - r)/r^3\,(r^2 - \bar{z}^2)^{\frac{1}{2}}$$

Thus the loci P = 0, SH = 0, SV = 0 are cones through the origin,

$$(P = 0): x^2X + y^2Y + z^2Z = 0 \tag{6}$$

$$(SH = 0): yz\gamma_x\,(Y - Z) + z\,x\gamma_y\,(Z - X) + xy\gamma_z\,(X - Y) = 0 \tag{7}$$

$$(SV = 0): \bar{z}\,(x^2X + y^2Y + z^2Z) - r^2\,(x\gamma_xX + y\gamma_yY + z\gamma_zZ) = 0 \tag{8}$$

PROJECTION AND GEOMETRY

The most convenient projection for mapping these surfaces on a plane is to project from the origin on the central plane, $\bar{z}+R=0$, where R is the radius of the sphere (Figure 2). Rectangular coordinates may be introduced by the transformation (4) with $\bar{z}=-R$. The actual amplitudes are then the expressions (5) when multiplied by a factor OP′/OP = $\frac{1}{2}\sec^2 i$

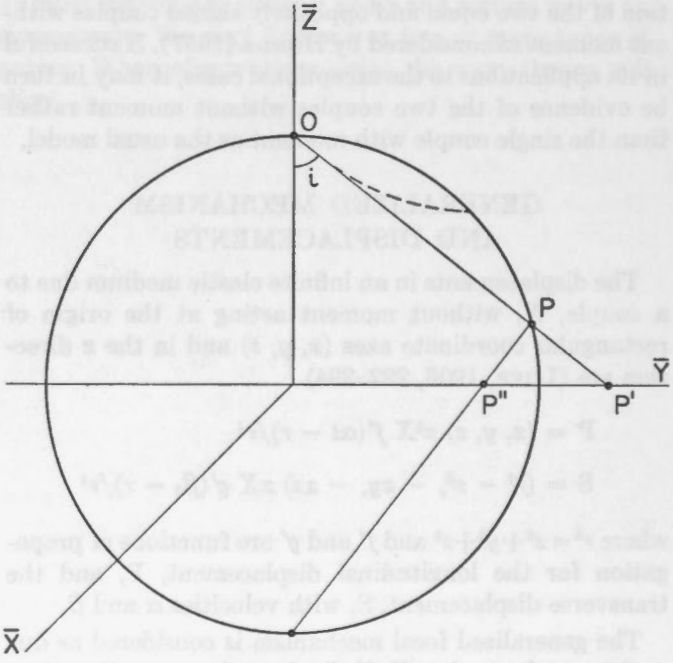

Figure 2. The projection, from the origin, of P on the central plane gives P′. The projection from the antipodal point gives P″, the inverse of P′ with respect to the circle in which the sphere cuts the central plane.

For non-metrical results the coordinates (x, y, z) may be used as homogeneous coordinates in the plane $\bar{z}=-R$, the base triangle being the intersections of the coordinate planes with the central plane. The line at infinity is then the line $\bar{z}=x\gamma_x+y\gamma_y+z\gamma_z=0$ and the point where the $\bar{z}$

axis meets the plane is the point $(\gamma_x, \gamma_y, \gamma_z)$. The conic $x^2X+y^2Y+z^2Z=0$ has the base triangle as a self-conjugate triangle and the point $(\gamma_x YZ, \gamma_y ZX, \gamma_z XY)$ as its centre. The polar line of $(\gamma_x, \gamma_y, \gamma_z)$ is $x\gamma_x X+y\gamma_y Y+z\gamma_z Z=0$ The conic $yz\gamma_x(Y-Z)+zx\gamma_y(Z-X)+xy\gamma_z(X-Y)=0$ passes through the point $(\gamma_x, \gamma_y, \gamma_z)$ and through the vertices of the triangle. The cubic $\bar{z}(x^2X+y^2Y+z^2Z)-r^2(x\gamma_x X+y\gamma_y Y+z\gamma_z Z)=0$ is a circular cubic having two circuits and an asymptote parallel to the line $x\gamma_x X+y\gamma_y Y+z\gamma_z Z=0$. A real tangent, parallel to the assymptote, meets the cubic in a vertex of the triangle or in the point $(\gamma_x, \gamma_y, \gamma_z)$.

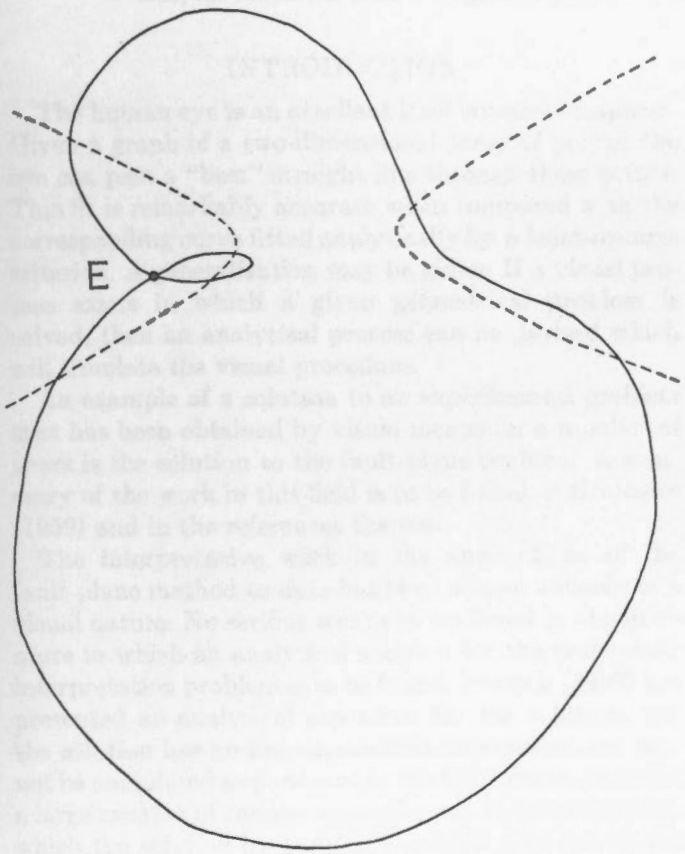

Figure 3. A hyperbola (dotted line) has a quartic (full line) as its inverse. The hyperbola is similar to its asymptotes, and the quartic evidently similar to a pair of circles.

The projection from the antipodal point may also be used (P″ in Figure 2), but this introduces an inversion in the circle of radius R and consequent higher degree curves in the plane. The conic becomes, in general a quartic. One such curve is drawn (Figure 3) where it may be seen that the hyperbola is approximately its asymptotes and the quartic approximately a pair of circles. This shows that the introduction of a small third component couple at the origin may allow a wider interpretation of the curves separating the compressions and dilatations. The condition that the S motion pass through a fixed point is verified if two of the couples are equal (2).

AN APPLICATION

An example of the fitting of a conic, a hyperbola, to points as mapped in the projection described above is given. The earthquake is that of 1949, April 25 at 13 hrs 15 min 00 sec, with epicentre at 20S. 69.5W. at a depth 0.01 R(U.S.C.G.S.). The information was collected and kindly supplied by Dr. J. Hodgson of Dominion Observatory, Ottawa. It is listed as one for which no solution was obtained. The solution using a hyperbola (Figure 4) is consistent with a very large proportion of the observations. From this point of view it is satisfactory, but at this stage of the investigation it is not possible to say what the directions of the couples or their relative magnitudes are.

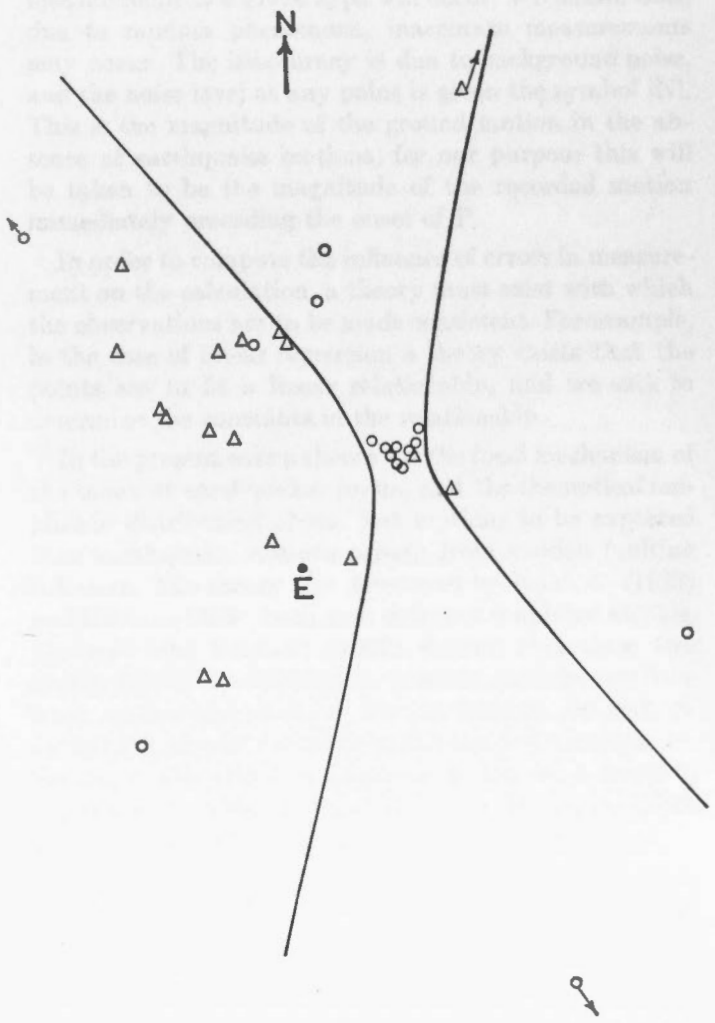

Figure 4. The distribution of compressions and dilatations for the earthquake of 1949 April 25, at 20°S, 69.5°W is solved by a hyperbola. Note that not all the observations are entered. The number of inconsistent points is reduced to a minimum.

References

BYERLY, P., 1938, The earthquake of July 6, 1934: amplitudes and first motion: *Seismol. Soc. Am. Bull.*, **28**, 1.

HODGSON, J. H., 1957. Nature of faulting in large earthquakes: *Geol. Soc. Am. Bull.*, **68**, 611.

HODGSON, J. H., and STOREY, R. S., 1954. Direction of faulting in some of the larger earthquakes of 1949: *Seismol. Soc. Am. Bull.*, **44**, 57.

HONDA, H., 1957. The mechanism of the earthquakes: *Sci. Repts. Tôhoku Univ.*, Ser. 5, **9**, supplement 1.

HONDA, H. and MASATSUKA, A., 1952. On the mechanism of earthquakes and the stresses producing them in Japan and its vicinity: *Sci Repts. Tôhoku Univ.*, ser. 5, **4**, 42.

KEYLIS-BOROK, V. I., 1957. The determination of earthquake mechanism using both longitudinal and transverse waves: *Annali Geofis.*, **10**, 105.

LOVE, A. E. H., 1906. The mathematical theory of elasticity: Cambridge University Press.

RITSEMA, A. R., 1957. On the use of transverse waves in earthquake mechanism studies and the direction of faulting in S.E. Asian earthquakes: *Verhand.* **52**, *Meteor. and Geophys. Inst. Djakarta.*

Analytical Calculation of the Fault-Plane Problem*

L. KNOPOFF

Institute of Geophysics, University of California, Los Angeles

ABSTRACT

Machine calculation of the solution to the fault-plane problem is possible, if an analytical formulation of the problem can be made. An analytical formulation is made in terms of the probability that a station report the correct sign of first motion in the presence of disturbing influences such as background noise. The location of the orthogonal planes depends upon the maximization of a certain probability function. The probability function is simplified if it is assumed that the ground motion noise level is constant at all stations. The maximization is then made with respect to four variables: the three independent angular variables describing the orientation of the two orthogonal planes and the noise. An example of the machine calculation of the maximization is given for the Alaska earthquake of July 10, 1958; the machine solution is compared with the solution obtained by visual means.

INTRODUCTION

The human eye is an excellent least-squares computer. Given a graph of a two-dimensional array of points, the eye can pass a "best" straight line through these points. This fit is remarkably accurate when compared with the corresponding curve fitted analytically by a least-squares criterion. A generalization may be given. If a visual process exists in which a given geometrical problem is solved, then an analytical process can be devised which will simulate the visual procedure.

An example of a solution to an experimental problem that has been obtained by visual means for a number of years is the solution to the fault-plane problem. A summary of the work in this field is to be found in HODGSON (1959) and in the references therein.

The interpretative work in the applications of the fault-plane method to date has been almost entirely of a visual nature. No serious work can be found in the literature in which an analytical solution for the fault-plane interpretation problem is to be found. INGRAM (1959) has presented an analytical procedure for the solution, but the solution has no firm theoretical foundation and cannot be considered as pertinent to the fault-plane problem; a large number of counter examples can be constructed in which the solution by INGRAM'S method does not fit the visual solutions and, as stated above, the visual fits are quite reliable. INGRAM'S solution cannot be considered to be accurate.

In this paper we shall present an analytical scheme for the calculation of the fault-plane solution. Since the method is analytical, it will be amenable to machine calculation. We shall review the fault-plane procedure from the point of view of the statistical solution, offer a basis for a solution, list the assumptions and present the solution to the equations. An example of the calculation is provided in the result obtained for the Mount Fairweather earthquake of July 10, 1958.

PROBABILITY AND FAULT-PLANE SOLUTIONS

The conversion of a visual procedure into an analytic procedure requires a theory of the probability that a measurement of a given type will occur. We admit that, due to random phenomena, inaccurate measurements may occur. The inaccuracy is due to background noise, and the noise level at any point is given the symbol $|N|$. This is the magnitude of the ground motion in the absence of earthquake motions; for our purpose this will be taken to be the magnitude of the recorded motion immediately preceding the onset of P.

In order to compute the influence of errors in measurement on the calculation, a theory must exist with which the observations are to be made consistent. For example, in the case of linear regression a theory exists that the points are to fit a linear relationship, and we seek to determine the constants in the relationship.

In the present case a theory for the focal mechanism of the onset of earthquakes exists, and the theoretical amplitude distribution of the first motions to be expected from earthquake motions arising from sudden faulting is known. The theory was developed by NAKANO (1923) and HONDA (1932); both used different simplified models. KNOPOFF and GILBERT (1960) showed that these two simple models correspond to possible models resulting from earthquake motions due to sudden dislocations along fault planes. In either model the first motions are the same; the first compressional motion at a point in space can be shown to be radial from the focus and to have a spatial dependence,

$$U_r = \frac{A}{r} \sin 2\theta \sin \phi = \frac{2Az'y'}{r^3} \qquad (1)$$

where A is a measure of the strength of the source, r is the distance along the ray to the seismograph, and

*Publication No. 203, Institute of Geophysics, University of California

spherical polar co-ordinates (r, θ, ϕ) have been taken with θ the polar angle, measured from the normal to the fault surface and ϕ the azimuthal angle measured from the null vector. The corresponding cartesian co-ordinate system is (x', y', z'). The geometry is shown in Figure 1. No corrections are applied in the above theory for the inhomogeneity of the elastic medium; this is usually done in the reduction of the data. The radiation pattern (1) holds for a linear dislocation at the source.

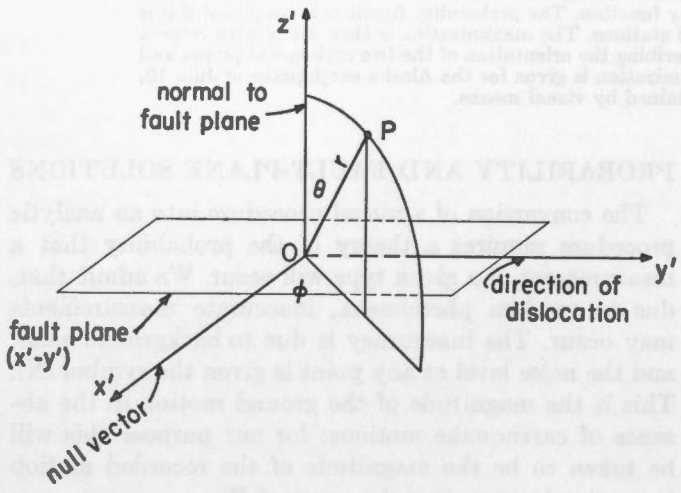

Figure 1. Geometry for a plane dislocation.

If the front of the source dislocation is not linear but instead the dislocation spreads out uniformly in a radial direction in the source plane, the spatial dependence is

$$U_r = \frac{A \sin 2\theta}{r} \qquad (2)$$

The development of a statistical theory will depend upon the ratio of the signal-to-noise amplitudes S/|N|. The signal level in this problem is taken as the theoretical result due to the fault-plane model. The noise level is as before. Our problem, therefore, is to find a function f(S/|N|) which describes the probability of correctness of the measurement.

If the quantities to be compared were the amplitudes of the events at the seismic stations the optimization problem would be a relatively simple one. A gaussian theory of errors could be assumed, as is customary, and the problem would then be reduced to maximizing the likelihood of fit of the function to the observations of amplitudes. The statistical fault-plane problem gains piquancy, since the quantity being measured is not the amplitude of the arriving P waves, but is merely the sign of the motion; seismic stations remote from the focus usually report merely whether the motion is compressional or dilatational at the stations. Hence the problem becomes one of determining the direction of the initial

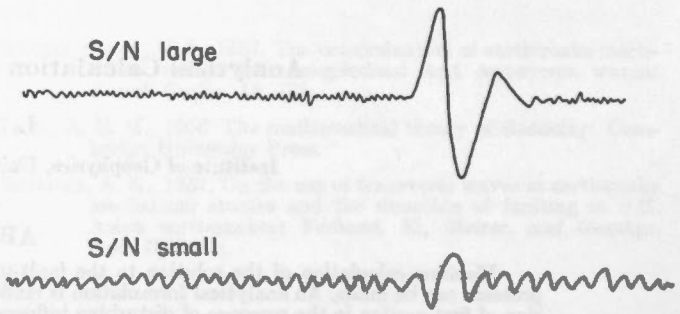

Figure 2. Schematic diagram illustrating the detection of a pulse in the presence of low and high noise levels.

motion in the presence of noise. Figure 2 illustrates some of the difficulty that may occur in determining the direction of the initial motion when the noise level is high, and the comparable ease of this determination when S/|N| is large.

If a three-dimensional map of the relative initial compressions and dilatations corresponding to each of the seismic stations is made, then it should be possible, for infinite signal-to-noise ratio, to pass the co-ordinate planes (x', y', z') among the points so that for $y' > 0$, $z' > 0$ only motion of one sign is to be found, for $y' > 0$, $z' < 0$ only motion of the opposite sign is found, and so on. Of course at those points for which low values of S/|N| occur, there is a finite probability that the sign of the first motion will be reported incorrectly; this is a purely statistical problem and is independent of systematic errors such as those due to reversed galvanometer leads, etc. Our problem is therefore to determine the way in which the co-ordinate planes can be passed through the data points so as to maximize the likelihood that a station will have a sign observed that is appropriate to the quadrant in which it appears. The stations are located exactly in space; only the sign of the reading has a finite probability of being incorrect.

In order to solve this problem we shall have to know the probability that a station will report the "correct" sign, that is, the sign report in the case of zero noise. We shall define a "proper" point as a station reporting a sign in agreement with the sign required for the case of zero noise; an "improper" station will report a disagreement between the two signs. The motion that a proper point reports will itself be called proper.

We assume that the probability of reporting an *incorrect* sign, i.e. that we have an improper point, is given by the function $\frac{1}{2}\exp-(S/N)^2$. This condition is plotted in Figure 3. We note that if $S=0$, the sign has a probability $\frac{1}{2}$ of being reported incorrectly. As S increases the probability of incorrectness decreases.

We compute the probability that we have a proper point. This is obtained by integrating the probability of incorrectness; we obtain $\frac{1}{2}(1 + \text{erf } S/|N|)$ for the

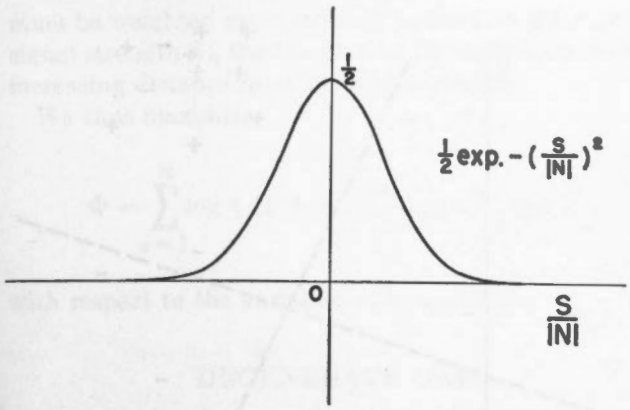

Figure 3. The probability of reporting an incorrect first motion.

probability of correctness. This function is plotted in Figure 4. This result indicates that, for large proper compressional values of S/|N| the probability of correctly reporting a reading as a compression is very nearly unity, but the probability that a point be reported as a compression when the point is geographically located in a proper rarefaction quadrant is small. If S = 0, a reading may be reported as either a compression or rarefaction with equal probability.

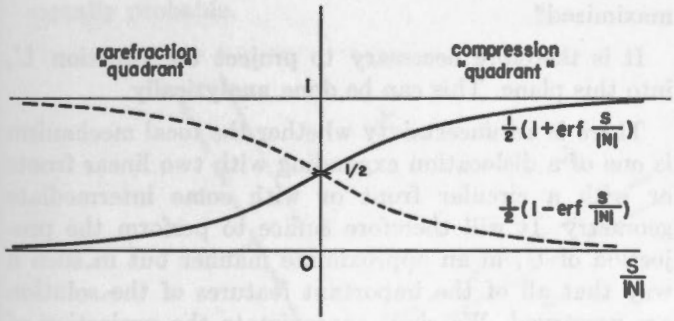

Figure 4. The probability of reporting a compression (solid) and a rarefaction (dashed) first motion.

Let the ith seismic station P_i have co-ordinates (x'_i, y'_i, z'_i) with respect to the focus; let the theoretical signal level at P_i be S_i. Let $|N_i|$ be the noise level at P_i. Let sgn R_i be the sign of the reading reported at P_i where a compression is reported as $+1$ and a rarefaction as -1. Then the probability that station P_i is proper is

$$\tfrac{1}{2}\,(1 + \operatorname{erf}\,(S_i/|N_i|)\ \operatorname{sgn} S_i\ \operatorname{sgn} R_i)\ .$$

The analytical problem is therefore to determine the location of the direction of the co-ordinate axes so that the function

$$\prod_{i=1}^{M} \tfrac{1}{2}\,(1 + \operatorname{erf}\,(S_i/|N_i|)\ \operatorname{sgn} S_i\ \operatorname{sgn} R_i)$$

is maximized. The total number of stations is M. Alternatively we may maximize the function

$$\sum_{i=1}^{M} \log \tfrac{1}{2}\,(1 + \operatorname{erf}\,(S_i/|N_i|)\ \operatorname{sgn} S_i\ \operatorname{sgn} R_i) \qquad (3)$$

with respect to the directions of the co-ordinate axes.

It will be noted that, stated in this way, a uniform distribution of seismic stations throughout space is not required. This is convenient since large parts of the Earth's surface, the oceans, are not adequately canvassed by seismic monitors.

NOISE ASSUMPTION

The function S_i is a theoretical function, and we assume it to be given by equations (1) or (2) where the co-ordinate system is to be determined by the maximization of (3). The function $|N_i|$ is also a function of the co-ordinates and unfortunately is not given theoretically. The noise is usually mainly microseismic. A factor must be included in N that also indicates the changes in magnitude of the ground motion due to changes in nature of the material upon which the seismograph is placed; there is a difference in the amplitudes of ground motions between seismographs placed on unconsolidated soils and those on bedrock.

Since information concerning $|N_i|$ is extremely difficult to collect, we shall assume $|N_i|$ is a constant $|N|$ at all stations. This is a strong oversimplification; perhaps its only virtue is that it leads to a tractable solution. However, if, for a given earthquake, data covering the world-wide distribution of $|N_i|$ became available, the present assumption would not have to be made, and the calculations would proceed according to equation (3).The present assumption is all that can be made without further information and represents a starting point for this calculation.

In view of the assumption, the function to be maximized becomes

$$\Phi = \sum_{i=1}^{M} \log \tfrac{1}{2}\,(1 + \operatorname{erf}\,(U_{r_i}/\alpha)\ \operatorname{sgn} R_i\ \operatorname{sgn} U_{r_i}) \qquad (4)$$

where α is a dimensional constant $\alpha = |N|$, and we have set $A = 1$. We shall determine α in the solution. The maximization of (4) will be made with respect to α and the three angles determining the co-ordinate axes.

PROJECTIVE SYSTEMS

In general the co-ordinate axes (x', y', z') are not simply related to the vertical and the geographic directions at the focus. Simplifications in visualization have been introduced by many authors. One such device consists of

projecting the geometry of Figure 1 onto a plane. This projection does not diminish the number of variables in the maximization.

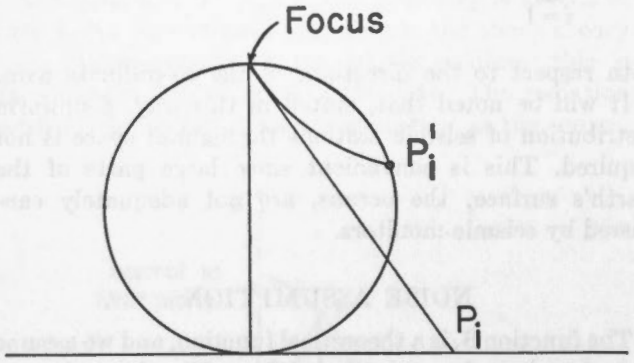

Figure 5. Projection into antipodal plane.

Figure 5 illustrates the projective procedure. A spherical Earth is drawn with the focus at one pole. At the antipodal point to the focus a tangent plane is drawn. The seismic stations are then projected onto the antipodal plane by extending the rays from the focus as straight lines along the tangent to the rays at the focus. A seismic station P_i' is thus mapped into the point P_i. Planes through the focus are mapped as straight lines in the projective plane. Of the three projected coordinate planes and axes only the planes $z'=0$ and $y'=0$ are of importance here. Their intersection, the null vector or x'-axis, projects as a point Q; the two planes project as straight lines intersecting at Q (Figure 6).

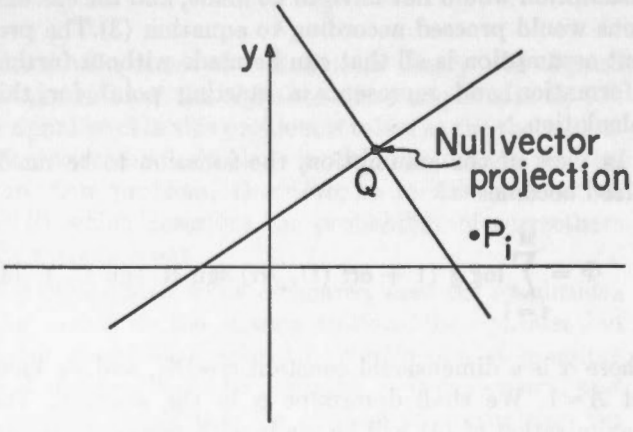

Figure 6. Projection of null planes and axes.

The above projection is advantageous for the present problem, because the maximization problem is now reduced to a problem in cartesian coordinates. The problem may now be restated as follows: if a map (Figure 7) of accurately located points in a projective plane is given,

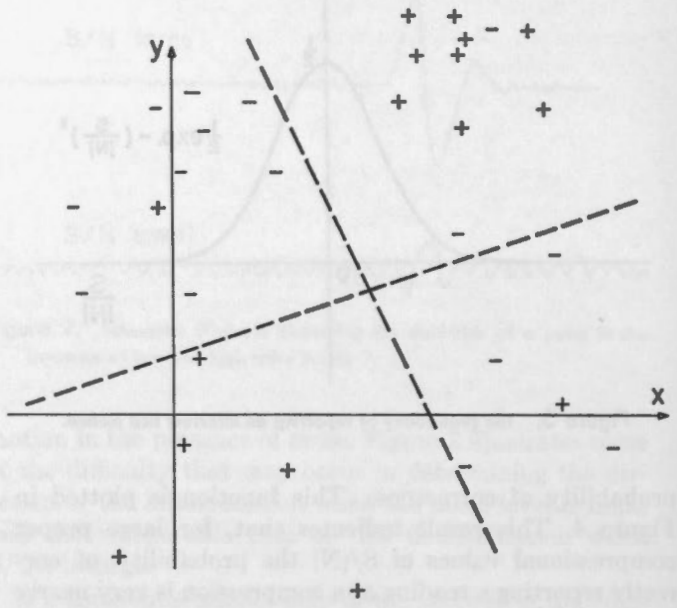

Figure 7. Hypothetical map of first motions in projection.

and to each point a sign of a seismic first motion is assigned, is it possible to pass a pair of straight lines through these points such that the function (4) is maximized?

It is therefore necessary to project the function U_r into this plane. This can be done analytically.

There is an uncertainty whether the focal mechanism is one of a dislocation expanding with two linear fronts or with a circular front or with some intermediate geometry. It will therefore suffice to perform the projection of U_r in an approximate manner but in such a way that all of the important features of the solution are preserved. We shall approximate the projection of U_{r_i} by the expression

$$\Omega_i = (ax_i + b - y_i)\,(cx_i + d - y_i) \tag{5}$$

$$ac + bd + 1 = 0 \tag{6}$$

where (x_i, y_i) are the co-ordinates of a seismic station in the projective plane. The two straight lines that are the projections of the planes $y'=0$ and $z'=0$ are taken to be

$$y = ax + b$$

$$y = cx + d$$

These lines, of course, are related through the condition (6). The function in (5) is reasonable for the following reasons: Ω_i vanishes for points on the planes $z'=0$ and $y'=0$ and in the projective plane for points on either of the straight lines. In addition, points close to the focus (small r) project to great distances; since these points

must be weighted more strongly because of their greater signal strength S_i, the function in (5) must increase with increasing distance from the intersection Q.

We thus maximize

$$\Phi = \sum_{i=1}^{M} \log \tfrac{1}{2} (1 + \text{erf } \Omega_i/\alpha \text{ sgn } R_i \text{ sgn } \Omega_i) \qquad (7)$$

with respect to the variables a, b, c, and α.

DEGENERATE CASE

We consider the cases in which all the points are all proper and evidently separable into quadrants by pairs of orthogonal straight lines. A hypothetical example of such a distribution of first motions corresponding to world-wide seismic stations is shown in Figure 8. Evidently, in the figure no stations are improper points. By visual means we may pass the pair of straight lines, shown as solid curves, through the data, defining the quadrants. But by any criterion, the curves shown as dotted also perform this task with equal ease. Indeed without further data, there is an infinity of solutions that will perform the task of separating the data into quadrants; it is to be expected that each of these solutions is equally probable.

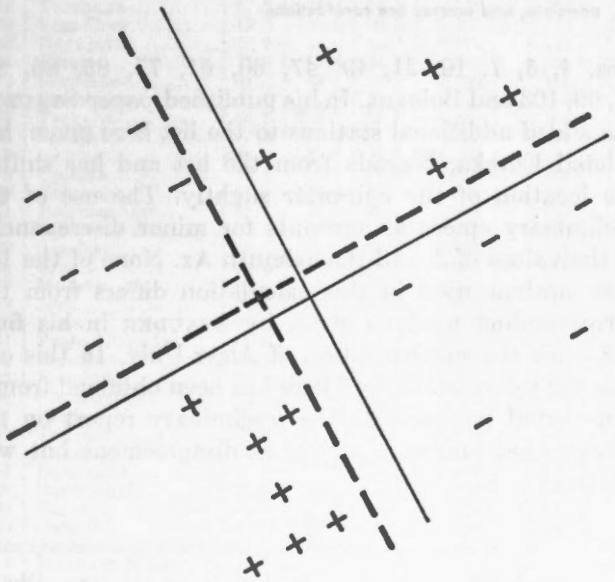

Figure 8. A map without improper points.

We seek the solution to the maximization problem for the present degenerate case. We note that the variable α in (7) is related to the characteristic width of the probability curves of Figure 3 and 4. We further note that as the noise $\alpha \to 0$, the probability curves of Figure 4 approach a step function

$$\lim_{N \to 0} \tfrac{1}{2} (1 + \text{erf } S/|N|) = \begin{matrix} 1 \text{ for } S > 0 \\ 0 \text{ for } S < 0 \end{matrix}$$

Since the error function is bounded $0 < \frac{1}{2}(1 + \text{erf } x) < 1$, the maximum value of the function in (7) is $\Phi = 0$. However the value $\Phi = 0$ is easily attained in the present degenerate example for any solution which keeps all points as proper points and if we set $\alpha = 0$. We note that for proper points

$$\text{sgn } R_i \text{ sgn } \Omega_i = 1$$

Thus all solutions that keep the data as proper points are permissible if the noise level α is set equal to zero. This result is consistent with the visual observation indicated above.

A comment may be made concerning the visual solutions that are made when it is impossible to fit solutions so that all points are proper points. An example of this problem is to be found in the hypothetical projective map of Figure 9. The visual solution should not be made

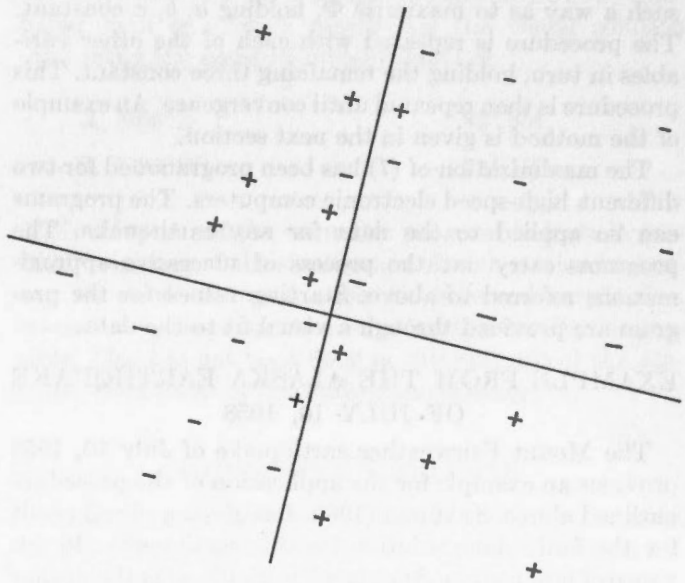

Figure 9. A map with improper points along the null plane projections.

to fit the points along the boundaries too rigorously. This conclusion is correct, since the signal strength S for points close to the boundary is small; hence these points should be weighted least when compared with the weights assigned to the points remote from the two straight lines. The actual fit must await the numerical solution. From the observation made in the preceding paragraph, it is the improper points that contribute to a non-zero value of α; the noise variable α will be one of the variables used to determine the ultimate solution to the maximization problem of (7).

NUMERICAL SOLUTIONS

Equation (7) differs from the maximization function in linear "least-squares" problems, since it is a non-linear expression. Two alternatives are presented: it must be decided whether to linearize equation (7) and solve the four simultaneous linear equations that are obtained or to maximize (7) numerically without any further mathematical manipulation. An investigation of the problem has shown that linearization of non-linear expressions of this type leads to the possibility of non-convergence of the result, especially if attempted by an iteration. The reason for this is that although starting values for the quantities a, b, c are easily made by a visual fit, a starting estimate of α is not simply made. A starting value of α that is sufficiently far from the solution may lead to divergence because of the non-linearity of the original expressions.

Through the application of high-speed digital computers, equation (7) is easily maximized numerically without linearization. Initial guesses as to α, a, b and c, the latter three obtained from a visual solution, are used to generate a starting value of Φ. Then α is varied in such a way as to maximize Φ, holding a, b, c constant. The procedure is repeated with each of the other variables in turn, holding the remaining three constant. This procedure is then repeated until convergence. An example of the method is given in the next section.

The maximization of (7) has been programmed for two different high-speed electronic computers. The programs can be applied to the data for any earthquake. The programs carry out the process of successive approximations referred to above. Starting values for the program are provided through a visual fit to the data.

EXAMPLE FROM THE ALASKA EARTHQUAKE OF JULY 10, 1958

The Mount Fairweather earthquake of July 10, 1958 provides an example for the application of the procedure outlined above. STAUDER (1960) has given a visual result for the fault-plane solution for this earthquake. In advance of publication, STAUDER has kindly sent the author a preliminary list of station co-ordinates and his observations on the first motions at these stations. It was from this preliminary listing that the calculation here reported has been made.

The list of stations included 118 stations. Of these stations 17 have not been included in this calculation because of conflict in the station reports of first motions obtained from long- and short-period instruments or because the sign of the motion was uncertain at the time of the preliminary listing. The 101 stations used in this calculation are given in Table I along with their co-ordinates in the projective plane and the first motions. The identification numbers correspond to STAUDER'S list. The 17 stations not used in this calculation were

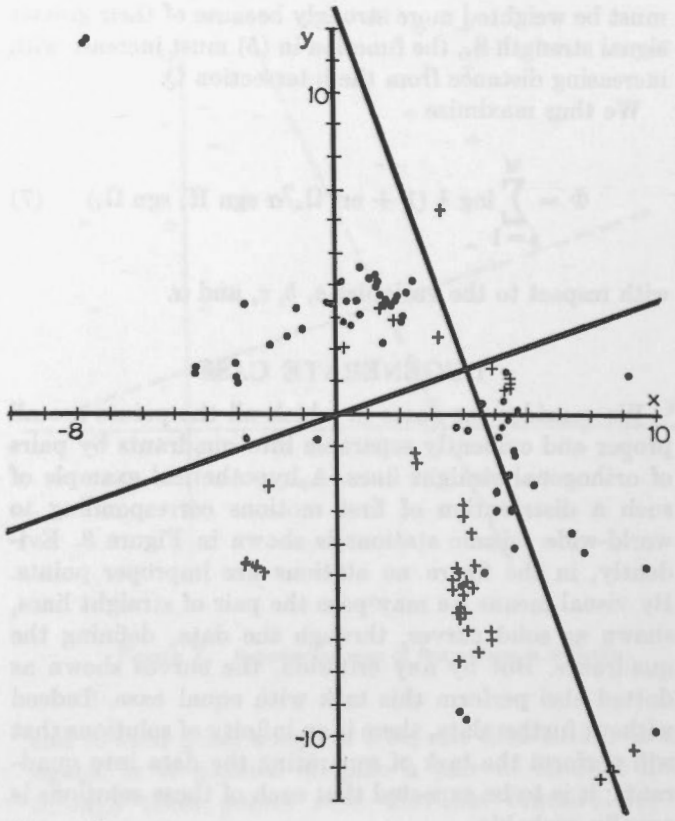

Figure 10. Mapping of the Alaska earthquake of July 10, 1958. The machine optimization of the fault-plane solution is shown. Circles are compressions, and crosses are rarefactions.

Nos. 4, 5, 7, 10, 21, 40, 47, 60, 61, 77, 85, 86, 88, 98, 99, 103 and Bologna. In his published paper STAUDER has added additional stations to the list here given, has deleted Eureka, Nevada from the list and has shifted the location of the epicenter slightly. The use of the preliminary epicenter accounts for minor discrepancies in the values of Δ and the azimuth Az. None of the 101 first motions used in this calculation differs from the corresponding motions given by STAUDER in his final list, with the sole exception of Alger-Univ. In this one case the information used here has been obtained from a long-period instrument; the preliminary report on the short-period first motion was in disagreement but was uncertain.

TABLE I

No.	Station	Δ	Az	i_0	x	y	Motion
1	Sitka	1.5°	143.7°	54.4°	8.270	−11.260	D
2	College	8.4	326.5	54.4	−7.711	11.651	C
3	College Outpost	8.4	326.7	54.4	−7.670	11.679	C
6	Victoria	12.7	134.8	54.4	9.919	− 9.849	C
8	Tumwater	14.1	138.5	54.4	9.262	−10.464	D
11	Corvallis	16.1	142.5	54.4	8.508	−11.078	D
12	Hungry Horse	16.8	116.3	47.0	9.605	− 4.749	C
13	Saskatoon	18.4	83.2	42.8	9.195	1.093	C
14	Butte	19.2	119.1	41.4	7.709	− 4.286	C
15	Arcata	19.3	149.0	40.9	4.460	− 7.422	D
16	Ferndale	19.5	153.3	40.5	3.834	− 7.626	D
17	Shasta	19.9	145.9	40.1	4.724	− 6.972	D
18	Bozeman	20.2	116.6	39.7	7.420	− 3.718	C

TABLE I—*Concluded*

No.	Station	Δ	*Az*	i_0	*x*	*y*	Motion
19	Mineral	20.5	144.7	39.7	4.797	− 6.773	D
20	Ukiah	21.1	148.9	38.3	4.076	− 6.762	D
22	Berkeley	22.6	148.5	36.2	3.828	− 6.244	D
23	Resolute Bay	22.5	27.5	35.8	3.331	6.395	D
24	San Francisco	22.6	148.8	36.2	3.792	− 6.259	D
25	Palo Alto	23.0	148.6	35.8	3.756	− 6.157	D
26	Mt. Hamilton	23.2	147.8	35.4	3.790	− 6.015	D
27	Salt Lake City	23.7	126.8	34.9	5.591	− 4.181	C
	Eureka, Nev.	24.0	136.4	34.5	4.603	− 4.974	C
28	Fresno	24.3	144.9	34.2	3.910	− 5.562	D
29	Tinemaha	24.5	141.7	34.2	4.216	− 5.338	D
30	Rapid City	25.3	109.6	33.4	6.208	− 2.208	D
31	King Ranch	25.6	146.1	33.4	3.677	− 5.470	D
32	Isabella	25.8	143.6	33.4	3.908	− 5.305	C
33	Fort Tejon	26.3	145.0	33.0	3.725	− 5.315	C
34	Boulder City	26.7	137.1	32.5	4.338	− 4.663	D
35	Pasadena	27.2	144.3	32.1	3.662	− 5.091	D
36	Boulder	27.3	118.3	32.1	5.518	− 2.972	C
37	Riverside	27.6	143.1	33.4	3.454	− 5.272	D
38	Palomar	28.4	142.7	31.7	3.745	− 4.913	D
39	Barrett	29.1	142.0	31.4	3.758	− 4.807	D
41	Lubbock	34.1	121.1	30.6	5.059	− 3.050	C
43	Florissant	35.6	102.5	29.8	5.592	− 1.238	C
44	Fayetteville	35.9	109.6	29.8	5.398	− 1.920	C
45	St Louis	35.9	102.6	29.8	5.592	− 1.249	C
46	Chihuahua	36.5	130.7	29.4	4.268	− 3.671	D
48	Dallas	37.0	115.7	29.4	5.073	− 2.443	C
49	Cleveland	38.3	88.7	29.8	5.728	.129	C
50	Ottawa	38.7	81.9	28.7	5.415	.771	D
51	Shawinigan Falls	39.4	78.5	28.7	5.361	1.088	D
52	Montreal	39.7	80.3	28.7	5.393	.919	D
54	Seven Falls	40.0	76.4	28.7	5.317	1.285	C
55	Honolulu	40.0	211.6	28.7	−2.833	4.677	D
56	Morgantown	40.5	92.0	28.3	5.375	− .188	C
58	HVO	41.1	206.9	28.3	−2.432	4.800	D
59	Uwekahuna	41.1	206.1	28.3	−2.367	4.831	D
62	Fordham	42.8	85.5	27.9	5.274	.413	C
63	Weston	43.0	81.9	27.9	5.237	.746	D
64	Chapel Hill	43.8	94.6	27.5	5.184	− .416	C
65	Columbia	44.2	98.4	27.5	5.143	− .759	C
66	Halifax	45.3	74.0	27.1	4.920	1.413	D
67	Tacubaya	47.6	128.4	26.8	3.959	− 3.136	D
68	Vera Cruz	49.0	125.0	26.0	3.997	− 2.801	D
69	Reykjavik	50.0	31.0	25.7	2.477	4.122	C
71	Kiruna	52.9	10.5	24.9	.844	4.561	C
72	Bermuda-C	54.0	85.5	24.5	4.546	.356	C
74	Skalstugan	56.0	15.9	24.2	1.230	4.319	C
75	Tsukuba	56.5	285.5	24.2	−4.328	1.199	C
76	Matsushiro	57.2	287.5	24.2	−4.283	1.351	C
78	Irkutsk	59.1	321.1	23.8	−2.769	3.431	C
79	Uppsala	60.3	14.4	23.8	1.098	4.269	C
80	Goteborg	61.6	18.3	23.5	1.366	4.128	C
81	Rathfarnham	61.7	31.0	23.5	2.240	3.728	C
82	Copenhagen	63.6	18.7	23.1	1.367	4.034	C
83	San Juan	64.6	96.2	22.7	4.155	− .451	C
84	Kew	64.9	28.3	22.7	1.981	3.678	C
87	Moscow	65.9	3.4	22.3	.229	4.092	C
89	Jena	68.0	20.8	21.6	1.406	3.703	C
90	Paris	68.0	27.6	21.6	1.833	3.508	C
91	Ponta Delgada	68.6	53.0	21.6	3.164	2.384	D
92	Stuttgart	69.6	23.2	21.3	1.537	3.584	C
95	Neuchatel	70.8	25.3	20.9	1.631	3.453	C
96	Clermont	71.0	28.4	20.9	1.818	3.362	C
101	Pavia	73.0	24.1	20.5	1.526	3.415	C
102	Trinidad	73.4	96.8	20.5	3.714	− .441	C
104	Toledo	74.5	35.8	20.2	2.164	3.001	C
106	Bucarest	76.5	12.2	19.8	.760	3.517	C
107	Simferopol	76.7	6.5	19.5	.400	3.519	C
108	Rome	76.8	22.9	19.5	1.377	3.260	D
109	Cartuja	77.1	36.6	19.5	2.110	2.843	C
110	Tashkent	78.3	340.2	19.1	−1.173	3.256	C
111	Makhach-Kala	79.0	356.7	19.1	− .201	3.453	C
112	Alger-Univ	79.0	31.7	18.8	1.785	2.893	D
113	Tiflis	80.3	358.8	18.8	− .071	3.399	C
114	Hong Kong	80.4	297.4	18.8	−3.019	1.564	C
115	Baguio	82.6	289.1	17.7	−3.014	1.043	C
116	Athens	82.6	15.1	17.7	.829	3.078	C
118	Manila	83.8	287.8	17.3	−2.961	.952	C
119	Suva	84.6	222.2	17.0	−2.053	2.267	D
120	Huancayo	86.0	120.4	16.3	2.517	− 1.478	D
121	Shillong	87.1	317.1	16.3	−1.988	2.137	C
122	Ksara	87.8	6.0	16.0	.298	2.853	C
123	Quetta	89.6	339.7	15.6	− .968	2.617	C
125	Agra	90.0	329.3	15.6	−1.423	2.399	C
126	Port Moresby	90.7	253.2	15.6	−2.670	.806	C
127	Helwan	91.3	10.2	15.6	.494	2.745	C
128	La Paz	93.2	116.4	15.2	2.437	− 1.210	D
129	Tamanrasset	93.3	34.3	15.2	1.528	2.238	C

96705–9—2½

Table I also lists the station co-ordinates (x, y) in the projection plane. The scale values are

$$x = 10 \tan i_0 \sin Az$$

$$y = 10 \tan i_0 \cos Az$$

The result of the maximization of Φ on the digital computer gave, for the Mount Fairweather earthquake, the values

$$\alpha = 41.0$$
$$a = .36$$
$$b = -.002$$
$$c = -2.707$$
$$d = 12.8$$

Translated into units of dip and strike of the orthogonal planes we obtain

I. Strike N70.2°E	Dip 90.0°
II. Strike N20.2°W	Dip 66.0° NE

These results from the machine calculation are to be compared with STAUDER's results for the visual solution (and using the non-preliminary data) of

I. N68°E	82° SE
II. N25°W	72° NE

Modification of the computer program to include possible weighting of the significance of each station according to some criterion, such as observed amplitudes, measured noise or general reportorial reliability, is possible. This has not been done in this example of the machine calculation of the fault-plane solution.

ACKNOWLEDGEMENTS

The author would like to express his deep appreciation to Dr. WILLIAM STAUDER, S.J., for his having made available the results of his calculations and observations.

References

HODGSON, J. H. (*Editor*), 1959. The mechanics of faulting (a symposium): *Dom. Obs. Pub.*, Ottawa, **20**, 251.

HONDA, H., 1932. On the mechanism and types of seismograms of shallow earthquakes: *Geophys. Mag.*, **5**, 69.

INGRAM, E. L., 1959. Statistics and the fault plane, *in* Hodgson, J. H., *Editor*, The mechanics of faulting, (a symposium) *Dom. Obs. Pub.*, Ottawa, **20**, 263.

KNOPOFF, L. and GILBERT, F., 1960. First motions from seismic sources: *Seismol. Soc. Am. Bull.*, **50**, 117.

NAKANO, H. 1923. Notes on the nature of forces which give rise to the earthquake motion: *Seismol. Bull., Central Meteorol. Obs., Japan*, **1**, 92.

STAUDER, W., S.J., 1960. The Alaska earthquake of July 10, 1958; seismic studies: *Seismol. Soc. Am. Bull.*, **50**, 293.

Statistical Accuracy of the Fault-Plane Problem*

L. KNOPOFF

Institute of Geophysics, University of California, Los Angeles

ABSTRACT

The statistics of the probability function used in the analytical calculation of the fault-plane problem is shown, by numerical means, to closely approximate that of a gaussian distribution function. The definitions of error are obtained from gaussian statistics. A numerical example is given for the Alaska earthquake of July 10, 1958.

In order to calculate the numerical solution to the fault-plane problem, the probability function was introduced (KNOPOFF, 1960):

$$\Phi = \prod_{i=1}^{M} \tfrac{1}{2}\,(1 + \operatorname{erf} \Omega_i/\alpha) \qquad (1)$$

where M is the number of seismic stations reporting first motions, Ω_i is proportional to the theoretical signal strength at the ith station and α is a constant. In one system of mapping, a convenient form for Ω_i is

$$\Omega_i = (ax_i + b - y_i)\,(cx_i + d - y_i)$$

subject to an equation of constraint

$$ac + bd + 1 = 0$$

where (x_i, y_i) are the coordinates of the ith seismic station in the map. The function Φ is then maximized with respect to the parameters α, and three of a, b, c, d. From this program, optimum values of a, b, c, d and the corresponding angular orientation parameters of the fault planes can be determined. The calculation is complicated and requires, in a practical case, the application of digital computing techniques.

Before investigating the statistical reliability of the optimum values corresponding to a given set of observations, it is necessary to investigate the analytic properties of the function Φ. The function Φ is evidently not a gaussian function. The properties of some nongaussian probability functions are given by JEFFREYS (1939); this case is not included. However Φ does have certain elementary properties. The function Φ has a maximum. It is, in general, not symmetric about the maximum. It goes to zero for values of the parameters remote from the values at the maximum. It is always positive. There must be at least one curve on the surface in *abcd* space where the curvature changes sign. A detailed description of the remaining properties of this function will not be given in this paper.

Assume the four independent parameters are x_n $(n = 1, 2, 3, 4)$. Then if Φ_m is the value of Φ at its maximum and x_{no} are the values of x_n at this maximum, we can write

$$\log \Phi = \log \Phi_m + \tfrac{1}{2} \sum_{i=1}^{4} \sum_{j=1}^{4} \frac{\partial^2 \log \Phi}{\partial x_i\, \partial x_j} \cdot (x_i - x_{io})\,(x_j - x_{jo}) + \ldots \qquad (2)$$

If the terms beyond the second order can be neglected, then it is evident that what remains is merely the ordinary gaussian distribution function. It is the terms beyond the second order which provide the deviations of Φ from gaussian and symmetric behavior.

The magnitudes of the terms beyond the second order are investigated numerically. An example of the maximization of (1) by machine computation has been presented (KNOPOFF 1961) for the case of the Alaska earthquake of July 10, 1958. A description of the numerical field of $\log \Phi$ in the vicinity of $\log \Phi_m$ was obtained. The values of the parameters at the maximum were $a_o = .36$, $b_o = -.002$, $c_o = -2.707$, $d_o = 12.8$, $\alpha_o = 41.0$. A mapping of the $\log \Phi$ field in the a-d plane for values of $\alpha = 38.0$, $b = .00$ is given in Figure 1. The contours are constant values of $\log_{10}\Phi$. A cross-section of the field along the line $a = .35$ is given in Figure 2. A parabola has been fitted to the points d:10(2)18. The fit to the computed values in this interval is good. The discrepancy between the fitted curve and the computed value at $d = 8$ corresponds to the difference between values that are $10^{-18}\,\Phi_m$ and $10^{-20}\,\Phi_m$. This discrepancy is therefore not significant. Hence a gaussian is an excellent approximation to Φ in the vicinity of the maximum and even to extremely small values of Φ. Deviations from the gaussian only appear when the values of Φ are negligibly small. Hence, for our purposes, we neglect the higher order terms in (2).

*Publication No. 204, Institute of Geophysics, University of California.

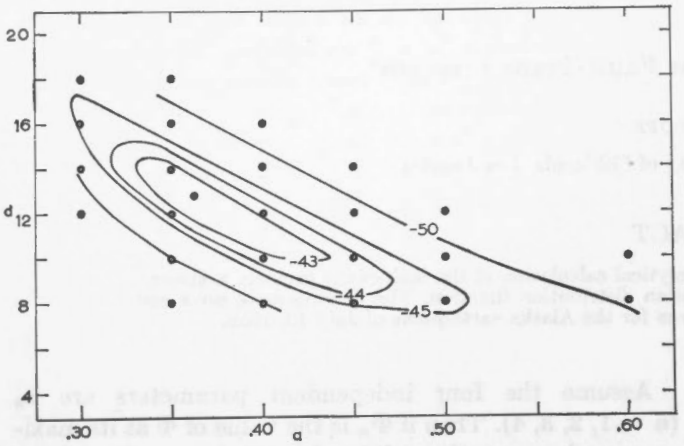

Figure 1. Portion of the field $\log_{10} \Phi$ for $\alpha = 38.0$, $b = .00$. Curves are constant values for $\log_{10} \Phi$. Dots indicates a numerical value obtained from the computer.

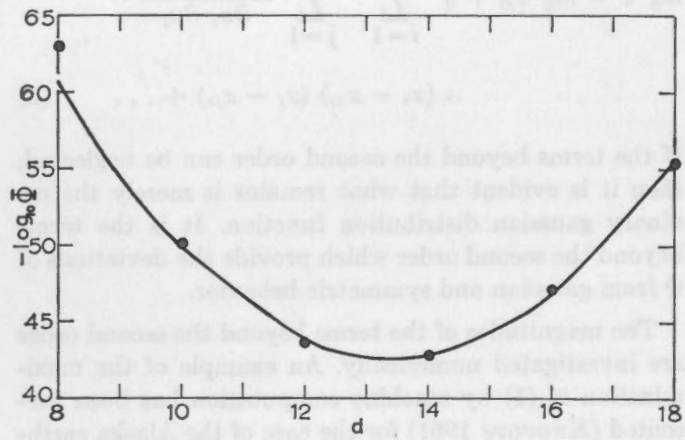

Figure 2. Section of Figure 1 along line $a = .35$. Curve is parabola fitted in region d:10(2)18.

Since the function Φ is approximately gaussian in the vicinity of the maximum, it follows that ordinary definitions of error, derived from gaussian statistics, will suffice to determine the statistical errors of the prediction in this problem as long as we keep the order of the moments small. In ordinary gaussian statistics, standard error is defined by $\Phi_s = e^{-\frac{1}{2}}\Phi_m$ where Φ_s is the value of the probability function Φ at the locus of the standard error. The problem of determining the standard error is therefore that of finding the locus of $\log_{10}\Phi_m - .217$ in the numerical field of $\log_{10}\Phi$ in *abc* space for $\alpha = \alpha_{.0}$. It is an elementary procedure to convert these loci into the four coordinates in angular space defining the standard errors of the dip and strike of the two null planes.

In the example of the Alaska earthquake, the numerical fault-plane solution was

I. Strike N70.2°E,	Dip 90.0°
II. Strike N20.2°W,	Dip 66.0°NE

The standard error in the variable b, in this case, is less than .001. The locus in *abd* space need only be plotted in the $a-d$ plane, $b = -.002$. The corresponding uncertainty in the dip and strike of II is plotted in Figure 3

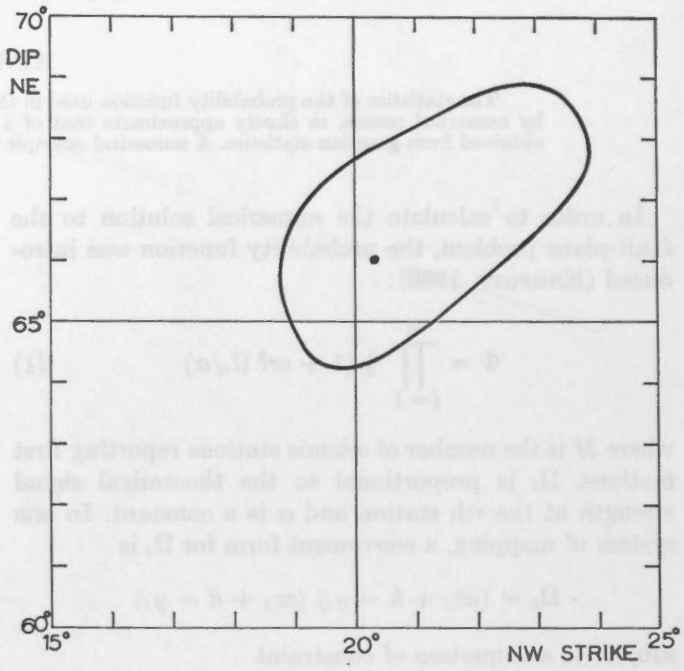

Figure 3. Standard error locus for II.

as a closed curve; points along this curve give the values of the angular co-ordinates which differ by the standard error from the solution, the latter plotted as a point in the interior of the curve. The values of dip for II lie within the standard error between the extremes of 64.2° NE and 68.9° NE while the strike lies in the interval N18.7° W and N23.9° W. The standard error in the strike of I lies between the limits of N66.4° E and N71.6° E. The uncertainty in the dip of I is less than .03°.

In the projective plane, envelopes are defined within which the solutions must lie, subject to the condition of orthogonality, if the solution is to be within the standard error. This is shown, for the example, in Figure 4; the shaded region defines solutions which are within the standard error of the optimum solution.

Because of the steepness of Φ near the standard error locus and because of the flatness of Φ near Φ_m, there is actually greater precision in the determination of the standard error locus from the numerical values than the determination of the optimum fault-plane solution itself. The fault-plane solution could as easily have occurred at the center of the locus as at one side, the latter the situation reported here; this is due to the extremely flat nature of the function near Φ_m and the poor resolution of the numerical procedure. Computing techniques with

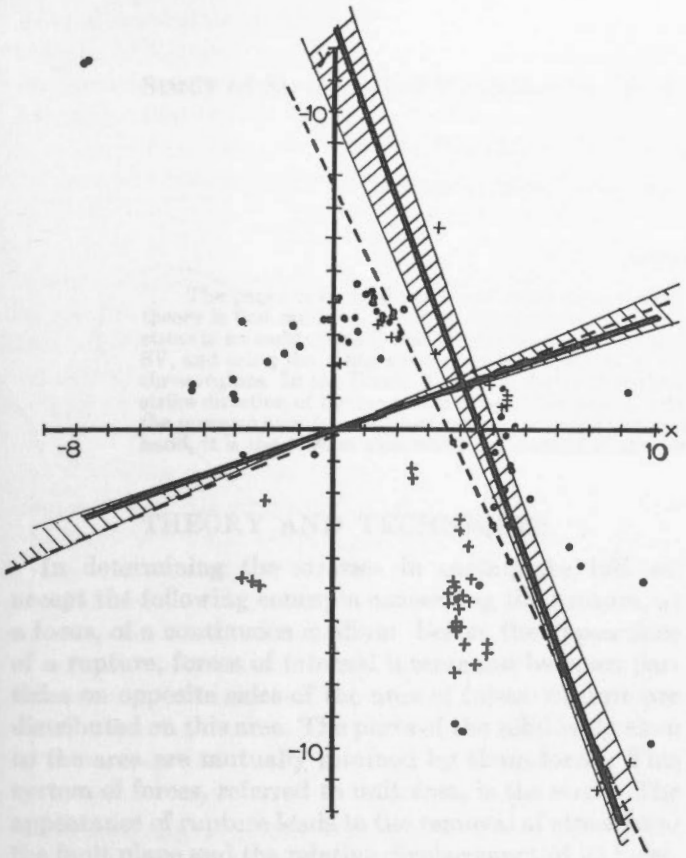

Figure 4. Antipodal projection for the earthquake of July 10, 1958. The heavy lines are the null planes obtained by machine calculation. The dotted lines are the visual solution (after Stauder). The shaded area indicates solutions within the standard error locus. Circles are stations reporting compressional first motions; crosses are first-motion reports of rarefactions.

higher resolution than those used here are required to resolve this uncertainty. If Φ_m must lie at the center of the standard error locus, then we modify the result for the Alaska earthquake to the values

I. N69.0° E ± 2.6°, 90.0° ± 0°

II. N21.3° W ± 2.6°, 66.6° NE ± 2.4°

In Figure 4 we compare the visual solution (STAUDER, 1960) for this earthquake and the numerical solution. STAUDER'S solution is

I. N68° E, 82° SE

II. N25° W, 72° NE

Plane I falls close to the limits of standard error obtained numerically. The reasons for the discrepancy between II and the numerical solution are several. The numerical solution is based upon a theoretical signal distribution that suggests that near stations be weighted very heavily and that stations near the null planes be weighted lightly. In the visual procedure this type of weighting is difficult. In addition, "improper points" (KNOPOFF 1961), far removed from the null planes, strongly influence the solution obtained numerically; such points in the visual solution are often weighted weakly since they are surrounded by a number of "proper points".

References

JEFFREYS, H., 1939. Theory of probability: Oxford University Press.

KNOPOFF, L., 1960. Analytical calculation of the fault-plane problem: *Dom. Obs. Pub.*, Ottawa, **24**, no. 10, page 309.

STAUDER, W., S.J., 1960. The Alaska earthquake of July 10, 1958; seismic studies: *Seismol. Soc. Am. Bull.*, **50**, 293.

Study of Stresses and Ruptures in Earthquake Foci with the Help of Dislocation Theory

L. M. Balakina, H. I. Shirokova and A. V. Vvedenskaya

Institute of Earth Physics, U.S.S.R. Academy of Sciences, Moscow

ABSTRACT

The paper reviews the authors' work done mainly during the three-year period since the Toronto meetings. A theory is first outlined, based on the theory of dislocations, which permits the determination of the principal axes of stress in an earthquake focus. The technique for the application of the method, based on the first motion in P, SH and SV, and using the Wulff stereographic projection, is then described. This method has been applied to earthquakes in three regions. In the Hindu Kush it is shown that the regional pressure acts in a horizontal plane and normal to the strike direction of the mountain range. The tension acts along the direction to the zenith. In the northwestern Pacific the pressure axes for most foci are also oriented perpendicular to the geological features. In Prebaikalye, on the other hand, it is the tension axes which are normal to the geological features.

THEORY AND TECHNIQUES

In determining the stresses in earthquake foci we accept the following concepts concerning the rupture, at a focus, of a continuous medium. Before the appearance of a rupture, forces of internal interaction between particles on opposite sides of the area of future rupture are distributed on this area. The parts of the solid body close to the area are mutually retained by these forces. This system of forces, referred to unit area, is the stress. The appearance of rupture leads to the removal of stress from the fault plane and the relative displacement of its faces. Under the conditions which occur in the earth's crust and in the upper part of the mantle, in which stresses may be supposed to have a considerable duration, a rupture accompanied by slipping is the most probable form of movement in the earthquake foci.

From these considerations we believe that a limited fault area, whose opposite faces move relative to each other in the slipping plane, is the most probable theoretical model of an earthquake source. The static stresses acting on this area before dislocation, and which rebound at the moment of the appearance of rupture, we name the stresses acting in the focus (Vvedenskaya, 1960). They are determined, by methods established in the theory of dislocations (Nabarro, 1951), from a force model of a rupture accompanied by slipping that is determined as follows. Let a limited area of rupture, including the origin of the x, y, z co-ordinate system, lie in the xz plane, and let the normal to it be oriented along the y axis. The faces of the rupture are abruptly shifted, relative to each other, in the xz plane. The face that is on the side of the positive direction of the y axis is shifted a distance $b/2$ in the $-z$ direction; that on the side of the negative direction of the y axis is shifted a distance $b/2$ in the $+z$ direction. The appearance of a rupture area accompanied by slipping causes the same field of displacement in the elastic medium that is formed by a system of mutually balanced forces uniformly distributed within this area (Vvedenskaya, 1956, 1959). The system of these forces forms a tensor. It can be represented by two perpendicular double forces without moment (forces of compression and dilatation) that act abruptly on each element of the area, parallel to the yz plane and making an angle of 45° to the area (Figure 1). These forces are equal and opposite to those that determined the tensor of stresses at each point of the area before the appearance of rupture and which vanished at the moment of rupture. Therefore the principal directions of this stress tensor, corresponding to its two principal non-zero values, are parallel to the yz plane at each point of the area. The axis of pressure (i) is parallel to the bisector of the co-ordinate angle (yoz), while the axis of tension (k) is parallel to the bisector of the co-ordinate angle ($-yoz$). The intermediate stress (equal to zero) is parallel to the x axis. This is not the only possible concept of a force model; it is well known that an opinion exists that the appropriate model is the double force with moment.

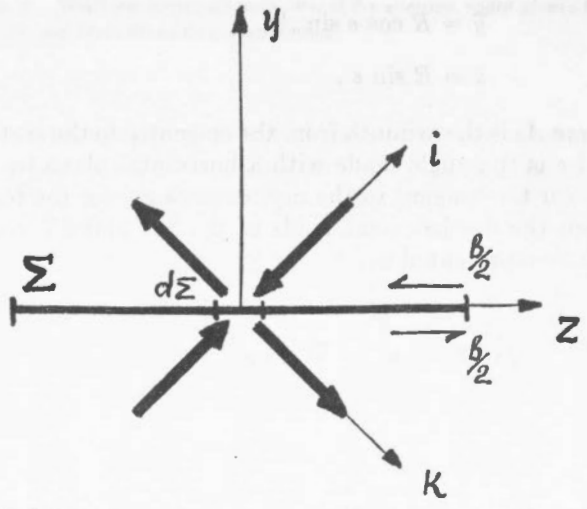

Figure 1. The system of forces that is equivalent to a rupture accompanied by slipping.

We determine the position of the principal stresses by comparing the observed displacements of the first longitudinal and transverse waves with the theoretical displacement field calculated for a system of forces found in the theory of dislocations and forming the tensor.

The expressions for this displacement field, for distances from the rupture great as compared with its size, can be represented as follows (VVEDENSKAYA, 1959):

$$U_p = -\frac{c^2}{\pi a^2}\frac{yz}{R^2\sqrt{R^2-y^2}}\rho b \quad , \qquad (1)$$

$$U_{sj} = \frac{1}{\pi R^3\sqrt{R^2-y^2}}\left[x_j yz - \frac{R^2}{2}\frac{\partial(yz)}{\partial x_j}\right]\rho b, \qquad (2)$$

where U_p is the displacement in the first arrival of the longitudinal wave, U_{sj} is the displacement component in the direction of the x_j axis ($x_j = x, y, z$) in the arrival of the transverse wave; x, y, z are the coordinates of the observation point; a and c are the velocities of propagation of the longitudinal and transverse waves;

$$R = \sqrt{x^2+y^2+z^2} \ ;$$

ρ is the radius of the rupture area, taken to be circular.

From this point b, ρ and R are excluded from the computations and formulae (1) and (2) are reduced to a form convenient for direct use. For this purpose a system of coordinates is introduced, the origin of which coincides with the focus of the earthquake, and for which the axes $\bar{x}, \bar{y}, \bar{z}$ are directed north, east and zenith respectively. The coordinates of the observatories are given in this system by the following formulae:

$$\bar{x} = R\cos e\cos Az$$

$$\bar{y} = R\cos e\sin Az$$

$$\bar{z} = R\sin e \ ,$$

where Az is the azimuth from the epicentre to the station, and e is the angle made with a horizontal plane by the ray (or the tangent to the ray) emerging from the focus. Then the displacement fields of the SH and SV waves can be represented as:

$$U_{SH} = \frac{\rho b}{2\pi R^2\sqrt{R^2-y^2}\cos e}\cdot$$

$$\cdot\left[y(\bar{x}n_z - \bar{y}m_z) + z(\bar{x}n_y - \bar{y}m_y)\right], \qquad (3)$$

$$U_{SV} = \frac{\rho b}{2\pi R^2\sqrt{R^2-y^2}\cos e\sin e}\cdot$$

$$\cdot\left[-2yz\sin^2 e + \bar{z}(zl_y + yl_z)\right] \quad , \qquad (4)$$

where m_j, n_j, l_j are the cosines of angles that are made by the directions x_j ($x_j = y, z$) and the axes $\bar{x}, \bar{y}, \bar{z}$ respectively. The displacement in the longitudinal wave is considered positive if it is directed *from* the focus; the displacement U_{sv} is also regarded as positive when it is directed *from* the focus while U_{SH} is regarded as positive when, looked at from the epicentre, it moves counterclockwise.

The most simple method for the determination of the two possible positions of the fault plane, and of the axes of principal stresses acting in the focus is to construct nodal lines for the P, SV and SH waves, using the observed signs of displacement in these waves. It follows from expression (1) that the displacement field for longitudinal waves has two nodal planes, $y = 0$ and $z = 0$, the fault plane in the focus coinciding with one of them. These planes are most simply constructed in the Wulff stereographic projection. In this projection the origin of coordinates is taken at the centre of a sphere of unit radius and the projection is on a diametral plane of the sphere. The earthquake focus then projects to the centre of the projection, the vertical diameter of the projection is oriented north, the horizontal diameter east, and the direction to zenith is projected in the centre of the projection.

The location of the observatories on the stereographic projection is determined by means of two known spherical co-ordinates of the observatories in relation to the focus: Az and e. Az is measured in a clockwise direction from the vertical diameter, along the equator of the projection; the angle e is measured from the equator to the centre. The sign of the arrival of the longitudinal wave at each observatory is entered at the corresponding point. Then in the projection plane two mutually perpendicular diametral arcs are constructed so as to separate the regions with different displacement signs. These arcs are the projections of the intersections of the two nodal planes with the unit sphere. The point of intersection of the arcs determines the projection of the point of intersection of the x axis with the sphere. It is the pole of the arc corresponding to the plane $x = 0$. On this arc lie points which determine the axes i and k in space, making angles of 45° with the nodal planes.

The directions of the axes of pressure and tension are determined by examination; the pressure axis is in the region of dilatational waves, the tension axis in the region of compressional waves.

To establish the position of the axes more precisely the observations of the displacement signs in the SH and SV waves are compared with the signs obtained from formulae (3) and (4). The technique for the determination of the principal direction axes on the basis of the observed displacement amplitudes in P, SV and SH arrivals is described elsewhere (VVEDENSKAYA, 1960).

The determination of the y and z axes by the signs in P, SV and SH waves does not unambiguously establish which of the two axes obtained is the y axis and which the z axis. This follows from the symmetry of the stress tensor. However the position of the principal stress axes is independent of the choice of the y and z axes.

RESULTS

By means of the techniques described above, stresses in the focus have been determined for earthquakes in the Hindu Kush, in the region of Prebaikalye and in the northwestern part of the Pacific Ocean. These results will now be discussed.

Hindu Kush

Stresses have been determined (Shirokova, 1959) for 14 earthquakes in the Hindu Kush. Solutions were based on the seismograms from the Soviet seismic stations, augmented with data from the BCIS bulletin, and chiefly depended on the displacement directions in the longitudinal waves. However these data gave some ambiguity in the construction of the nodal lines; therefore the signs of displacement in the SV and SH waves were used where possible.

The results are given in Table I, which lists, for each earthquake, the directions of the pressure, tension and intermediate stress axes. Measurements are in terms of azimuth (Az) and of the angle i that the axis makes with the zenith. For earthquakes 1, 2, 4, 9, 10 and 11 the positions of the nodal lines differ little one from another, and for them we can accept one and the same stress system in the focus. For other earthquakes the direction of the stress axes is somewhat different. However this difference was established on the basis of observations of the displacement signs in the longitudinal waves at three station, Khorog, Kulyab and Obigarm, located relatively close to the epicentre ($\Delta \leqslant 350$ km) where the error in the determination of the angle e can be very great. Since the angular distance of these stations from the average nodal lines of the above 6 earthquakes is of the same order as the possible error in e, we may assume that these nodal lines apply to all the earthquakes, ignoring the small observed differences.

The system of stresses obtained is shown in Figure 2 in a Wulff projection. The figure shows that one of the nodal planes for P waves strikes N85°E, dipping to the south at an angle of about 55°, while the other plane strikes N70°E and dips to the north at an angle of 35°. Apparently, in whichever of these planes rupture occurs,

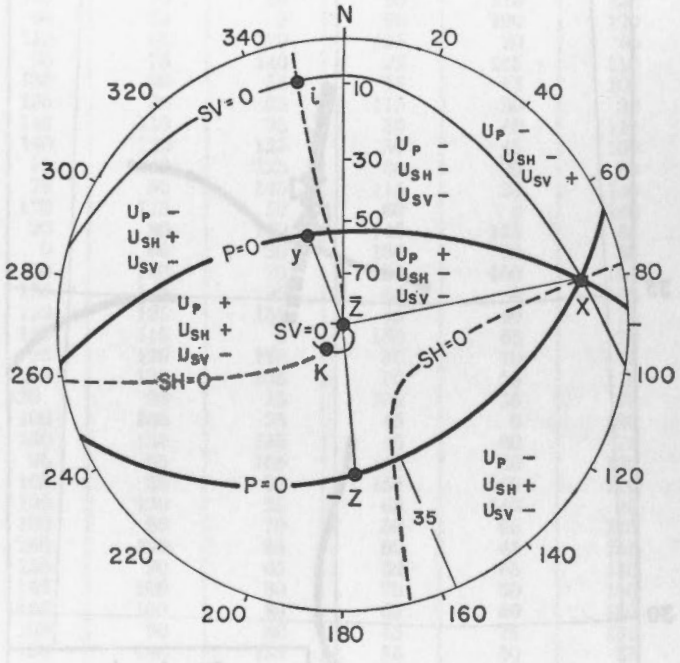

Figure 2. Wulff stereographic projection of the average nodal planes for P, SV and SH in Hindu Kush earthquakes.

Table I

No.	Date	Origin Times	Coordinates of Epicentre		Focal Depth	Pressure Axis		Tension Axis		Intermediate Stress Axis	
		h	φ°N	λ°E	km	A_s°	i°	A_s°	i°	A_s°	i°
1	Jan. 6 1951	05	36.6	70.9	220	170	100	25	170	75	80
2	June 12 1951	22	36.7	70.5	200	170	100	25	170	75	80
3	Oct. 4 1951	05	36.6	70.5	200	20	60	0	150	110	110
4	July 5 1952	17	36.9	70.8	200	160	100	25	170	70	80
5	Nov. 27 1952	07	36.9	70.1	180	12	80	160	10	100	95
6	Aug. 7 1954	15	36.7	70.6	200	25	70	160	25	110	120
7	Sept. 9 1954	18	36.7	70.5	200	35	65	175	30	120	120
8	Mar. 10 1955	20	36.7	69.8	200	45	85	05	175	140	90
9	Apr. 6 1956	07	36.5	70.7	200	170	80	30	170	80	80
10	May 18 1957	13	36.8	70.8	210	170	80	30	170	80	80
11	June 11 1957	04	36.6	70.3	170	170	80	30	170	80	80
12	Feb. 17 1958	05	36.5	70.6	180	0	80	50	160	90	75
13	Mar. 28 1958	04	36.6	71.0	210	165	105	145	15	60	95
14	Mar. 28 1958	12	36.6	70.9	190	170	100	110	25	85	160

the movement in the focus of the earthquake will correspond to a thrust, with a very insignificant component along the strike. As is seen from the figure, the axis of the pressure is directed almost along the meridian (the azimuth is about 170°) and makes an angle of about 100° with the zenith. The axis of tension is directed about in the azimuth 30° and makes an angle of about 170° with the vertical.

In Figure 3 the direction of the axis of pressure is designated by a black arrow, that of tension by a white arrow. The length of the arrow is equal to the sine of the angle made by the axis of stress with the direction to the zenith. The angle made by the arrow with the north direction is equal to the azimuth of the axis of the corresponding stress. Axes making acute angles with the direction to zenith are drawn by solid arrows, those making obtuse angles by dashed arrows.

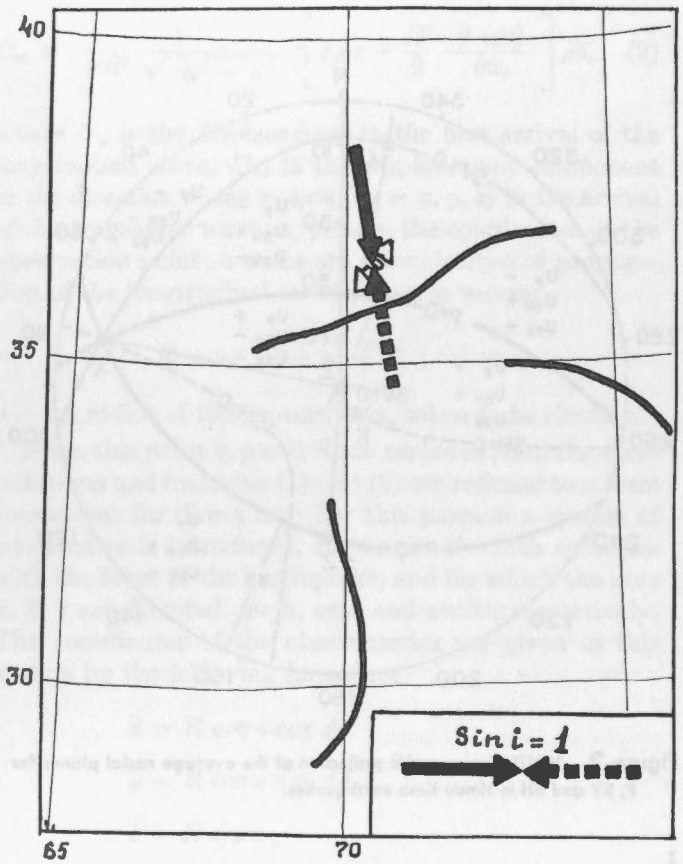

Figure 3. Average direction of pressure axis (black arrow) and tension axis (white arrow) in the Hindu Kush. See text for description of units used.

The strike directions of the main structure are shown by thick lines in Figure 3. It will be seen that the pressure acting in the foci of the Hindu Kush earthquakes makes an angle close to 90° with the strike direction of the mountain system.

Prebaikalye

The results of the determination of stresses acting in the foci of earthquakes in Prebaikalye with M $\geqslant$6 are given in Table II, (Vvedenskaya and Balakina, 1960).

For all the earthquakes in the table the following laws govern the directions of the principal axes of stress. For the earthquakes of northeastern and central Prebaikalye the axes of tension are directed almost perpendicular to the geological structures and make great angles (>75°) with the zenith (*see* Figure 4). The axes of pressure are directed almost along the structure and make small angles (<45°) with the zenith directions. When the slipping was directed along the plane occupying the position of either of the two possible fault planes, the upper face of the rupture lowered, the lower one lifted.

In the foci of earthquakes of southwestern Prebaikalye, as compared with the earthquakes of the regions located farther to the north, the angles between the zenith direction and the axes of tension decrease, while the angles between the zenith direction and the axes of pressure increase.

Northwestern Pacific

In the Pacific seismic zone, the stresses acting in the foci of 44 earthquakes, in Japan, the Bonin Islands, the Kuriles, Kamchatka and the Aleutians, have been determined (Balakina, 1959). As a result of this study we have established that the axes of the principal stresses in the region do have preferred directions (*see* Table III).

Table II

No.	Date	Origin Times	Coordinates of Epicentre		Focal Depth	Pressure Axis		Tension Axis	
		h	φ°N	λ°E	km	A_s°	i°	A_s°	i°
1	Apr. 29 1917	11	55–56	115–116	In Crust	97	136	18	80
2	Apr. 4 1950	18	51.6	102.7	In Crust	9	55	9	145
3	Feb. 6 1957	20	50.0	105.5	In Crust	64	128	115	53
4	June 27 1957	0	56.1	116.6	In Crust	82	136	174	93
5	Jan. 5 1958	11	56.5	121.0	In Crust	72	33	2	103
6	June 23 1958	5	48.7	103.2	In Crust	67	93	156	56
7	Sept. 14 1958	14	56.5	122.0	In Crust	99	8	127	97
8	Aug. 29 1959	17	52.6	107	In Crust	48	19	144	88

TABLE III

No.	Date	Origin Times	Coordinates of Epicentre		Focal Depth	Pressure Axis		Tension Axis		Intermediate Stress Axis	
		h	φ°N	λ°E	km	A_p°	i°	A_t°	i°	A_s°	i°
1	Mar. 23 1948	18	52.9	153.3	200	165	5	125	95	35	85
2	Apr. 5 1949	09	41.6	131.6	570	95	75	70	165	5	80
3	May 3 1949	05	48.6	153.5	150	140	75	50	90	135	155
4	May 21 1949	21	37	142.0	40–50	75	105	85	15	160	90
5	Aug. 17 1949	18	43.5	146.2	70	155	120	30	140	85	60
6	Nov. 3 1949	01	48.5	156.0	180	40	90	130	80	145	170
7	Feb. 23 1950	08	48.0	148.2	570	115	85	65	165	10	85
8	Feb. 28 1950	10	45.0	144.5	340	110	75	35	135	5	50
9	May 17 1950	11	39.0	131.5	580	105	125	115	35	20	95
10	June 27 1950	15	41.0	139.5	30–100	95	85	60	175	5	90
11	July 13 1950	04	27.5	140.0	520	95	75	170	130	20	140
12	Apr. 16 1951	20	30.5	137.0	480	105	70	15	95	115	160
13	July 11 1951	18	29.0	141.0	480	90	30	5	95	100	120
14	Aug. 10 1951	23	45.5	143.7	350	110	65	120	155	20	95
15	Aug. 24 1951	14	46.8	150.8	180	20	75	140	25	105	110
16	Mar. 5 1952	16	42.0	145.0	In Crust	135	90	55	15	45	105
17	Mar. 7 1952	07	35.0	136.0	In Crust	155	80	65	115	50	30
18	Mar. 9 1952	17	41.5	144.0	30	140	110	95	30	40	110
19	Apr. 28 1952	10	42.0	142.6	80	140	120	120	30	45	100
20	May 28 1952	07	35.0	136.0	380	75	140	125	60	20	65
21	Oct. 26 1952	08	34.5	137.0	300	75	60	145	115	25	140
22	Nov. 4 1952	16	52.5	159.0	In Crust	120	115	50	60	0	140
23	Oct. 11 1953	13	49.5	156.4	90	20	80	100	145	115	55
24	Oct. 14 1953	14	43.0	144.4	100	0	60	20	150	90	80
25	Nov. 25 1953	17	34.0	141.0	40	50	140	70	50	150	100
26	Nov. 26 1953	08	34.0	141.0	40	170	145	90	85	0	125
27	Dec. 25 1953	01	52.0	159.8	60	120	125	155	40	40	70
28	July 6 1954	08	46.0	152.0	60	145	115	0	150	65	75
29	July 29 1954	03	48.0	156.0	In Crust	95	125	120	35	10	75
30	Aug. 9 1954	19	53.0	158.0	In Crust	165	130	125	50	55	110
31	Aug. 30 1954	07	44.0	146.0	In Crust	120	95	15	160	35	70
32	Sept. 6 1954	18	51.0	155.0	In Crust	100	105	25	45	0	130
33	Sept. 23 1954	21	49.0	154.0	In Crust	150	135	135	45	60	75
34	Nov. 19 1954	05	40.1	132.5	500	95	65	165	130	30	130
35	May 14 1955	06	28.0	139.5	500	105	35	20	155	160	110
36	June 12 1955	20	49.0	155.0	In Crust	100	120	25	65	145	40
37	Mar. 9 1957	20	52.0	168.5W	In Crust	160	95	70	50	65	140
38	Mar. 11 1957	03	51.0	176.5W	In Crust	150	100	65	60	45	145
39	Mar. 11 1957	09	53.0	169.0W	In Crust	155	90	65	50	65	140
40	Mar. 11 1957	14	51.0	178.5W	In Crust	165	100	80	70	50	150
41	Mar. 16 1957	02	51.0	178.5W	In Crust	165	100	80	65	50	150
42	Mar. 22 1957	14	54.0	165.0W	In Crust	165	90	80	45	75	135
43	May 4 1959	07	59.1	160.3	20	130	140	135	55	50	75
44	June 18 1959	15	53.9	160.5	In Crust	45	90	135	110	130	20

The pressure axes are mostly directed perpendicular to the strike of the main structures, and make large angles with the zenith direction. This is most clearly observed in foci at great depths; in the foci of shallow earthquakes this rule is sometimes violated (Figure 5). In foci at depths to 100 km inclusive the pressure axes make angles greater than 90° with the zenith direction, while in foci at depths over 300 km the angles are less than 90°. The insufficient number of observations with focal depths between 100 and 300 km prevents us from establishing a direction for the pressure axes at these depths.

For the tension axes (Figure 6) the predominant direction cannot be established for the whole region under consideration. We can only say that in most of the foci the tension axes make angles equal to or greater than 45° with the zenith direction. A certain system in the orientation of the tensions is observed in limited areas of the investigated region.

For the axes of intermediate stress two predominant directions can be distinguished. One of them is parallel to the strike of the main structures, and makes a great angle with the zenith direction. The second is perpendicular to the strike of the structures, and makes small angles with the zenith direction (Figure 7).

The orientation of the possible fault planes and the direction of movements on them vary considerably. Only a small number of them agree with the concept that a fault exists under the continent, on which the lower, oceanic face moves downward relative to the upper one. No predominance of transcurrent movements are observed in the ruptures; movements along the dip and along the strike are encountered equally often.

The variations in the orientation of the fault planes and in the direction of motion, as well as the considerable width of the zone of foci, seems to suggest that the zone is not a single focal surface, but a zone of instability in the region of stresses.

The distribution of stresses in this unstable zone will determine the surface of greatest tangent stress along which rupture is most likely to occur.

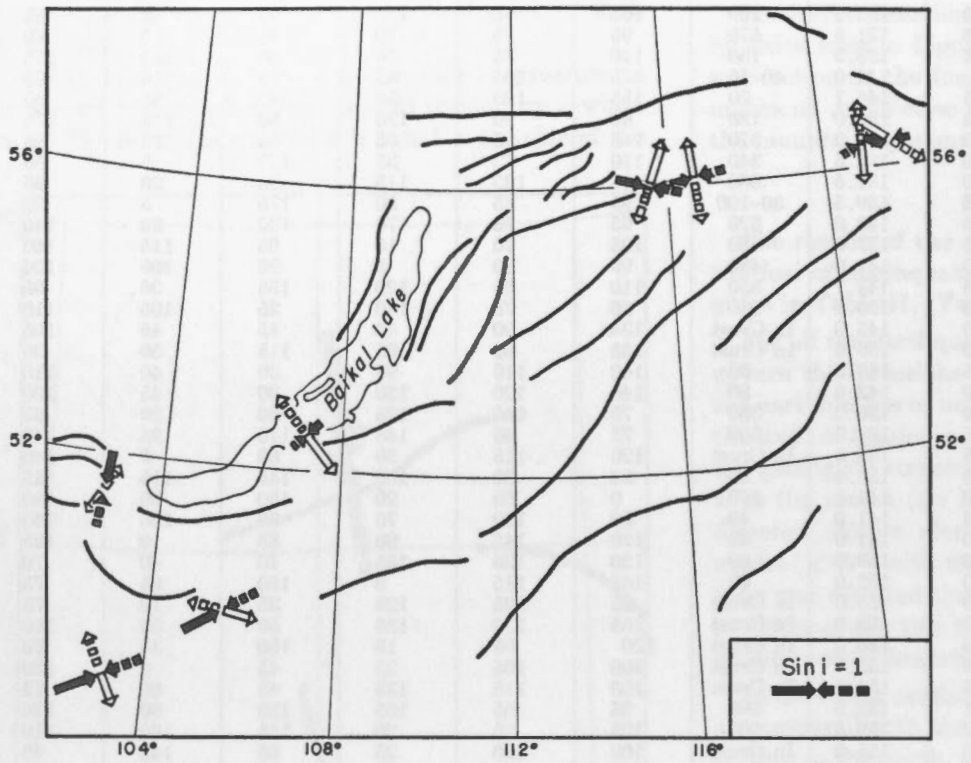

Figure 4. Pressure axes (black arrows) and tension axes (white arrows) for foci in Prebaikalye.

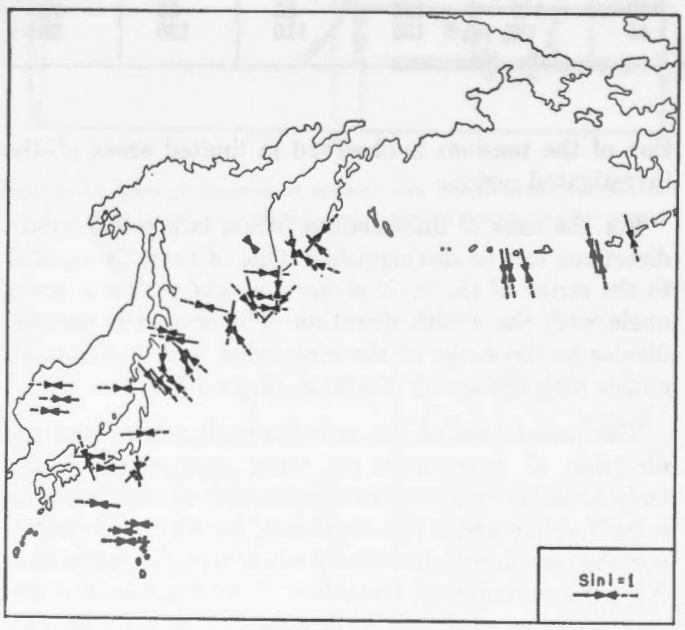

Figure 5. Pressure axes for foci in the northwest Pacific.

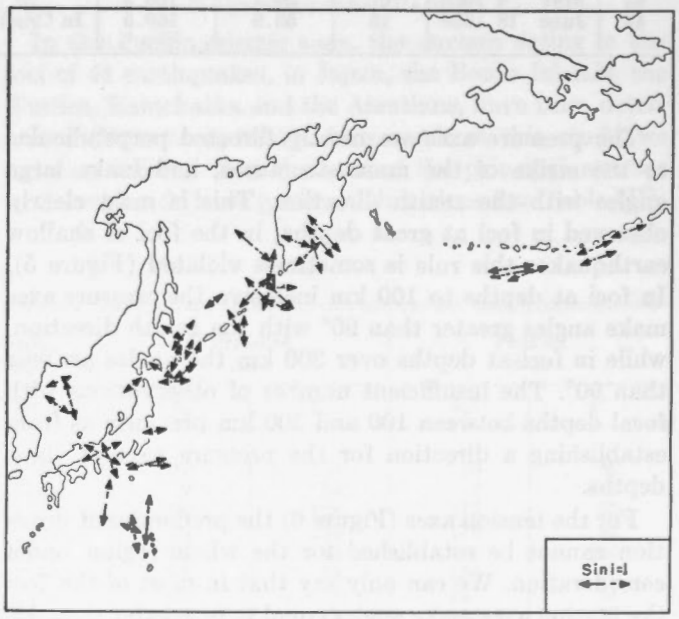

Figure 6. Tension axes for foci in the northwest Pacific.

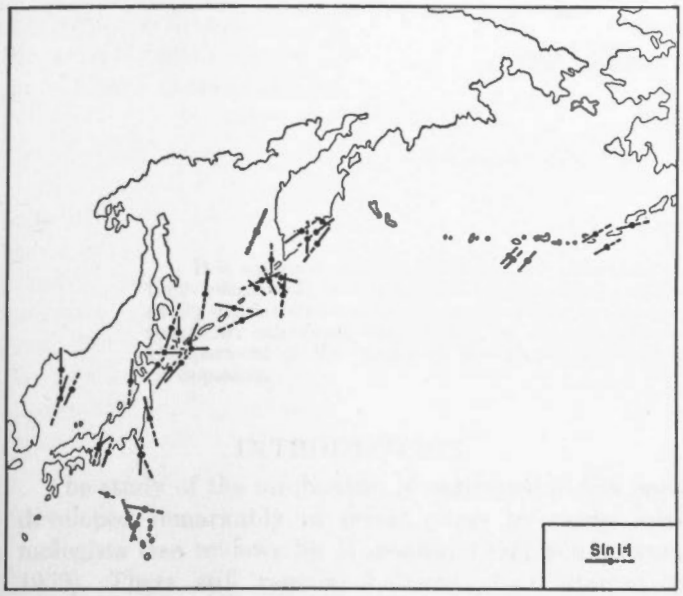

Figure 7. Axes of intermediate stress for foci in the northwest Pacific.

References

Balakina, L. M., 1959. The distribution of stresses effective in earthquake foci in the northwestern Pacific: *Akad. Nauk SSSR Izv.* ser. Geofiz., **11**, 1599; in the English edition, *Am. Geophys. Union*, 1131.

Nabarro, F. R. N., 1951. The synthesis of elastic dislocation fields *Phil. Mag.*, **42**, no. 334, 1224.

Shirokova, H. I., 1959. Determination of the stresses effective in the foci of the Hindu Kush earthquakes: *Akad. Nauk SSSR Izv.* ser. Geofiz., **12**, 1739; in the English edition, *Am. Geophys Union*, 1223.

Vvedenskaya, A. V., 1956. The determination of displacement fields by means of dislocation theory: *Akad. Nauk SSSR Izv.* ser. Geofiz., **3**, 277.

———— 1959. The displacement field associated with discontinuities in an elastic medium: *Akad. Nauk SSSR Izv.* ser. Geofiz., **4**, 516; in the English edition, *Am. Geophys. Union*, 357.

———— 1960. The determination of stresses acting in earthquake foci from observations at seismic stations: *Akad. Nauk SSSR Izv.* ser. Geofiz., **4**, 513; in the English edition, *Am. Geophys. Union.*, 341.

Vvedenskaya, A. V. and Balakina, L. M., 1960. Method and results of determination of the stresses acting in earthquake foci of Prebaikalye and Mongolia. *Akad. Nauk SSSR* Byull. Soveta Seysmol. no. 10.

The Generation of Seismic Waves

H. HONDA

Geophysical Institute, Faculty of Science, Tokyo University

ABSTRACT

It is assumed that an earthquake is caused by the release of deviatoric stresses, and further that the effects of their release will be represented by the radial and transverse impulsive forces acting on the surface of a spherical cavity constructed around the source of the earthquake. The motions of the P and S waves at large distances from the source are calculated theoretically, in the case when the patterns of the first motions of the waves are quadrantal. Comparisons of the results of the calculations with those of the observations are made for some deep Japanese earthquakes.

INTRODUCTION

The study of the mechanism of earthquakes has been developed remarkably in recent years by many seismologists (see reviews by HODGSON, 1957; SCHÄFFNER, 1959). There still remain, however, two alternative assumptions on the earthquake mechanism, one of them being represented by the force system of type I, i.e. a single couple with moment, and the other by the force system of type II, i.e. a pair of coplanar couples with moment or a pair of compressive stress and tension of equal magnitude acting at right angles to one another. The distinction between the two assumptions can be recognized from the study of the S waves, and it has been shown that the force system of type II represents the mechanism in the foci of many earthquakes which have occurred in and near Japan (HONDA, 1957). Recently, BYERLY and STAUDER (1958) showed that the pattern of the first motions of the S waves of the earthquake which occurred off the coast of northern California on July 6, 1934, indicates a quadrantal distribution such as would be expected for the force system of type II. ICHIKAWA (1959) also proved that similar relations hold for the S waves of the deep earthquake off the southern coast of central Japan on October 26, 1952. In the investigation of long-period Love waves, AKI (1960 a, b) found some facts which can be well explained by postulating a force system of type II for the earthquake source.

In the present paper, the author intends to assume an earthquake mechanism equivalent to the mechanism of type II, to investigate the nature of the P and S waves which are generated from the focus and to give some examples for earthquakes to illustrate the agreement between observation and theory.

THEORIES

TWO-DIMENSIONAL CASE

For the sake of simplicity, we shall first treat the problem in two dimensions, although the actual earthquake phenomena may not be represented in this simple way.

Let the x_1 and y_1 axes be the principal axes of stress, making the angle $\pi/4$ with the x and y axes, and σ_1 and σ_2 the principal stresses, and assume that $0>\sigma_1>\sigma_2$, σ_1 and σ_2 being both pressures (Figure 1).

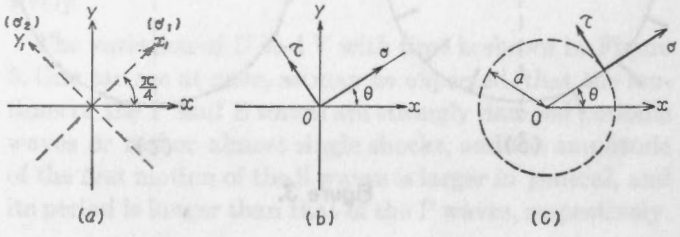

Figure 1. (a), (b), (c).

The normal and tangential stresses σ and τ across a plane whose normal is inclined at θ to the x-axis, are

$$\sigma = \tfrac{1}{2}(\sigma_1 + \sigma_2) + \tfrac{1}{2}(\sigma_1 - \sigma_2)\sin 2\theta$$
$$\tau = \tfrac{1}{2}(\sigma_1 - \sigma_2)\cos 2\theta \qquad (1)$$

where $(\sigma_1 - \sigma_2)>0$. In these expressions $\frac{1}{2}(\sigma_1 + \sigma_2)$ is the hydrostatic pressure and $\frac{1}{2}(\sigma_1 - \sigma_2)$ and $-\frac{1}{2}(\sigma_1 - \sigma_2)$ are the principal deviatoric stresses. The hydrostatic pressure does not generally cause appreciable yield in the rocks, and it is usual to assume that only the deviatoric stresses produce yield (JAEGER, 1956). The stresses which play a principal part in an earthquake and are released by the earthquake may be considered to be the deviatoric stresses. The direction of the stresses is assumed to be uniform throughout a certain region around the origin, and is illustrated in Figures 2 and 3.

We may assume that, when the deviatoric stresses near the origin exceed a certain limit, some faults, fractures or collapses suddenly occur. We shall assume that these occur within a distance a of the origin, but we shall not concern ourselves with the nature of the actual failure. We shall simply assume that the failure results in the release of the deviatoric stresses. We shall assume

96705-9—3

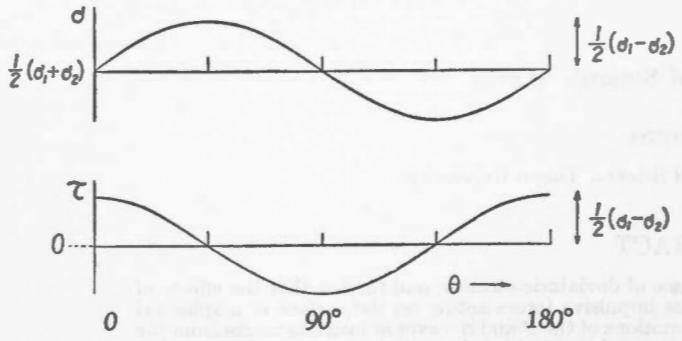

Figure 2.

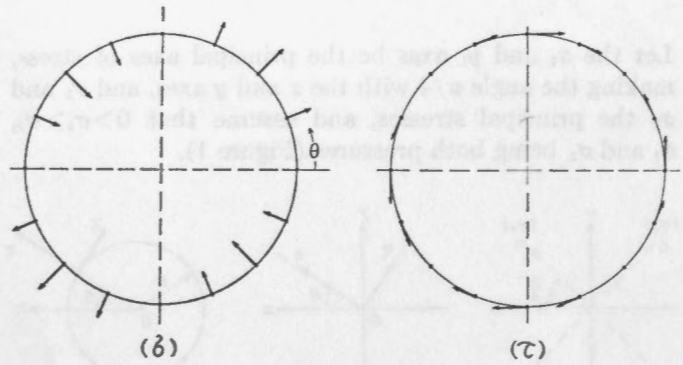

Figure 3.

further that the effect of the release of these stresses is equivalent to that of normal and tangential forces $F \sin 2\theta \cdot f(t)$ and $F \cos 2\theta \cdot f(t)$, acting on the inner surface of a cylindrical cavity of radius a constructed around the origin. $f(t)$ is a function which varies impulsively with time t, and $F = \frac{1}{2}(\sigma_1 - \sigma_2)$. The mechanism assumed in this way may be represented by following relations:

$$\left.\begin{aligned}(\widehat{rr})_{r=a} &= -F \sin 2\theta \cdot f(t),\\ (\widehat{r\theta})_{r=a} &= -F \cos 2\theta \cdot f(t).\end{aligned}\right\} \qquad (2)$$

The importance of the sudden release of the deviatoric stresses as the cause of earthquakes has been pointed out, for instance, by Byerly and Stauder (1958).

Three-Dimensional Case

Now we shall treat the problem in three dimensions. Let the x_1 and y_1 axes make the angle $\pi/4$ with the x and y axes respectively, and the z_1 axis coincide with the z axis, and the x_1, y_1, z_1 axes be the principal axes of stresses and F_1, F_2, F_3 the deviatoric stresses, where $F_1 + F_2 + F_3 = 0$. It is generally thought that fracture would occur along either or both of the planes which pass through the axis of the intermediate deviatoric principal stress and bisect the angle between the greatest and smallest stresses, when the maximum shear stress reaches a limiting value. In practice, however, the angle between the plane of fracture and the direction of the maximum pressure is usually considered to be less than 45°, due to the effects of the resistance to the shear fracture (Anderson, 1951; Jeffreys, 1959; Jacobs *et al.*, 1959). In the present paper, as in the foregoing section we ignore the details of the yielding, and consider only the effects of the release of the deviatoric stresses at somewhat large distances from the focus.

We take the y axis as the polar axis and represent the spherical coordinates by r, θ, φ (Figure 4).

The relation between the cartesian and polar axes is given in Table I.

The normal and tangential components σ, τ_θ and τ_φ of the deviatoric stresses acting on the plane whose normal is directed to (θ, φ), can be expressed by

$$\left.\begin{aligned}\sigma &= l_1^2F_1 + m_1^2F_2 + n_1^2F_3,\\ \tau_\theta &= l_1l_2F_1 + m_1m_2F_2 + n_1n_2F_3,\\ \tau_\varphi &= l_3l_1F_1 + m_3m_1F_2 + n_3n_1F_3.\end{aligned}\right\} \qquad (3)$$

When we assume that

$$F_1 = F,\ F_2 = -F,\ F_3 = 0,\ (F > 0) \qquad (4)$$

Table I

	x_1	y_1	z_1
r	$l_1 = \frac{1}{\sqrt{2}} \sin\theta \cos\varphi + \frac{1}{\sqrt{2}} \cos\theta$	$m_1 = -\frac{1}{\sqrt{2}} \sin\theta \cos\varphi + \frac{1}{\sqrt{2}} \cos\theta$	$n_1 = -\sin\theta \sin\varphi$
θ	$l_2 = \frac{1}{\sqrt{2}} \cos\theta \cos\varphi - \frac{1}{\sqrt{2}} \sin\theta$	$m_2 = -\frac{1}{\sqrt{2}} \cos\theta \cos\varphi - \frac{1}{\sqrt{2}} \sin\theta$	$n_2 = -\cos\theta \sin\varphi$
φ	$l_3 = -\frac{1}{\sqrt{2}} \sin\varphi$	$m_3 = \frac{1}{\sqrt{2}} \sin\varphi$	$n_3 = -\cos\varphi$

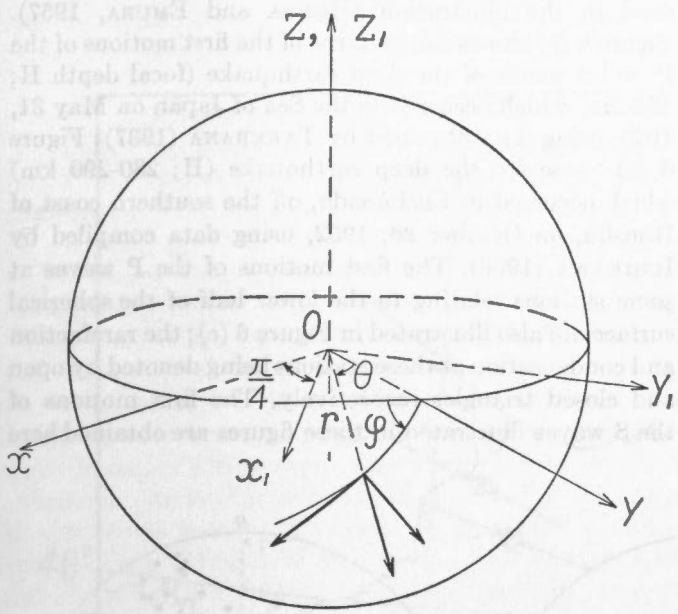

Figure 4.

(3) becomes as following

$$\left.\begin{aligned} \sigma &= F \sin 2\theta \cos \varphi , \\ \tau_\theta &= F \cos 2\theta \cos \varphi , \\ \tau_\varphi &= -F \cos \theta \sin \varphi . \end{aligned}\right\} \qquad (5)$$

Following the same arguments as in the two-dimensional problem, the mathematical relations representing the mechanism at the focus in three dimensions in this case, may be expressed as follows

$$\left.\begin{aligned} (\widehat{rr})_{r=a} &= -F \sin 2\theta \cos \varphi \cdot f(t), \\ (\widehat{r\theta})_{r=a} &= -F \cos 2\theta \cos \varphi \cdot f(t), \\ (\widehat{r\varphi})_{r=a} &= F \cos \theta \sin \varphi \cdot f(t). \end{aligned}\right\} \qquad (6)$$

The x_1 and y_1 axes in this case correspond to the author's directions of the 'maximum tension' and 'maximum pressure' in the theories of the earthquake mechanism, respectively (HONDA, 1957). The assumption may be considered to represent at least one of the most probable mechanisms of earthquakes, as may be seen from the fact that the patterns of the first motions of the P waves of most earthquakes have been shown generally to be quadrantal, in agreement with the results which will be derived from our present assumption.*

Let us assume that

$$f(t) = 1 \text{ for } t>0, \text{ and } f(t) = 0 \text{ for } t<0, \qquad (7)$$

and examine the displacements, at large distances from the source, which are generated by the step function source represented by (6) and (7). The radial component $\delta_{p,r}$ of the P waves and the transverse components $\delta_{s,\theta}$ and $\delta_{s,\varphi}$ of the S waves are given by the following expressions (HONDA, 1959):

$$\left.\begin{aligned} \delta_{p,r} &= U \frac{a^2 F}{r\mu} \sin 2\theta \cos \varphi , \\ \delta_{s,\theta} &= V \frac{a^2 F}{r\mu} \cos 2\theta \cos \varphi , \\ \delta_{s,\varphi} &= -V \frac{a^2 F}{r\mu} \cos \theta \sin \varphi , \end{aligned}\right\} \qquad (8)$$

where μ is the rigidity. When the reciprocals of the velocities of the P and S waves are denoted by c_1 and c_2, U and V vary with $t - c_1(r-a)$ and $t - c_2(r-a)$ respectively.

The variation of U and V with time is shown in Figure 5. One can see at once, as may be expected, that the motions of the P and S waves are strongly damped periodic waves or rather almost single shocks, and the amplitude of the first motion of the S waves is larger in general, and its period is longer than that of the P waves, respectively.

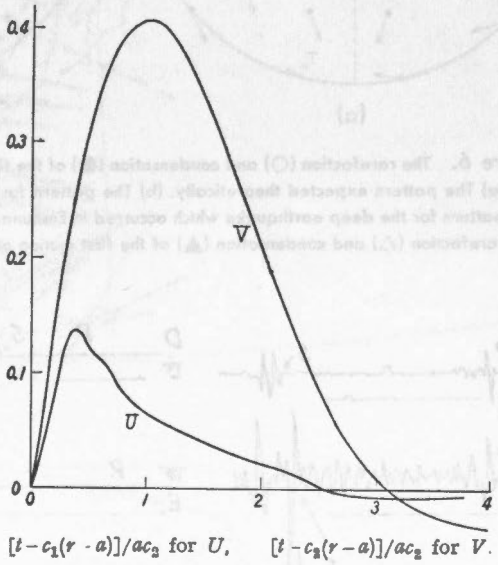

Figure 5. U and V.

Expressions quite similar to (8) with respect to (θ, φ), have been obtained from the assumption of the force system of type II, and have been used by us as the fundamental expressions which denote the patterns of the first motions of the P and S waves (HONDA, 1957).

* It may be mentioned here that when we assume the relations $F_1=F_2=-F$, $F_3=2F$, $(F \gtrless 0)$ in place of (4), then the conical surfaces constructed around the z axis with the vertex at the origin will become the nodal surfaces of the P waves. (*see* e. g. KAWASUMI, 1937).

ILLUSTRATIONS

As an example illustrating our theories, the patterns of the rarefaction and condensation of the first motions of the P waves and the directions of those of the S waves, expected theoretically on a spherical surface, whose radius is much larger than a, are shown in Figure 6 (a), when the axes of the model sphere ($r = a$) are oriented in certain directions, i.e. one of the nodal planes is inclined 30° in the direction N48°W, and the other one 25° in S27°W. Open and closed circles show the rarefaction and condensation of the first motion of the P waves, and the arrow the direction of the first motion of the S waves. The upper half of the spherical surface is shown in the figure, the chart of equal area projection being used in the illustration (HONDA and EMURA, 1957). Figure 6 (b) shows the patterns of the first motions of the P and S waves of the deep earthquake (focal depth H; 450 km) which occurred in the Sea of Japan on May 31, 1935, using data obtained by TAKEHANA (1937); Figure 6 (c) those for the deep earthquake (H; 280-290 km) which occurred in Enshunada, off the southern coast of Honshu, on October 26, 1952, using data compiled by ICHIKAWA (1959). The first motions of the P waves at some stations relating to the lower half of the spherical surface are also illustrated in Figure 6 (c); the rarefaction and condensation at these stations being denoted by open and closed triangles respectively. The first motions of the S waves illustrated in these figures are obtained here

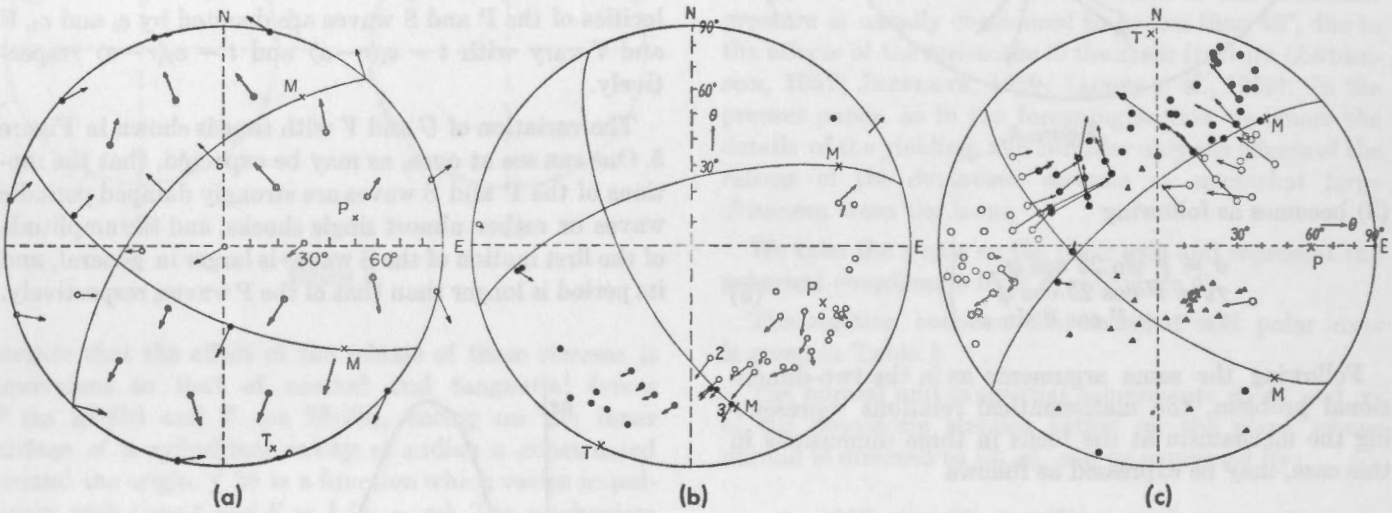

Figure 6. The rarefaction (○) and condensation (●) of the first motion of the P waves, and the direction (←) of that of the S waves, (upper half sphere). (a) The pattern expected theoretically. (b) The pattern for the deep earthquake of the Sea of Japan, May 31, 1935. Focal depth H: 450 km. (c) The pattern for the deep earthquake which occurred in Enshunada, off the southern coast of Honshu, on Oct. 26, 1952. The focal depth H: 280-290 km. The rarefaction (△) and condensation (▲) of the first motion of the P waves relate especially to the lower half sphere.

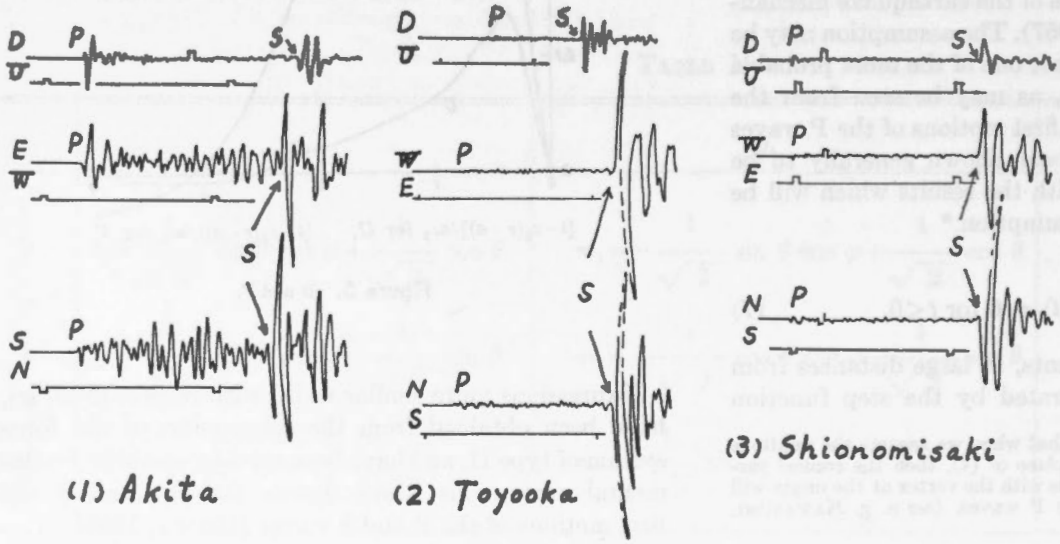

Figure 7. The seismograms of the deep earthquake of the Sea of Japan, May 31, 1935.

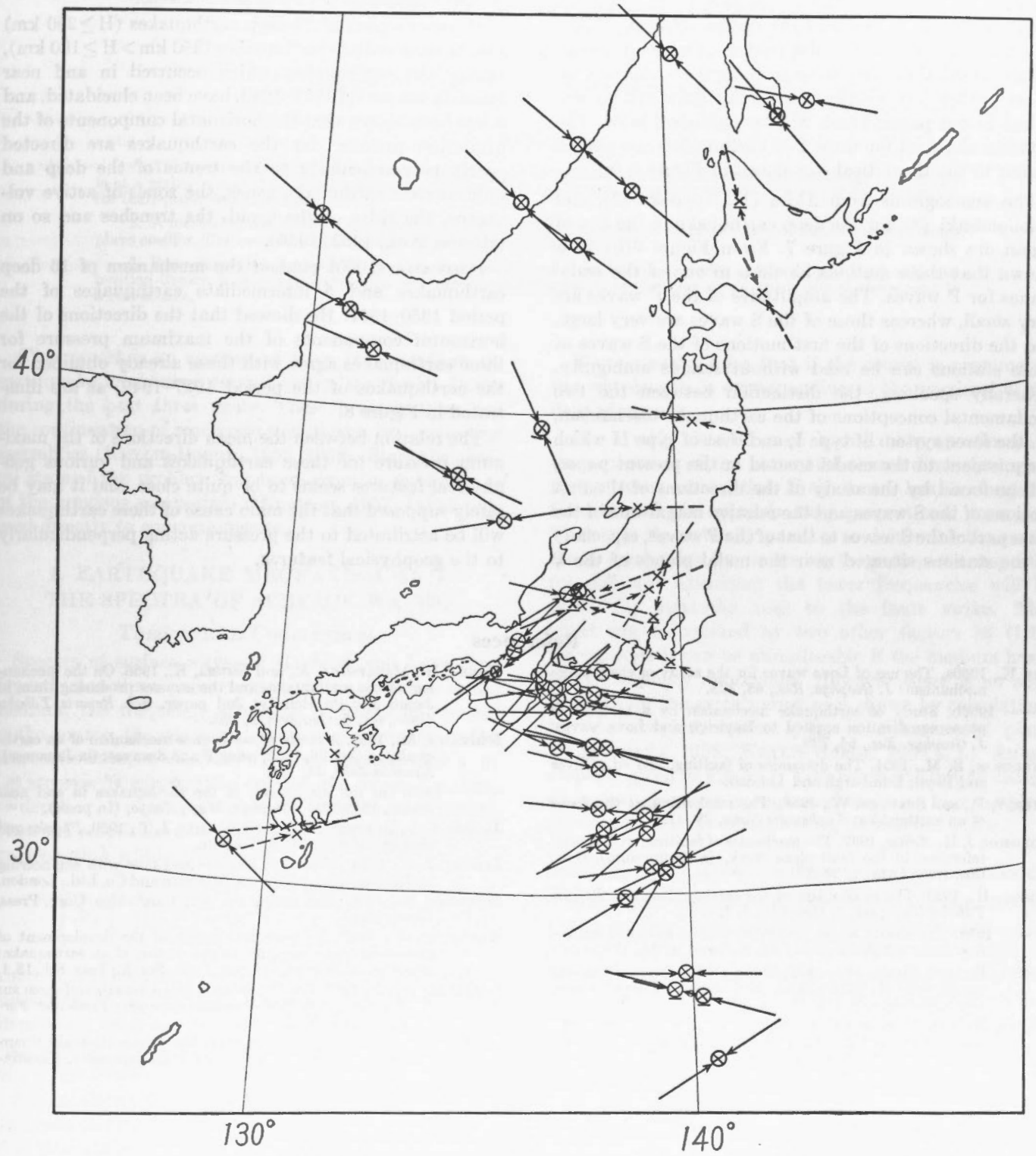

Figure 8. The direction of the horizontal components of the maximum pressure in Japan and adjacent areas. ⊕ deep earthquake; x intermediate earthquake, 1927-1949, (Honda et al., 1952, 1956). ⊕ deep earthquake; x intermediate earthquake, 1950-1957, (Ichikawa, 1960).

only approximately, by dividing the observed horizontal component of the S waves for each station, by the distance factor f, a factor which is related to the distance between the hypocenter and the station (HONDA, 1957), in order to reduce all the observed motions to the same distance from the source so as to make them comparable to each other. The details of these examples will be described in our paper which will be published later. The patterns obtained for these two earthquakes are almost similar to the theoretical one shown in Figure 6 (a).

The seismograms from Akita (1), Toyooka (2), and Shionomisaki (3), for the deep earthquake in the Sea of Japan are shown in Figure 7. From Figure 6(b) it is known that these stations lie close to one of the nodal planes for P waves. The amplitudes of the P waves are very small, whereas those of the S waves are very large, and the directions of the first motions of the S waves at these stations can be read without serious ambiguity. Generally speaking, the distinction between the two fundamental conceptions of the earthquake mechanism, i.e. the force system of type I, and that of type II which is equivalent to the model treated in the present paper, will be found by the study of the directions of the first motions of the S waves and the relative magnitude of the main part of the S waves to that of the P waves, especially at the stations situated near the nodal planes of the P waves. It is generally difficult to identify the first motions of the S waves at the stations near the middle azimuths between the nodal planes of the P waves.

The mechanism of 34 deep earthquakes ($H \geq 250$ km) and 10 intermediate earthquakes ($250 \text{ km} > H \geq 100$ km), among the earthquakes which occurred in and near Japan in the period 1927–1949, have been elucidated, and it has been shown that the horizontal components of the maximum pressure for the earthquakes are directed nearly perpendicularly to the trends of the deep and intermediate earthquake zones, the zones of active volcanoes, the ridge of the geoid, the trenches and so on (HONDA *et al.*, 1952, 1956).

ICHIKAWA (1960) studied the mechanism of 16 deep earthquakes and 5 intermediate earthquakes of the period 1950–1957. He showed that the directions of the horizontal components of the maximum pressure for these earthquakes agree with those already obtained for the earthquakes of the period 1927–1949, as are illustrated in Figure 8.

The relation between the mean directions of the maximum pressure for these earthquakes and various geophysical features seems to be quite close, and it may be safely supposed that the main cause of these earthquakes will be attributed to the pressure acting perpendicularly to the geophysical features.

References

AKI, K., 1960a. The use of Love waves for the study of earthquake mechanism: *J. Geophys. Res.*, **65**, 323.

——— 1960b. Study of earthquake mechanism by a method of phase equalization applied to Rayleigh and Love waves: *J. Geophys. Res.*, **65**, 729.

ANDERSON, E. M., 1951. The dynamics of faulting, 2nd ed.: Oliver and Boyd, Edinburgh and London.

BYERLY, P., and STAUDER, W., 1958. The mechanism at the focus of an earthquake: *Earthquake Notes*, **29**, 17.

HODGSON, J. H., *Editor*, 1957. The mechanics of faulting, with special reference to the fault-plane work, (a Symposium), *Dom. Obs. Pub.*, Ottawa, **20**, 251.

HONDA, H., 1957. The mechanism of the earthquakes: *Sci. Reports Tôhoku Univ.*, ser. 5, Geophys. **9**, 1.

——— 1959. The elastic waves generated from a spherical source: *Sci. Reports Tôhoku Univ.*, ser. 5, Geophys. **11**, 178.

HONDA, H., and EMURA, K., 1957. Some charts for studying the mechanism of earthquakes: *Sci. Reports Tôhoku Univ.*, ser. 5, Geophys. **9**, 113.

HONDA, H., and MASATSUKA, A., 1952. On the mechanism of the earthquakes and the stresses producing them in Japan and its vicinity: *Sci. Reports Tôhoku Univ.*, ser. 5, Geophys. **4**, 42.

HONDA, H., MASATSUKA, A., and EMURA, K., 1956. On the mechanism of the earthquakes and the stresses producing them in Japan and its vicinity: 2nd paper, *Sci. Reports Tôhoku Univ.*, ser. 5, Geophys. **8**, 186.

ICHIKAWA, M., 1959. A study of occurrence mechanism of an earthquake on Oct. 26, 1952, using P and S waves: (in Japanese), *Kenshin-Ziho*, **23**, 135.

——— 1960. On the mechanism of the earthquakes in and near Japan, 1950-1957: *Geophys. Mag., Tokyo*, (In press).

JACOBS, J. A., RUSSELL, R. D., and WILSON, J. T., 1959. *Physics and Geology*: McGraw-Hill, Toronto.

JAEGER, J. C., 1956. Elasticity, fracture and flow with engineering and geological applications: Methuen and Co. Ltd., London.

JEFFREYS, H., 1959. The earth, 4th ed.: Cambridge Univ. Press, Cambridge.

KAWASUMI, H., 1937. An historical sketch of the development of knowledge concerning the initial motion of an earthquake: *Bur. Central Seismol. Internat. Pubs.*, Ser. A., Trav. Sci., **15**, 1.

SCHÄFFNER, H. J., 1959. Die Grundlagen und Auswerteverfahren zur Bestimmung von Erdbebenmechanismen: *Freiberger Forschung.*, C. 63, Berlin.

TAKEHANA, M., 1937. The mechanism of the deep earthquake occurred in Japan Sea on May 31, 1935: (in Japanese), *Kenshin-Ziho*, **9**, 253.

Some New Investigations of Earthquake Mechanism

V. I. KEYLIS-BOROK

Geophysical Institute, U.S.S.R. Academy of Sciences, Moscow

ABSTRACT

1. Theory predicts that, in azimuths coinciding with the fault strike, the maximum in the surface-wave spectrum is at a higher period than in perpendicular azimuths. This can be used, together with body waves or independently, for fault-plane determinations.

2. A method is considered which permits one to investigate the selectivity of a system of stations used in fault-plane studies. The method also simplifies subsequent interpretation.

3. Some simplified methods to obtain a source model are investigated. A model, obtained by analogy with dislocation theory, is shown to correspond to a peculiar distribution of pre-faulting stress which cannot correspond to a real source.

This report is an account of some investigations on earthquake mechanism carried out in the Soviet Union during the past three years. These investigations are the continuation of work reported at the two preceding assemblies (KEYLIS-BOROK, 1956, 1959). Since the general state of the problem has been given in publications of the previous symposium (HODGSON, 1957) I shall proceed directly to concrete results.

1. EARTHQUAKE MECHANISM AND THE SPECTRA OF SURFACE WAVES.

THEORETICAL CONCLUSIONS

Spectra of surface waves of Rayleigh and Love type depend upon three main factors: the constitution of the medium, the frequency spectrum of forces or stresses in the source, the space distribution of intensity in the source (EWING, *et al.*, 1957; KELYIS-BOROK, 1960 a, b) Let stresses $f(t)\varphi(r, \alpha, f)$ be applied in a source (t = time, z = depth, r, α = polar coordinates in horizontal plane). Then the amplitude of surface waves of frequency p and wavelength λ will be proportional to

$$\int M_\varphi\left(\frac{\lambda}{H}, z\right) Q(p)\, \Phi\left(\frac{\lambda}{D}, \alpha, z\right) \ldots\ldots (1.1)$$

where H is thickness of layers, D is a linear dimension of the source, M_φ is the frequency response of the medium (depending upon source depth and different for Rayleigh and Love waves), $Q(p)$ is the Fourier transform of $f(t)$, Φ is a Bessel-Fourier transform of φ.

A more detailed consideration of the problem is given elsewhere (KEYLIS-BOROK, 1960 a, b). It can be seen from (1.1) that surface-wave amplitudes are proportional not to the integral intensity of the source but only to the component of its space Fourier transform with the wavelength the same as of a surface wave.

We can easily infer that if the source is asymmetric the wavelength λ_r corresponding to the maximal Φ will depend upon α.

For a wide class of cases λ_r will be proportional to the projection of the horizontal source dimension upon the epicentre-station line. If the source has an elongated form then λ_r is approximately proportional to $\cos \alpha$. Thus it is theoretically possible to determine the earthquake mechanism by measuring the surface-wave spectra for different azimuths; the lower frequencies will be found for azimuths near to the fault strike. This effect can be masked by two other factors in (1.1); for example it can be unnoticeable if the medium has a sharp frequency reasonance. However there is no such masking for the earth's crust as is shown by calculations for the simplest source lying in a horizontal plane (IANOVSKAYA 1958; KEYLIS-BOROK 1960 a, b). An example is given in Figure 1. This result will not be changed in analysing more complicated sources—for example if the sources are distributed along an inclined plane.

SOME CONSIDERATIONS ON PRACTICAL INTERPRETATION

It is known (EWING *et al.* 1957, KEYLIS-BOROK 1960a), that a surface wave consists of two phases: one—preliminary—is represented by oscillations with a continuously changing period; another—adjacent to the Airy phase—is represented by beatings with constant periods which depend only on the constitution of the medium and corresponds to extrema of group velocity.

The earth's crust usually has several possible periods (corresponding to a resonance with different layers) for the Airy phase. However in fact only some of these periods are realized.

The change with azimuth of λ_r will lead to the following observations if the azimuth of an observational point approximates to the fault strike:

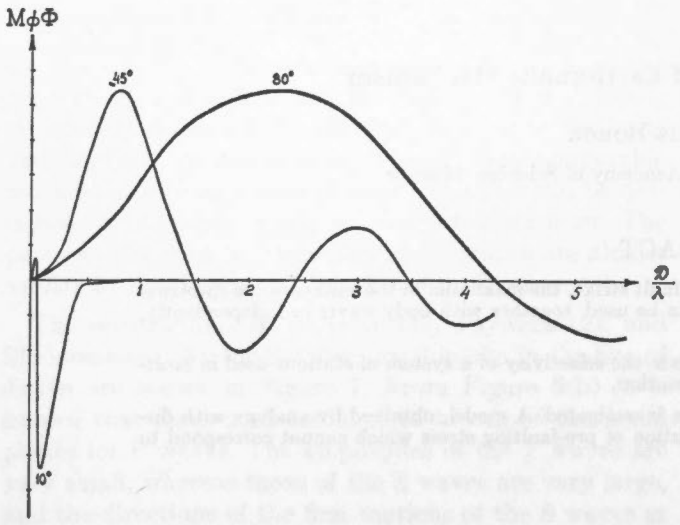

Figure 1. Dependance of maximum of Rayleigh wave spectra (vertical component) an angle α between the strike of the source and direction to station. Elongated (10:1) source. D-length of source, λ-wave-length. For details see Keylis-Borok (1960 a, b).

a. In the preliminary phase the predominant period will be continuously increasing.

b. Near the Airy phase the period can increase discontinuously (if one of the Airy phases are observed simultaneously).

c. The relative intensity of waves near the Airy phase with larger period will be continuously increasing (if several of the Airy phases are observed simultaneously).

If we succeed in finding these changes in practice they may easily be used to study the earthquake mechanism, independently of the use of body waves. The corresponding practical procedure is obvious. However it is necessary to take account of the variation of spectrum to be expected from peculiarities in crustal constitution in various azimuths.

2. AN ANALYSIS OF OBSERVATIONAL SYSTEMS.

The main problem in studying earthquake mechanism is to distinguish the general properties of faults in a region to be studied. However, if the number of stations is limited, the determination of faults with some particular orientation turns out to be impossible.

Consider for example the extreme case when all virtual points of observation (the stereographic projections of the straightened rays) are situated near each other in a single direction from an epicentre. Then it will be possible to obtain unambiguous fault-plane solutions only for earthquakes with nodal lines passing between the virtual points. As a result all the sources studied in the region will have the same fault strike. However this must be explained by the fact that it is impossible to study other sources, not by the actual predominance of this strike. In this case it is worth while to study the earthquake mechanism only if a very exceptional problem is stated—to examine whether there are any earthquake sources with that particular strike in the region.

Obviously there is no point in beginning to study the earthquake mechanism in a particular region (nor in general to make any mass interpretation of observations) without a preliminary analysis of the selectivity of the available observational system. The necessity of such analysis was indicated by J. H. Hodgson at the Toronto meetings of the U.G.G.I.

The method of analysis is simple, though it requires a good deal of work. It consists of the following operations.

a. Virtual points corresponding to waves recognized at each station are plotted on a Wulff projection for a typical epicentral location.

b. A set of variants of fault-plane orientation ($y=0$) and motion direction ($x=0$) is given so that the complete range of possible fault-plane solutions is computed (azimuths of fault dip varying from 0° to 360°; for each dip azimuth the dip angles varying from 0° to 90°; for each combination of dip and strike the angles between the dip line and the motion direction varying from $-90°$ to $+ 90°$).

c. For each variant nodal lines are drawn (see Bessonova, *et al.*, 1957) and the theoretical signs of waves to be used at the virtual point are determined. Then the unambiguity and accuracy of solution of the inverse problem is examined; i.e. the possibility of determining the nodal lines with the given sign distribution is appraised.

Practically, the signs of displacements for different variants are compared first to determine whether the same sign distribution corresponds to several variants. Then it is necessary to determine how much the nodal lines can be displaced consistent with given signs of displacements in the virtual points. If this displacement of nodal lines is within the admissible error (usually $\pm$ 10° to 15°) then the considered variant can be determined using the given observational system.

d. It is convenient to represent the considered variants in the usual notation on a Wulff projection (see Bessonova *et al.*, 1957). An example is given in Figure 2. Variants which can and cannot be determined are plotted by solid and dashed lines respectively. Three possible motion directions are given for each fault plane. Inversion of this direction does not change the result. Quite similarly cases are considered when amplitudes of displacement are used as well as their sign, or when more complicated source models are considered, etc.

This method seems to take much time. However this is compensated for by the further simplification of the most complicated part of the interpretation—the drawing of the nodal lines.

In fact, as a result of operations *a* to *c* the set of all possible variants is obtained; for each variant we have nodal lines and signs of displacements in P, SH and SV waves in virtual points. If a real earthquake is studied, the drawing of the nodal lines will be reduced to the choice of variants with signs coinciding to the observed ones. Thus, from this part of the interpretation, which has been the least formalized up till now, the element of art is excluded.

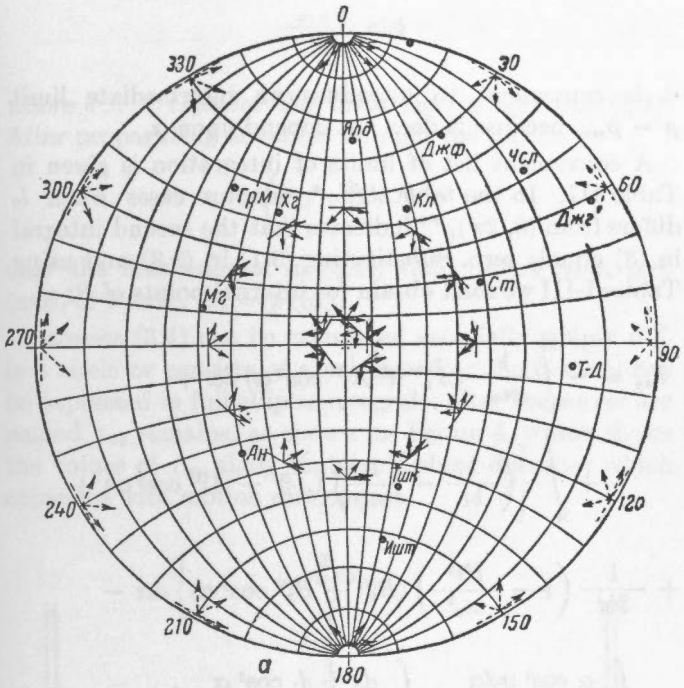

Figure 2. Example of analysis of the system of stations. Solid and dashed line—fault-plane solutions, which can and cannot be determined. Heavy points are stereographic projections of stations. For details see Bessonova et al., 1957; Pavlova, 1960.

3. ON ONE SIMPLIFIED METHOD OF OBTAINING THE MODEL OF AN EARTHQUAKE SOURCE.

Three factors must be considered in the theoretical treatment of the generation of waves from the source: non-ideal elasticity in the zone of crushing and large displacements near the source; diffraction of waves at the fault plane; conditions of fault formation (friction, speed of fault expansion, etc.).

At the present time it is difficult to allow for non elastic displacements. In terms of ideal elasticity the problem of waves generated at the source may be stated as follows (see STARR, 1928). The field of initial stress is given. At some moment shear stress at a given boundary—a fault plane—begins to vanish according to some time law; simultaneously the given boundary may expand. The problem is to find the elastic waves generated, and then to construct an equivalent source model.

One can consider the model in which the initial field is zero, and the initial moment the stresses or forces begin to act. The stresses on the fault plane in such a model must compensate those in the initial field.

Even the simplified elastic problem is very difficult. The question arises whether it is possible to construct and to base a source model more simply, by using the dislocation theory (*see* BALAKINA *et al.* this volume). The answer is as yet negative. However the analysis of the problem has some interest.

STRESSES

According to dislocation theory (more precisely, analogously to it, since this is a statical theory) a finite source can be constructed by integration of a point source —a double couple (Figure 3b)—along the fault surface S.

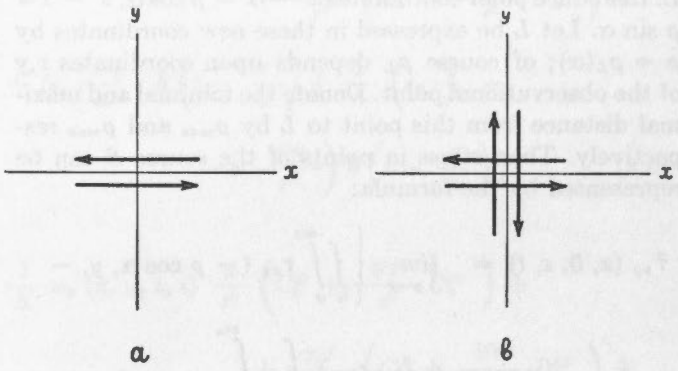

Figure 3. Single couple and double couple.

Let the intensity $K(t)$ of a point source be of the form $K(t) = 0$ for $t = 0$ and $K(t) = 4\pi\mu K$ for $t>0$, where K is a positive constant, t is time and μ is the shear modulus.

It is not essential for the final conclusions whether $K(t)$ reaches a final value instantly or not. For such $K(t)$ and the choice of axes as in Figure 3b we have, for a point source and for $t>r/a$:

$$\frac{1}{K}\,\tau_{xy}(x,y,t) = \frac{1}{r^3}\left(A_1^{(0)} + \frac{b^2t^2}{r^2}B_1^{(0)}\right) + \frac{x^2}{r^5}\left(A_2^{(0)} + \frac{b^2t^2}{r^2}B_2^{(0)}\right) + \frac{y^2}{r_5}\left(A_3^{(0)} + \frac{b^2t^2}{r^2}B_3^{(0)}\right) + \frac{x^2y^2}{r^7}\left(A_4^{(0)} + \frac{b^2t^2}{r^2}B_4^{(0)}\right) + \frac{f}{a}\left(\frac{c_1x^2}{r^4} + \frac{c_1y^2}{r^4} + \frac{c_2^2x^2y^2}{r^6}\right)\delta\left(t - \frac{r}{a}\right) + fc_3\,\frac{x^2y}{a^2r^5}\,\delta'\left(t + \frac{r}{a}\right) + \frac{1}{b}\left(\frac{d_0}{r^2} + \frac{d_1x^2}{r^4} + \frac{d_2y^2}{r^4} + \frac{d_3x^2y^2}{r^6}\right)\delta\left(t - \frac{r}{b}\right) + \frac{1}{b^2}\left(\frac{d_4x^2}{r^2} + \frac{d_5y^2}{r^3} + \frac{d_6x^2y^2}{r^5}\right)\delta'\left(t - \frac{r}{b}\right); \quad (3.1)$$

here a and b are P and S wave velocities,

$$r = \sqrt{x^2 + y^2 + z^2}$$

is the distance to the source, δ is the Dirak delta function, the constants $A_q^{(i)}$ $B_q^{(i)}$ c_q, d_q are given in Table I and in the first line of Table II, the subscripts $i = 1$ and $i = 2$ correspond to time intervals $r/a < t < r/b$ and $t > r/b$ (for $t < r/a$ of course $\tau_{xy} = 0$). All $B_q^{(2)} = 0$.

Proceed to consider a finite source S. Denote the stress aroused by it by $\tilde{\tau}_{xy}$. Obviously

$$_{xy}(x, y, z, t) = \int\int_S \tau_{xy}(x - x', y - y', z - z', t)\, ds, \quad (3.2)$$

where τ_{xy} is determined by 3.1. Let S be in the plane $y = 0$ and bounded by an arbitrary smooth contour L. Introduce polar coordinates $x' - x = \rho \cos\alpha$, $z' - z = \rho \sin\alpha$. Let L be expressed in these new coordinates by $\rho = \rho_L(\alpha)$; of course ρ_L depends upon coordinates x,y of the observational point. Denote the minimal and maximal distance from this point to L by ρ_{min} and ρ_{max} respectively. Then stress in points of the source S can be represented by the formula:

$$\tilde{\tau}_{xy}(x, 0, z, t) = \lim_{y \to 0} \left\{ \int_{l_1} \int_0^{m_b} \tau_{xy}(-\rho\cos\alpha, y, -\rho\sin\alpha, t)\, \rho\alpha\rho d\alpha + \int_{l_2} \int_{\sqrt{b^2t^2 - y^2}}^{m_a} \tau_{xy}(-\rho\cos\alpha, y, -\rho\sin\alpha, t)\, \rho d\rho d\alpha \right\}, \quad (3.3)$$

where $m_v = \min[\rho(\alpha), \sqrt{v^2t^2 - y^2}\,]$, $v = a, b$.

In the first and the second integrals τ_{xy} is determined by formula (3.1) for $i = 1$ and $i = 2$ correspondingly; l_1 for internal points S is the interval $(0, 2\pi)$; for boundary points l_i evidently depends upon form of L and on the coordinates (x, z). l_2 is the set of all intervals of α, $0 < \alpha < 2\pi$, for which $\rho_L(\alpha) > bt$.

For time

$$t > \frac{\rho_{min}}{a}$$

it is convenient to introduce an intermediate limit $\rho = \rho_{min}$ because it does not depend upon α.

A convenient list of limits of integration is given in Table III. In the table sign * denotes cases when l_2 differs from $(0, 2\pi)$, ** indicates that the second integral in (3) equals zero. Substituting (3.1) in (3.3) and using Tables I-III we shall obtain for internal points of S:

$$\tilde{\tau}_{xy} = -\int_0^{2\pi} \frac{1}{m_b}(A_1^{(2)} + A_1^{(2)}\cos^2\alpha)\, d\alpha + \int_{l_2} \left\{ \left(\frac{1}{bt} - \frac{1}{m_a}\right)(A_1^{(1)} + A_1^{(1)}\cos^2\alpha) + \frac{1}{3bt}\left(1 - \frac{b^2t^2}{m_a^2}\right)(B_1^{(1)} + B_2^{(1)}\cos^2\alpha) \right\} d\alpha - \int_{n_a} \frac{c_1\cos^2\alpha d\alpha}{at} - \int_{n_b} \frac{d_0 + d_1\cos^2\alpha}{bt}\, d\alpha, \quad (3.4)$$

TABLE I

$A_1^{(1)} = A_1^{(2)}$	$B_1^{(1)}$	$A_2^{(1)} = A_2^{(1)}$	$B_2^{(1)} = B_2^{(1)}$	$A_4^{(1)}$	$B_4^{(1)}$	$A_4^{(2)}$	$c_1 = -c_2 = d_2$	$C_2 = -d_2$	d_0
$-2f$	6	$6f$	-30	$-30f$	210	$-30f + 30$	-4	40	-2

TABLE II

Source	$A_2^{(2)}$	$A_2^{(2)}$	d_1	d_2	d_4	d_5
Two dipoles	$6f - 3$	$6f - 3$	7	7	1	1
Dipole along x	$3f - 3$	$3f$	2	5	0	1
Dipole along y	$3f$	$3f - 3$	5	2	1	0
One and a half dipoles	$3f - 3$	$9f - 3$	$7 - 3f$	$7 + 3f$	$1 - f$	$1 + f$

where $n_v(v = a, b)$ is a part of a circle $\rho = vt$ inside S. Analysing the second integral it is useful to note that

$$A_1^{(1)} + \tfrac{1}{3} B_1^{(1)} = 0$$

At the source boundary

$$\tau_{xy} = \lim_{y \to 0} \int_{\alpha_1} \left\{ \frac{5A_2^{(2)} + A_1^{(2)}}{15y} - \frac{1}{m_b} (A_1^{(2)} + \right.$$

$$\left. + A_2^{(2)} \cos^2 \alpha) \right\} d\alpha + \ldots\ldots (3.5)$$

where ..... replaces the three last integrals in (3.4). After propagating of waves through the source

$$\left(t > \frac{\rho_{max}}{b} \right)$$

only the first integral in (3.4), (3.5) differs from zero (and, of course, $m_b = \rho_L(\alpha)$).

Stresses (3.4) can be calculated especially simply if L is a circle or consists of a polygon. For the circle it can be expressed in full elliptic integrals; after the waves are passed τ_{xy} remains, as shown on Figure 4, which shows the values of τ_{xy} along that fault-plane diameter which coincides with motion direction x.

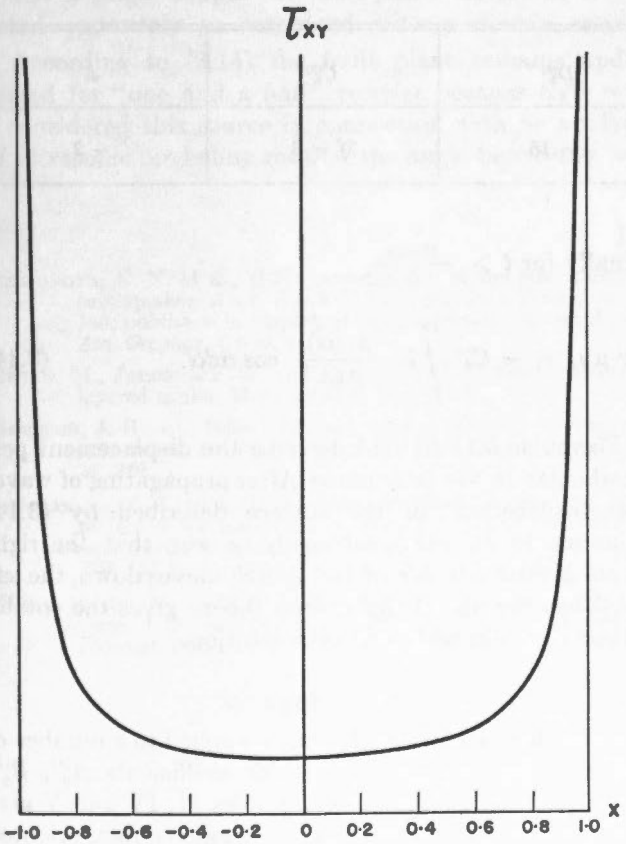

Figure 4. The stresses τ_{xy} corresponding to a source model obtained by integration of double couple along the circle of r=1.

The change of τ_{xy} in space (Figure 4) and in time determined by 3.4 is so peculiar inside S that there is little sense to take such a change as a real initial field before an earthquake.

Displacements

We shall also calculate the displacements of the fault surface S. Displacements produced by a double couple for the above mentioned choice of $K(t)$ have a form,

$$\text{for } t > \frac{r}{a}:$$

$$\frac{1}{K} u_x(x, y, z, t) = \frac{y}{r^3} \left(C_1^{(0)} + \frac{b^2 t^2}{r^2} D_1^{(0)} \right) +$$

$$+ \frac{x^2 y}{r^5} \left(C_2^{(0)} + \frac{b^2 t^2}{r^2} D_2^{(0)} \right) +$$

$$+ f e_1 \frac{x^2 y}{a r^4} \delta\left(t - \frac{r}{a}\right) + \frac{1}{b} \left(e_2 \frac{y}{r^2} - \right.$$

$$\left. - e_1 \frac{x^2 y}{r^4} \right) \delta\left(t - \frac{r}{b}\right), \qquad (3.6)$$

$$\frac{1}{K} u_y(x, y, z, t) \frac{x}{r^3} \left(C_3^{(0)} + \frac{b^2 t^2}{r^2} D_1^{(0)} \right) +$$

$$+ \frac{x y^2}{r^5} \left(C_2^{(0)} + \frac{b^2 t^2}{r^2} D_1^{(0)} \right) +$$

$$+ f e_1 \frac{x y^2}{a r^4} \delta\left(t - \frac{r}{a}\right) + \frac{1}{b} \left(\frac{x}{r^2} e_3 - \right.$$

$$\left. - e_1 \frac{x y^2}{r^4} \right) \delta\left(t - \frac{r}{b}\right), \qquad (3.7)$$

$$\frac{1}{K} u_z(x, y, z, t) = \frac{xyz}{r^5} \left(C_2^{(0)} + \frac{b^2 t^2}{r^2} D_1^{(0)} \right) +$$

$$+ f e_1 \frac{xyz}{a r^4} \delta\left(t - \frac{r}{a}\right) - e_1 \frac{xyz}{b r^4} \delta\left(t - \frac{r}{b}\right); \qquad (3.8)$$

here u_x, u_y, u_z are the displacement components along the x, y, z axes respectively. Coefficients $C_q^{(i)}$, $D_q^{(i)}$, e_q are given in Table IV and in the upper line of Table V. As before $i = 1$ and $i = 2$ correspond to intervals

$$r/a < t < r/b \quad \text{and} \quad r/b > t, \quad \text{and all} \quad D_q^{(2)} = 0.$$

Integrating as before we shall obtain for internal points of a finite source S:

For all $t > 0$

$$u_x = \mp 2\pi \left(C_1^{(2)} + \tfrac{1}{3} C_1^{(2)} \right) T_C, \qquad (3.9)$$

$$u_z = 0. \qquad (3.10)$$

TABLE III

Upper limits in integrals (3.3)

$$\frac{\rho_{max}}{a} < \frac{\rho_{min}}{b}$$

Time interval	$0 - \frac{\rho_{min}}{a}$	$\frac{\rho_{min}}{a} - \frac{\rho_{max}}{a}$	$\frac{\rho_{max}}{a} - \frac{\rho_{min}}{b}$	$\frac{\rho_{min}}{b} - \frac{\rho_{max}}{b}$	$\frac{\rho_{max}}{b} - \infty$
First integral	bt	bt	bt	$min\ (bt, \rho_L)$	ρ_L
Second integral	at	$min\ (at, \rho_L)$*	ρ_L*	ρ_L*	**

$$\frac{\rho_{max}}{a} > \frac{\rho_{min}}{b}$$

Time interval	$0 - \frac{\rho_{min}}{a}$	$\frac{\rho_{min}}{a} - \frac{\rho_{min}}{b}$	$\frac{\rho_{min}}{b} - \frac{\rho_{max}}{a}$	$\frac{\rho_{max}}{a} - \frac{\rho_{max}}{b}$	$\frac{\rho_{max}}{b} - \infty$
First integral	bt	bt	$min\ (bt, \rho_L)$	$min\ (bt, \rho_L)$	ρ_L
Second integral	at	$min\ (at, \rho_L)$*	$min\ (at, \rho_L)$*	ρ_L *	**

TABLE IV

$C_1^{(1)} = C_3^{(1)}$	$C_2^{(1)}$	$D_1^{(1)}$	$D_2^{(1)}$	$C_2^{(2)}$	e_1
$-f$	$3f$	3	-15	$3f-3$	-2

Upper and lower signs correspond to upper (from the side of positive y) and lower sides of S.

For $t < \rho_{min}/a$, $u_y = 0$. (3.11)

For $\rho_{min}/a < t < \rho_{min}/b$,

$$\frac{1}{K} u_y = -\int_0^{2\pi} \left\{ C_3^{(2)} ln \frac{m_a}{\rho_{min}} + \frac{b^2t^2}{2} D_3^{(1)} \left(\frac{1}{\rho_{min}^2} - \right. \right.$$

$$\left. \left. - \frac{1}{m_a^2} \right) \right\} \cos \alpha d\alpha. \quad (3.12)$$

For $\frac{\rho_{min}}{b} < t < \frac{\rho_{max}}{b}$

$$\frac{1}{K} u_y = -\int_0^{2\pi} C_3^{(2)} ln \frac{m_b}{\rho_{min}} \cos \alpha d\alpha - \int_{l_3(\alpha)} \left\{ A_3^{(1)} ln \frac{m_a}{bt} + \right.$$

$$\left. + \tfrac{1}{2} B_3^{(1)} \left(1 - \frac{b^2t^2}{m_a} \right) \right\} \cos \alpha d\alpha + \frac{e_3}{bt} \int_{n_b} \cos \alpha d\alpha. \quad (3.13)$$

Finally for $t > \frac{\rho_{max}}{b}$

$$4\pi \mu u_y = -C_3^{(2)} \int_0^{2\pi} ln \frac{\rho_L(\alpha)}{\rho_{min}} \cos \alpha d\alpha. \quad (3.14)$$

Formulae 3.11 to 3.14 describe the displacement perpendicular to the fault plane. After propagating of waves the displacement of the surface described by (3.14) remains. As $C_3^{(2)} < 0$ it can easily be seen that the right (from positive x) side of the source moves down, the left up. Thus the use of dislocation theory gives the combination of a slip with a specific rotation.

OTHER SOURCES

Formulae (3.1) to (3.14) can be applied to a number of other sources if other values for coefficients $A_q^{(i)}$, $B_q^{(i)}$, $C_q^{(i)}$, $D_q^{(i)}$, c_q, d_q, e_q are taken. Tables II, IV and V give formulae for three more sources: single couple, oriented along the x axis as in Figure 3a; single couple oriented along the y axis; the sum of a single couple oriented

TABLE V

Source	$2C_1^{(2)}$	$2C_3^{(2)}$	e_2	e_3
Two dipoles	$-2f$	$-2f$	-1	-1
Dipole along x	$-f-1$	$-f+1$	-1	0
Dipole along y	$-f+1$	$-f-1$	0	-1
One and a half dipoles	$-4f$	0	$-f-1$	$-1+f$

along the x axis with intensity $(1+f)K$ and a perpendicular couple with intensity $(1-f)K$. The latter source has been referred to as "one and a half" couples in Tables II and V. The coefficients given in Tables I and IV are applicable to two couples and to "one and a half" couples, but must be divided by two for the other cases.

It can be seen from Table IV that a discontinuous slipping along S is determined by a single couple orientated along the x axis; a perpendicular dipole added when other sources are formed changes only distortion of S.

For a single couple the fault-plane distortion is directed oppositely as compared with a double couple.

According to (3.14) the fault plane remains undistorted for "one and a half" couples because $C_3^{(2)} = 0$. I considered this source in connection with an analysis of ultrasonic modelling results; the angle between $y = 0$ and the SV node is nearly the same as in the experiment by PRESS (1959).

However for points on the fault boundary L integration gives the remaining distortion for all sources.

Conclusion

Waves generated by a plane source of finite dimensions essentially depend upon discontinuous as well as continuous displacements in the source itself. Such a source may be considered as an earthquake source model, if and only if the stresses in it correspond to stresses at the fault plane before and during the earthquake.

In a source constructed analogously to dislocation theory—by integrating of double couples—peculiar distributed shear stresses act which hardly correspond to any notion of earthquakes.

References

BESSONOVA, E. N. et al., 1957: Investigation of the mechanism of earthquakes: *Akad. Nauk SSSR Geofiz. Inst. Trudy*, no. 40, 166; published in English *in* Soviet Research in Geophysics *Am. Geophys. Union* 4.

EWING, M., JARDETSKY, W. and PRESS, F., 1957: Elastic waves in layered media: McGraw-Hill, New York.

HODGSON, J. H., ed., 1959: The mechanics of faulting, with special reference to the fault-plane work: *Dom. Obs. Pub.*, Ottawa, **20**, 249.

IANOVSKAYA, T. B., 1958. On the determination of the dynamic parameters of the focus of an earthquake from records of surface waves, I: *Akad. Nauk SSSR Izv.* ser. Geofiz., no. 3, 289; 161 in the English edition, *Am. Geophys. Union.*

KEYLIS-BOROK, V. I., 1956: Methods and results of the investigations of the earthquake mechanism: *Bur. Central Seismol. Internat. Pubs.*, Ser. A, Trav. Sci., **19**, 383.

——— 1959. The study of earthquake mechanism: *Dom. Obs. Pub.*, Ottawa, **20**, 279.

——— 1960*a*. Interferential surface waves: (in Russian), *Izdatel'stve Akad. Nauk SSSR*, Moscow.

——— 1960*b*. The difference in the spectrum of surface waves for earthquakes and explosions: (in Russian), *Akad. Nauk SSSR Inst. Fiz. Zem., Trudy* **5**.

KEYLIS-BOROK, V. I. and PAVLOVA, G. I., 1960. The generalization of data concerning the mechanism of earthquakes: (in Russian), *Akad. Nauk SSSR Inst. Fiz. Zem., Trudy*, **11**, 121.

PAVLOVA, G. I., 1960. The changes in a stress field resulting from an earthquake: (in Russian), *Akad. Nauk SSSR Inst. Fiz. Zem., Trudy*, **11**, 148.

PRESS, F., 1959. Elastic wave radiation in ultrasonic models: *Dom. Obs. Pub.*, Ottawa, **20**, 271.

STARR, A., 1928. Slip in a crystal and rupture in a solid due to shear *Cambridge Phil. Soc. Proc.*, **24**, 489.

An Application of S Waves to Focal Mechanism Studies*

WILLIAM STAUDER, S.J.
Saint Louis University, Saint Louis, Missouri, U.S.A.

ABSTRACT

Two methods are developed for relating the direction of polarization of S waves to the mechanism at the focus of an earthquake. Application to three or four earthquakes for which the fault-plane solutions from P waves were previously available show that in these cases the S wave data agree with the P wave solution and conform to a dipole with moment as the model of the focus. In three Kamchatka earthquakes the same methods of analysis indicate a new type of focus, represented by a single force.

INTRODUCTION

One of the problems frequently mentioned in discussions of fault-plane work concerns the question whether the mechanism at the focus of an earthquake better corresponds to a single dipole with moment or to two superposed dipoles of opposite moment as the mathematical point model of the earthquake focus. The matter was much discussed in the symposium on fault-plane work at the XIth General Assembly of the IUGG (HODGSON, 1959). As is well known, either model conforms equally well to the quadrant distribution of the direction of the initial motion of P waves which has been observed in so many earthquakes. It has also frequently been pointed out that, in theory, S waves can be used to discriminate between the two models.

The present paper is an observational study of this question. A selected set of earthquakes has been chosen and the character of the S motion determined at several stations distributed azimuthally about the source and at epicentral distances ($38° < \Delta < 82°$) favorable for the observation of S waves. The paper endeavors to study the relation between these observed S motions and the mechanism at the focus.

THEORY

In one way or another (Cf. SCHEIDEGGER, 1957) the methods of fault-plane determination all reduce data observed at stations on the surface of the earth to that which would be observed in an infinite homogeneous medium. For many purposes a convenient device is to consider the motion at points on the surface of an arbitrary unit sphere concentric with the focus (Figure 1, left). The sphere is called the focal sphere. In particular, in the present consideration attention is directed to the S wave motion over the surface of the focal sphere due to the action of a single dipole with moment as the source mechanism (Figure 1, right). The observed S motion, reduced to the focal sphere, will then be compared to that expected in theory.

*The matter presented in this paper is summarized from the articles of the author mentioned in the references.

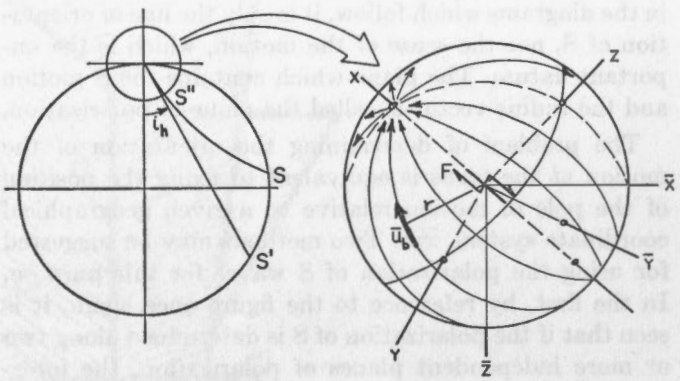

Figure 1. The focal sphere.

The theory of point sources has been worked out by several authors. The application of the theory to source mechanism determinations has been presented perhaps most completely by KEYLIS-BOROK and his associates (GOTSADZE *et al.*, 1957). The theory shows that an important property of the S motion for a single dipole-with-moment source is this: The S motion at any point in an infinite homogeneous elastic medium, the ray to that point, and the direction of the forces at the focus are all co-planar. This property is, in fact, common to all point sources whose component forces are directed along a single axis. Symbolically, this property may be represented (ADAMS, 1958) by the equation:

$$(\vec{u}_b \times \vec{r}) \cdot \vec{k}(t) = 0 \qquad (1)$$

where

$$\vec{u}_b$$

is a unit vector in the direction of the S motion at a point on the focal sphere,

$$\vec{r}$$

is a unit vector along the radius vector to the point, and

$$\vec{k}(t)$$

is a unit vector in the direction of the force.

Referring to the figure, the direction of the forces at the source may be designated as the x-axis. This axis is called the axis of motion. The point at which the axis of motion intersects the focal sphere is the pole of motion. Consequent upon the co-planar property, the S motion at points on the surface of the sphere is oriented along great circles or "meridians" which converge to the pole of motion on one side of the focal sphere and diverge from it on the other. It should be pointed out at this juncture, however, that the methods which are used in this paper do not depend upon the *direction* of first motion of S, but only upon the *polarization* of S. That is, while a direction will usually be assigned to the S motion in the diagrams which follow, it is only the line of orientation of S, not the sense of the motion, which is the important datum. The plane which contains the S motion and the radius vector is called the plane of polarization.

The problem of determining the orientation of the motion at the focus is equivalent to fixing the position of the pole of motion relative to a given geographical coordinate system, $\overline{xyz}$. Two methods may be suggested for using the polarization of S waves for this purpose. In the first, by reference to the figure once again, it is seen that if the polarization of S is determined along two or more independent planes of polarization, the intersection on the focal sphere of the meridian lines corresponding to these two or more planes of polarization fixes the position of the pole of motion. In the second method, since the plane of polarization of S contains the direction of motion at the source, the normal to the plane of polarization of S determined at a given station will lie in a plane normal to the axis of motion. The intersection of the normal to a plane of polarization with the focal sphere is the pole of the plane of polarization. The normals (poles) to two or more planes of polarization of S will therefore determine a plane which is perpendicular to the motion at the source. This plane is the "auxiliary plane" of the fault-plane terminology. Analytically, either method may be expressed (ADAMS, 1958) by the relation

$$(\vec{u}_{bi} \times \vec{r}_i) \times (\vec{u}_{bj} \times \vec{r}_j) = \vec{k}(t) \qquad (2)$$

where the subscripts refer to quantities determined at points on independent planes of polarization of S. The methods themselves will become clearer in the exposition which follows.

PRACTICAL PROCEDURE

In making use of the polarization of S waves in the two ways just suggested, two different methods of stereographic projection are adopted: a central projection, and the more customary stereographic or Wulff net. The first of these lends itself more readily to the determination of the intersection of two or more planes of polarization. The second will be used in determining the auxiliary plane or plane of the poles of the planes of polarization of S.

The central projection is the projection of the lower hemisphere of the focal sphere onto a plane tangent to the sphere at the bottom. Figure 2 shows the scheme of the projection. The point of projection is the center of the sphere. A point on the sphere projects onto the tangent plane a radial distance from the center of the projection equal to $\tan i_h$, where i_h is the angle between the downward vertical and the radius vector to the point. The figure shows the projected position of the pole of motion. There is also shown the direction of polarization of S at a point on the lower hemisphere. One of the hachured planes is the corresponding plane of polarization. The projection of the direction of polarization is a short line-segment along the intersection of the plane of polarization with the tangent plane. The line points to the pole of motion. Hence, in this projection the directions of polarization of S at many points on the focal sphere form a family of straight lines which converge to the pole of motion.

The angle ϵ, which is the angle between the plane of polarization and the vertical plane containing the ray, is the angle of polarization. This angle is defined by the relation $\epsilon = \tan^{-1} \mathrm{SH/SV}$. It projects as the angle γ_h through the cosine of i_h.

In practice ϵ is determined by particle motion diagrams of the S phase, that is, by a vector combination of the horizontal seismograms of the S motion. According to GUTENBERG (1952), for the epicentral distances used in this investigation the ratio of the amplitude of SH and the horizontal component of SV at the free surface is very closely proportional to the ratio of the same quantities in the incident wave. This permits the construction of a particle motion diagram directly from the trace amplitudes on the seismograms without reducing to the motion in the incident wave.

Figure 3 shows an example of a particle motion diagram for the earthquake of July 10, 1958. The S motion is oftentimes slightly irregular or elliptical. In these cases the major axis of the S motion is taken as the horizontal projection of the direction of polarization of S. The angle γ_o is measured off from the azimuth to the epicenter to the direction of polarization. This angle, in turn, is related to the angle of polarization by the equation

$$\tan \epsilon = \cos i_o \tan \gamma_o , \qquad (3)$$

where i_o is the angle of incidence of the ray at the surface.

Figure 4 illustrates the method of plotting the direction of polarization in the central projection. The azimuth of the station at the epicenter is measured off from north and the station located at a radial distance $r = \tan i_h$ from the center of the projection. At this

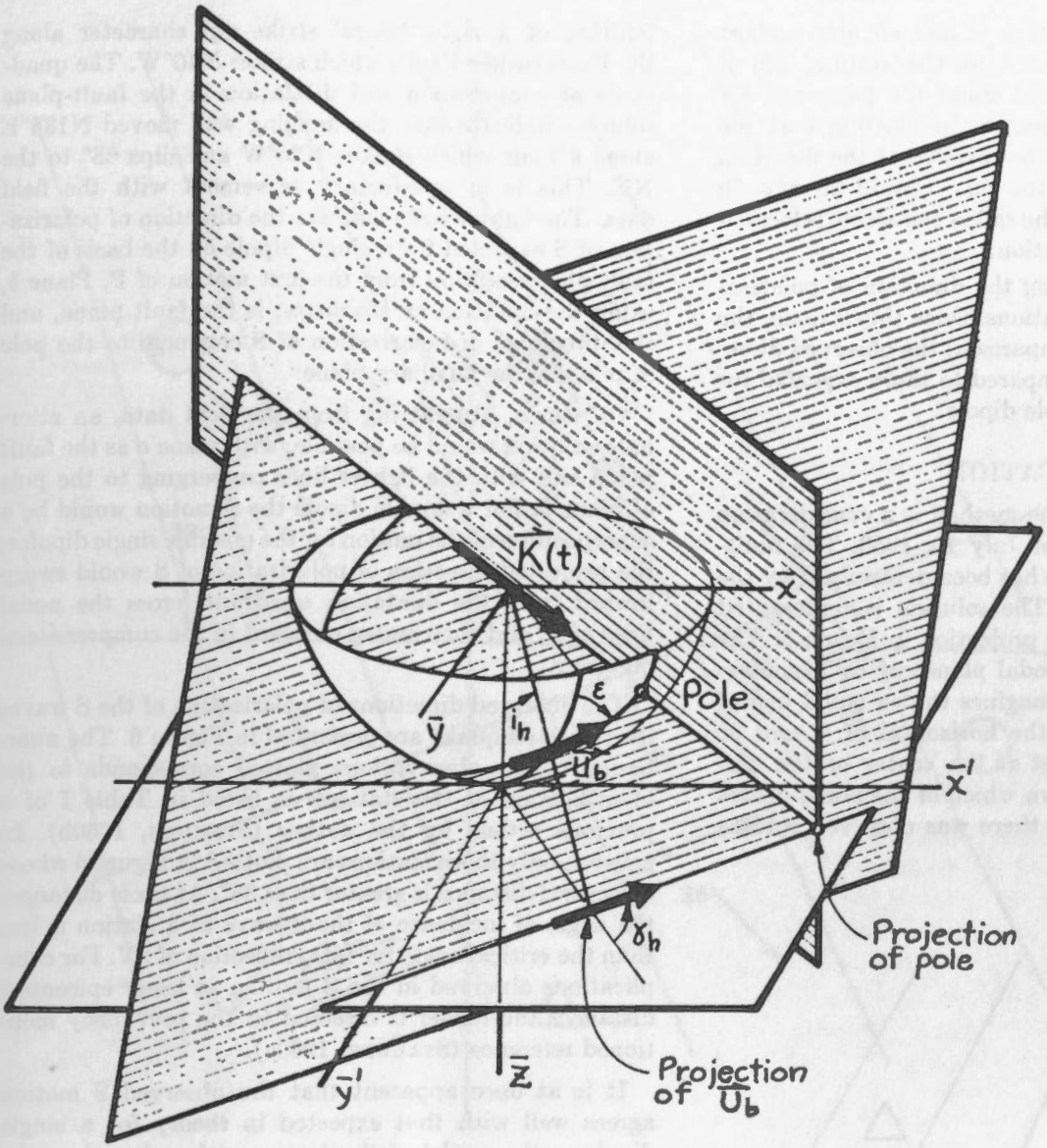

Figure 2. The central projection of S motion on the focal sphere onto the plane tangent to the sphere.

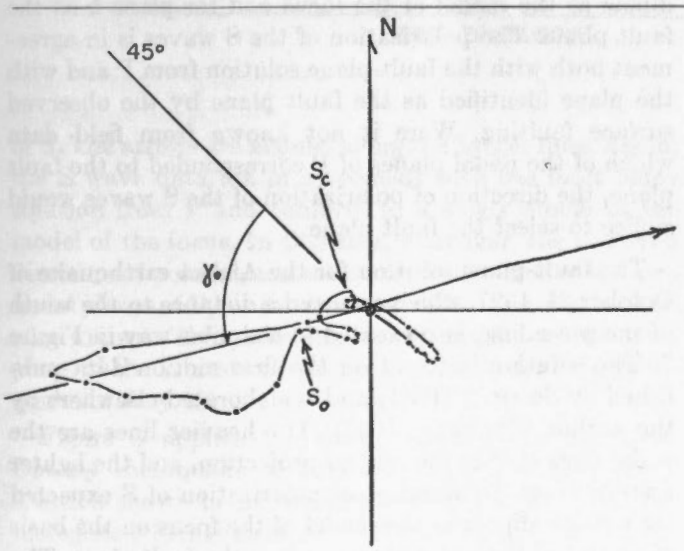

Figure 3. The particle motion diagram of the S phase recorded at Weston for the earthquake of July 10, 1958. $\Delta = 43°$.

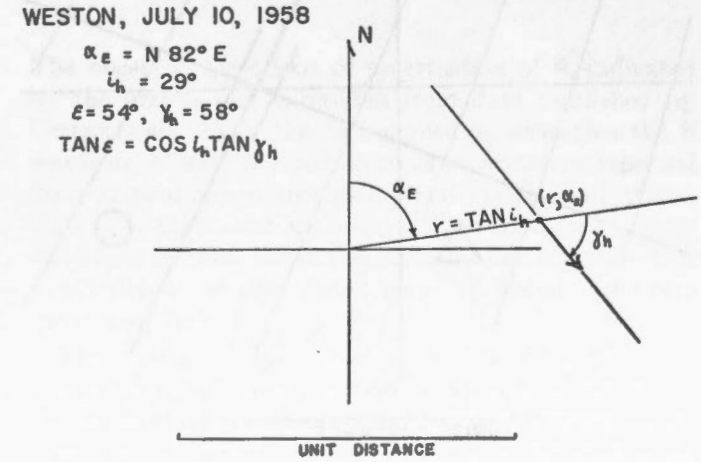

Figure 4. The method of plotting the direction of polarization of S in the central projection.

point the angle of polarization is laid off and a short arrow drawn. When measured at the station, SH is regarded as positive clockwise about the focus and SV as positive toward the epicenter. In plotting ϵ at the source, account is taken of the reversal of the direction of SV along the ray due to the curvature of the ray. In the drawings which follow, the tail of the arrow is located at the coordinates of the station.

This procedure for plotting the direction of polarization is carried out for all stations. Once this is done, the method is simply one of comparison: the observed directions of polarization are compared to those expected for a single dipole or for a double dipole.

APPLICATION

The first application of the method is a consideration of the Alaska earthquake of July 10, 1958. The fault-plane solution from P waves has been determined by the author (STAUDER, 1960a.) The solution is represented schematically in the central projection in Figure 5. The heavy lines represent the nodal planes of P. Visualization is not difficult if one imagines that a nodal line of P is the intersection with the horizontal of a card or plane inclined against a post at the center of the diagram. In this case it is known which of the nodal planes of P is the fault plane, for there was observed surface faulting of a right lateral strike-slip character along the Fairweather Fault, which strikes N40°W. The quadrants of compression and dilatation in the fault-plane solution indicate that the hanging wall moved N138°E along a fault which strikes N25°W and dips 68° to the NE. This is in satisfactory agreement with the field data. The lighter lines indicate the direction of polarization of S expected for a single dipole on the basis of the fault-plane solution from the first motion of P. Plane *b*, using the notation of HODGSON, is the fault plane, and the directions of polarization of S converge to the pole of plane *a*, the auxiliary plane.

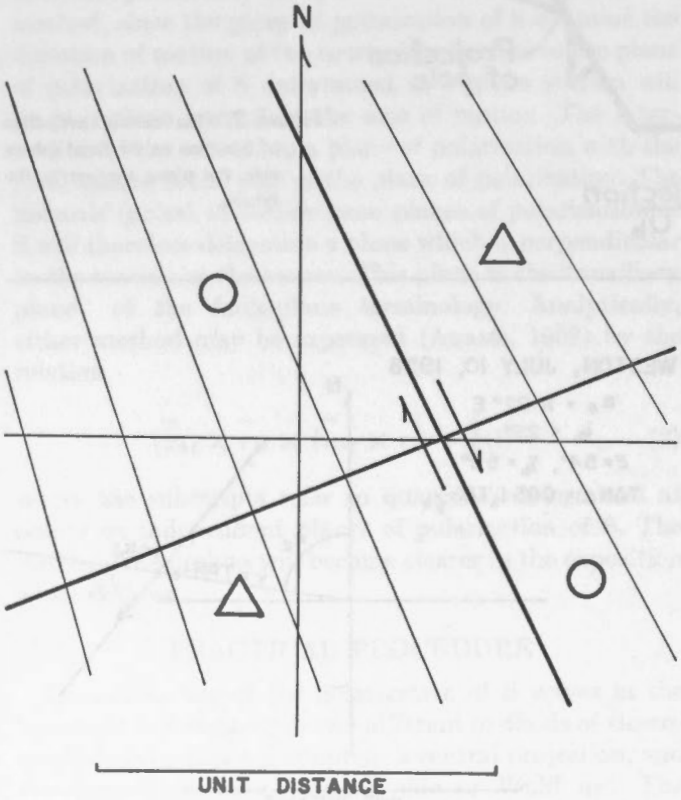

Figure 5. The central projection of the fault-plane solution of the earthquake of July 10, 1958, and the theoretical direction of polarization of S.

Of course, abstracting from the field data, an alternate solution would be possible, with plane *a* as the fault plane and with the lighter lines converging to the pole of plane *b*. For a double dipole the S motion would be a superposition of the motion for the possible single dipoles; the projected direction of polarization of S would sweep inward from the dilatation quadrant, cross the nodal lines of P, and then sweep outward in the compressional quadrant.

The observed directions of polarization of the S waves for this earthquake are presented in Figure 6. The numbering of the observations plotted corresponds to the identification of the stations as listed in Table I of a previous article by the author (STAUDER, 1960b). In general, only those stations are plotted in Figure 6 whose epicentral distance is greater than 38°. At these distances the angle of incidence of the S wave at a station is less than the critical angle for total reflection of SV. For complications observed in the S motion at lesser epicentral distances the reader is directed to the previously mentioned reference (STAUDER, 1960a).

It is at once apparent that the observed S motion agrees well with that expected in theory for a single dipole as the model of the focus and for plane *b* as the fault plane. The polarization of the S waves is in agreement both with the fault-plane solution from P and with the plane identified as the fault plane by the observed surface faulting. Were it not known from field data which of the nodal planes of P corresponded to the fault plane, the direction of polarization of the S waves would suffice to select the fault plane.

The fault-plane solution for the Alaska earthquake of October 24, 1927, which occurred a distance to the south of the preceding, is presented in a similar way in Figure 7. The solution is based on the first motion data published by SOMMER (1931) and is elaborated elsewhere by the author (STAUDER, 1959). The heavier lines are the nodal lines of P in the central projection, and the lighter lines indicate the direction of polarization of S expected for a single dipole as the model of the focus on the basis of plane *b* of the nodal planes of P as the fault plane. The arrows represent the observed directions of polarization

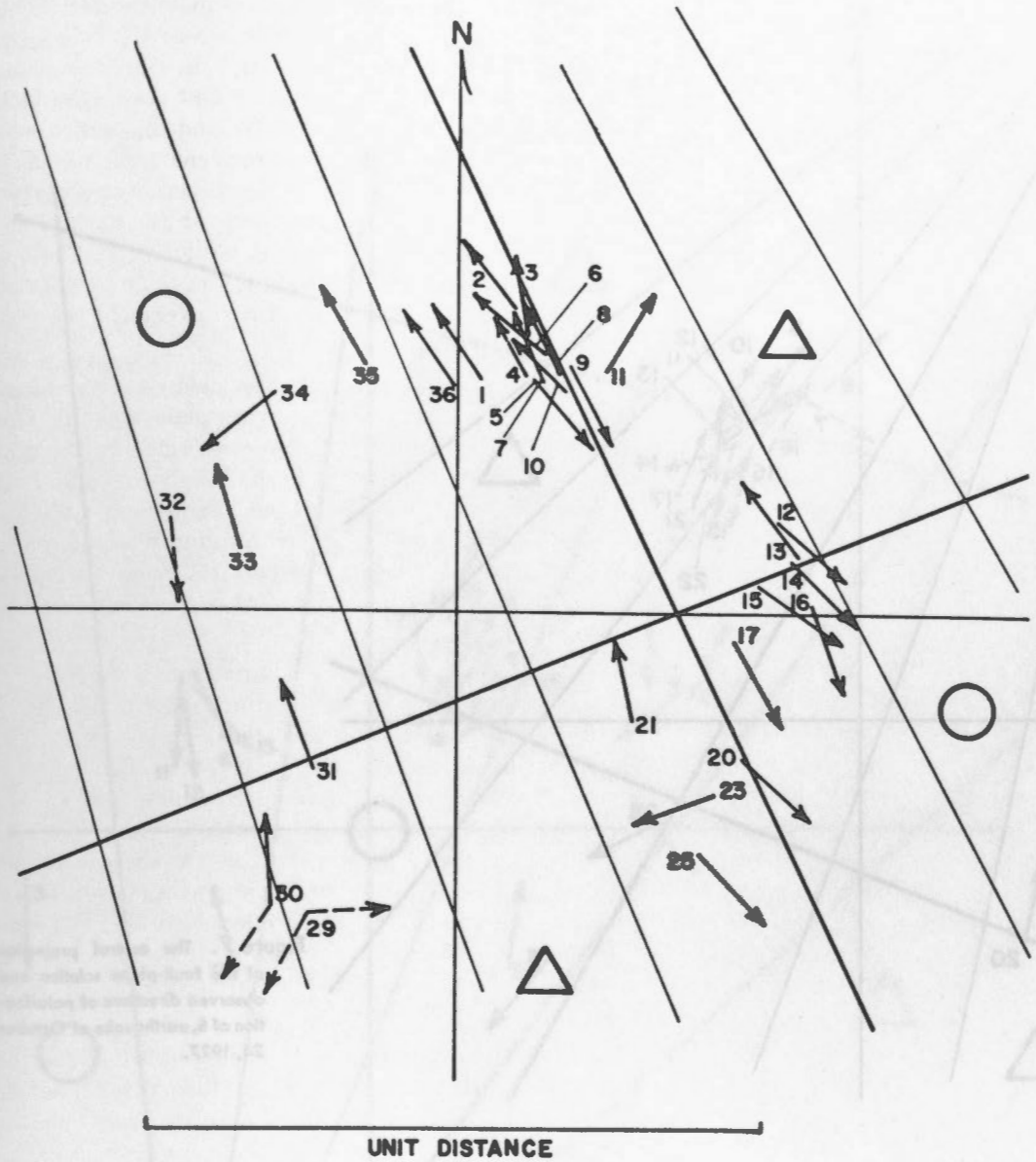

Figure 6. The observed directions of polarization of S, July 10, 1958.

of S. The arrows are aligned along the lighter lines. Again, the S wave data are in agreement with the fault plane solution from P and conform to a single dipole as the model of the focus. In this case, moreover, the observed direction of polarization *selects* the fault plane of the two nodal planes of P, for the direction of faulting is not otherwise known. The plane selected is parallel to the fault plane of the solution presented previously for this earthquake of July 10.

Figure 8 applies the same technique to the Kern County earthquake of July 21, 1952. The fault-plane solution shown is one worked out by the Russian seismologists (GOTSADZE et al., 1957, p. 62), using data from both P and S supplied to them by GUTENBERG. The solution differs slightly from that of GUTENBERG (1955). The observed directions of polarization of S, indicated by the arrows, are computed from data published by GUTENBERG. As in the two preceding examples the S waves agree with the directions of polarization expected for a single dipole source with plane *a* as the fault plane. This is in agreement with the surface fracture. A fuller discussion of these latter two earthquakes, together with a tabulation of the data, may be found elsewhere (STAUDER, 1960c).

The method of the central projection of the planes of polarization of S has also been applied to three Kamchatka earthquakes (STAUDER, 1960b). The three earthquakes selected were members of the aftershock sequence of the large earthquake of November 4, 1952. They occurred on March 5, September 23, and October 5, 1953.

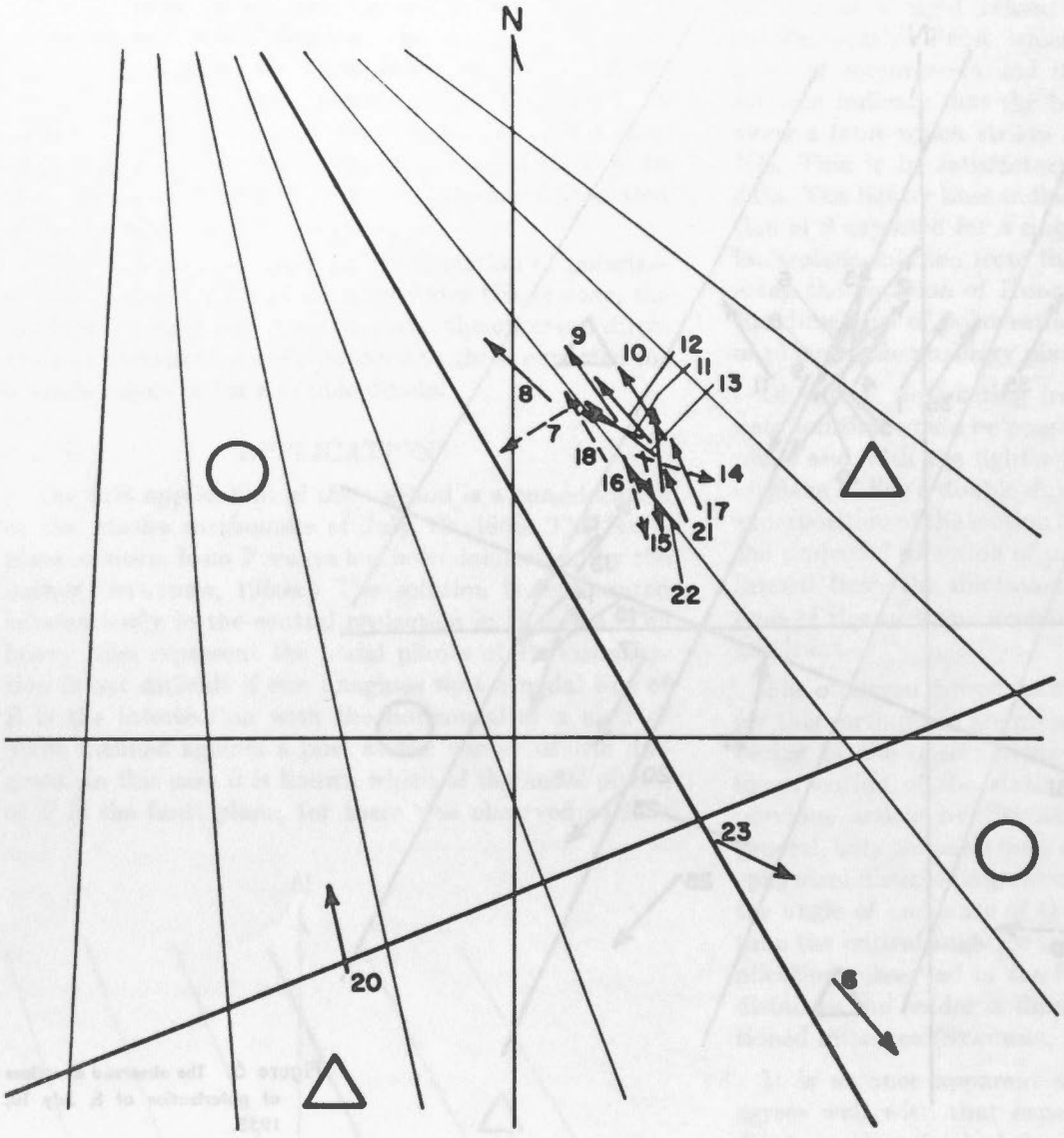

Figure 7. The central projection of the fault-plane solution and observed directions of polarization of S, earthquake of October 24, 1927.

All are of magnitude $6\frac{3}{4}$-7, and have a depth of focus of 40-60 km. HODGSON (1956) has determined fault-plane solutions from P waves for the earthquakes of March 5 and October 5. No solution was possible for the earthquake of September 23 because of conflicts in the data.

Examination of the polarization of the S waves for the earthquakes of March 5, and October 5, 1953, has shown (STAUDER, 1960b) that there is no agreement, either for a single dipole or for a double dipole source, between the S wave data and the P wave solution. The case of the earthquake of September 23, 1953, is more interesting and bears summary.

Since there is no fault-plane solution available for the earthquake of September 23, it is not possible to compare the data from S waves to the solution from P waves. Figure 9, however, presents the central projection of the observed directions of polarization of S. Two features are to be noted: 1) the direction of polarization of S is very consistent from one station to the next, and 2) the motion is highly SV-polarized.

Even though no fault-plane solution from P waves is possible, it is instructive to present the extended distance projection of the first motion of P (Figure 10). Inspection of the figure shows at once that, with but one definite exception (Quetta), the first motion of P is compressional in all quadrants.* One station (Matsushiro) is at an epicentral distance of 20°; all others are at epicentral distance of 40° or greater.

* It should be noted that the directions of first motion plotted in Figure 10 differ from those reported to HODGSON by questionnaire at four stations: College, Sitka, Basel, and Helwan. The direction of motion at these stations, except perhaps Basel, is unmistakable. The author has checked his own readings at College, Sitka, and Helwan with the trace-ground motion correlation by writing to the USCGS and to the director of the station at Helwan.

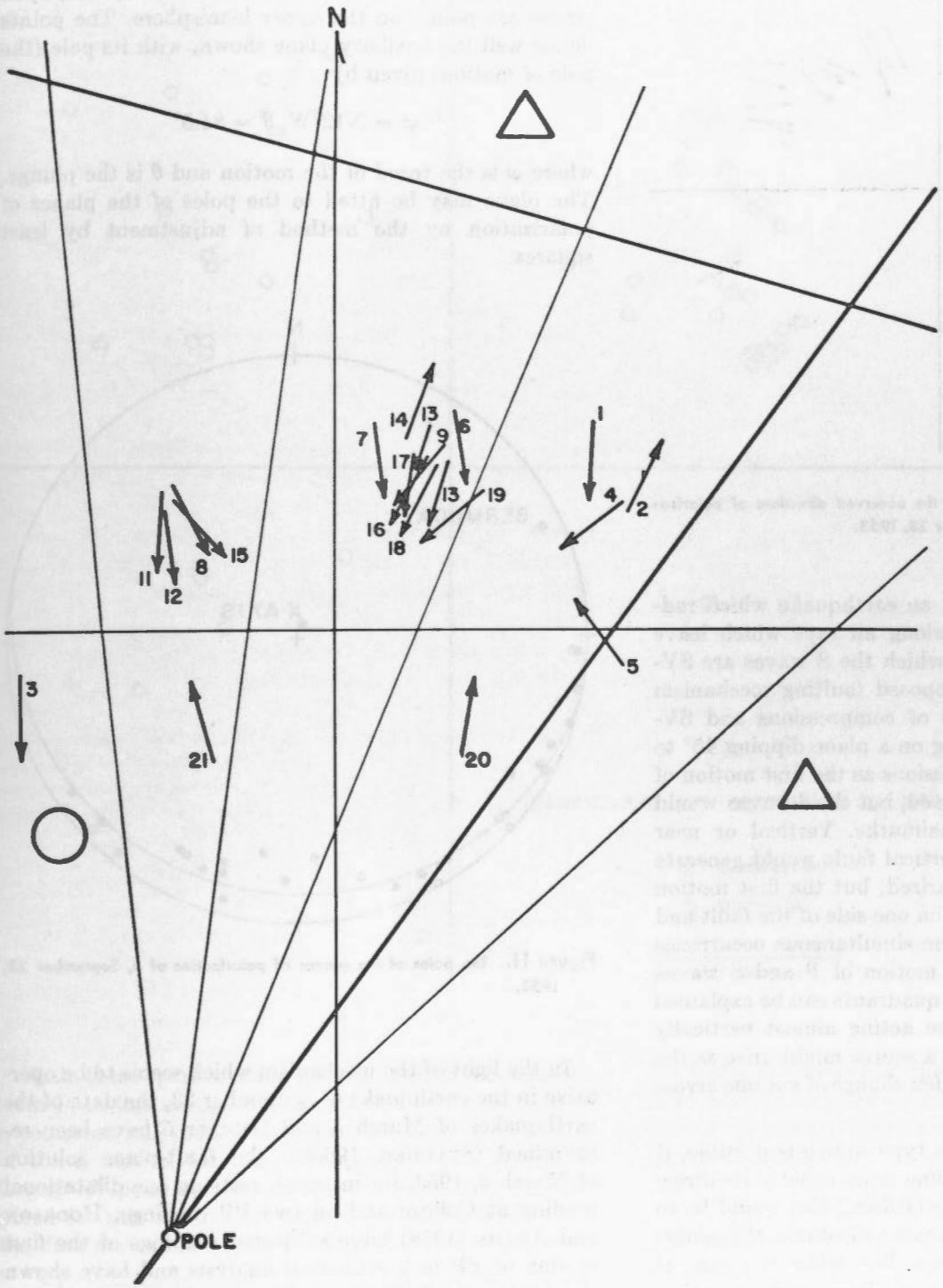

Figure 8. The central projection of the fault-plane solution and observed directions of polarization of S, Kern County earthquake of July 21, 1952.

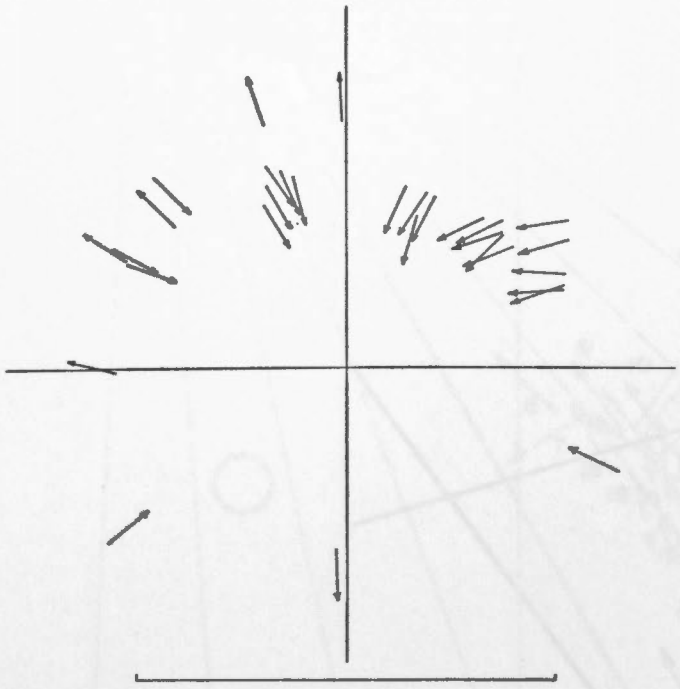

Figure 9. The central projection of the observed directions of polarization of S, earthquake of September 23, 1953.

There is here, apparently, an earthquake which radiates compressional energy along all rays which leave the focus downward and in which the S waves are SV-polarized. No commonly proposed faulting mechanism can explain this association of compressions and SV-polarization. Dip-slip faulting on a plane dipping 45° to 60° could give rise to compressions as the first motion of P in the distance range observed, but the S waves would be largely SH at certain azimuths. Vertical or near vertical motion on a near-vertical fault would generate S waves which were SV-polarized, but the first motion of P would be compressional on one side of the fault and dilatational on the other. The simultaneous occurrence of compressions as the first motion of P and S waves which are SV-polarized in all quadrants can be explained by a single force type source acting almost vertically downward at the focus. Such a source might arise as the model which represents a sudden change of volume across a horizontal surface.

Granted that a single force type source is possible, it would be desirable to determine more exactly its direction of action. One possibility of doing this would be to extend the arrows of the Figure 9 and obtain the center of gravity of their intersection. But while the central projection is good for comparing observed polarization of S motion to that expected for a given fault-plane solution, it exaggerates the scatter of the data. A better procedure is to make use of the second way of using S wave data mentioned in the introduction: the use of the Wulff net and the plotting of the poles of the planes of polarization of S. (Also Cf. STAUDER, 1960c).

The poles of the planes of polarization of S for the earthquake of September 23 are plotted in Figure 11. Closed circles are points on the lower hemisphere, open circles are points on the upper hemisphere. The points define well the auxiliary plane shown, with its pole (the pole of motion) given by

$$\varphi = \text{N12°W}, \theta = 84.5°$$

where φ is the trend of the motion and θ is the plunge. The plane may be fitted to the poles of the planes of polarization by the method of adjustment by least squares.

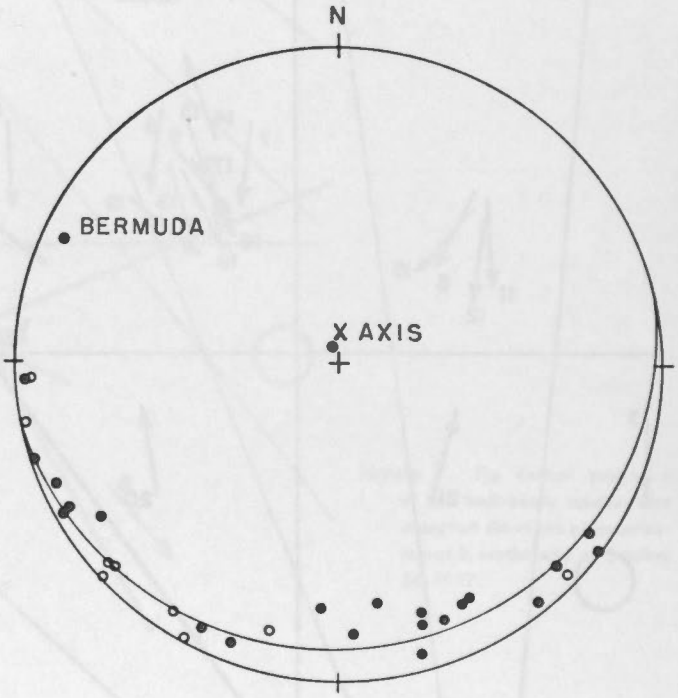

Figure 11. The poles of the planes of polarization of S, September 23, 1953.

In the light of the mechanism which seems to be operative in the earthquake of September 23, the data of the earthquakes of March 5 and October 5 have been re-examined (STAUDER, 1960b). the fault-plane solution of March 5, 1953, for instance, rests on one dilatational reading at College and on two PP readings. HODGSON and ADAMS (1958) have subjected readings of the first motion of PP to a statistical analysis and have shown them to be unreliable for fault-plane work. Further, the fault-plane solution from P for this earthquake makes inconsistent a very good compressional reading at Kirkland Lake. The reading at College is likewise very definite and has been read by the author as a compression.

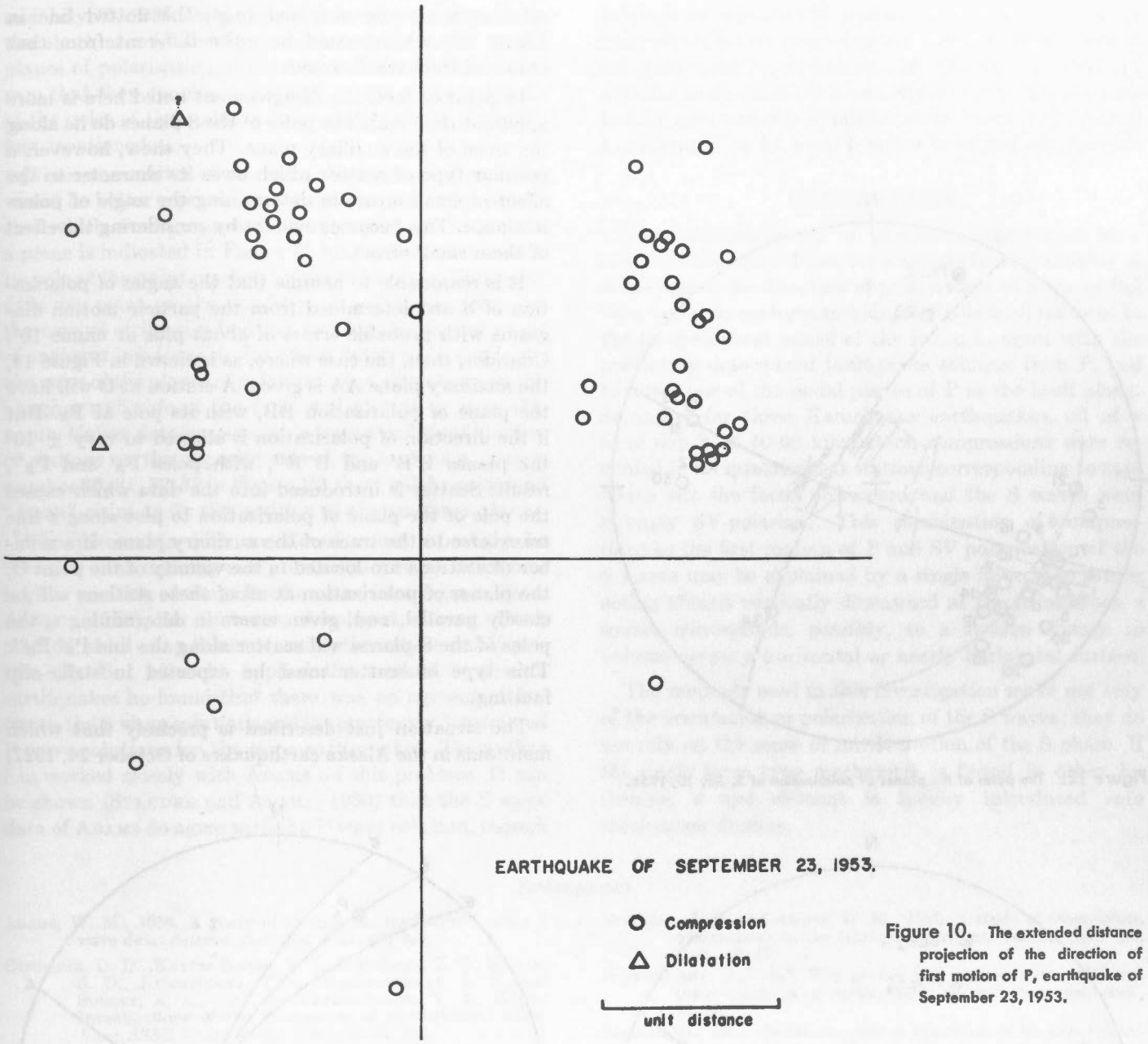

Figure 10. The extended distance projection of the direction of first motion of P, earthquake of September 23, 1953.

With these qualifications to the fault-plane solution from P, in this earthquake, again, the first motion of P is compressional in all quadrants. And since examination of the S motion for this earthquake shows that it is largely SV-polarized, the same conclusion may be proposed for this earthquake as for that of September 23: the data are explainable by a single force acting almost vertically downward at the source. This solution is at least equally as satisfactory as the fault-plane solution from P. A similar argument can be made for the earthquake of October 5.*

SCATTER OF THE DATA

A caution is necessary in applying the method of plotting the poles of the planes of polarization of S in order to determine the auxiliary plane or its pole. For example, Figure 12 is the plot of the poles of the planes of polarization for the earthquake of July 10, 1958. The poles of the planes of polarization by no means lie along the auxiliary plane, which is represented by the solid line on the

* An identical distribution of polarization of the S wave has been found in nine out of twelve other Kamchatka earthquakes currently under investigation. The author has also proposed that the data from these earthquakes may be interpreted as conforming either to a single force or to a double couple mechanism equivalent to the release of a principal stress system in which the maximum compressive stress is nearly horizontal and normal to the Kamchatka coast, and the least stress is nearly vertical.

figure. A similar configuration is obtained in the plot of the poles of the planes of polarization of S for October 24, 1927 (Figure 13). This technique of presenting the data does not seem to agree with the fault-plane solution from P. If a great circle on the Wulff net were passed through the points of either Figure 12 or Figure 13, a solution would be obtained (e.g., the dotted line in Figure 12) which would be quite different from that obtained from the P waves.

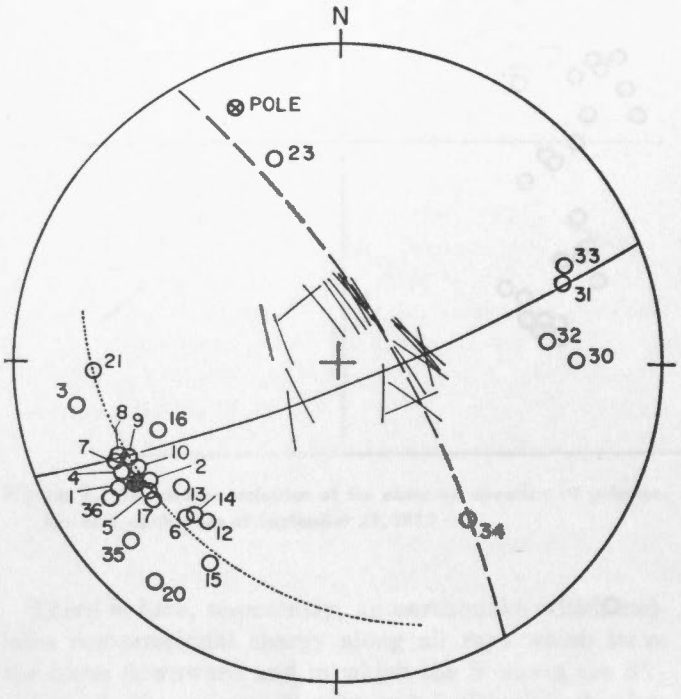

Figure 12. The poles of the planes of polarization of S, July 10, 1958.

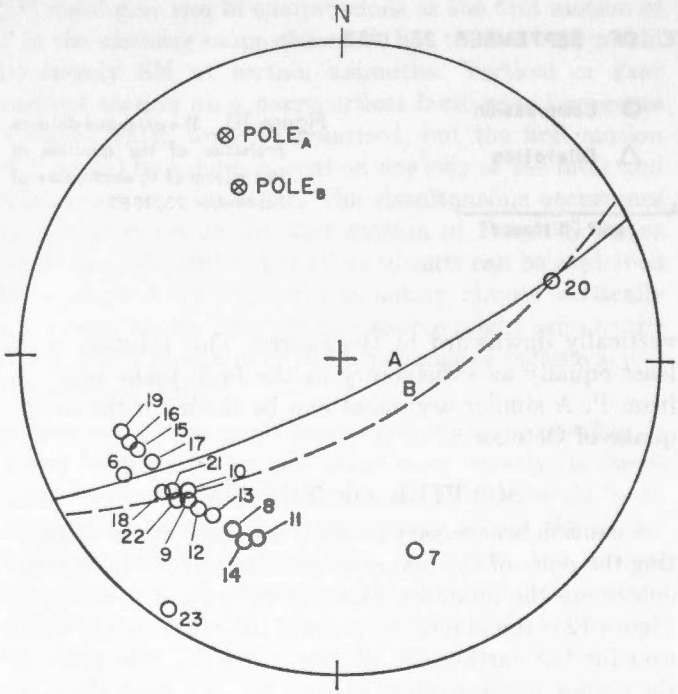

Figure 13. The poles of the planes of polarization of S, October 24, 1927.

In point of fact, the disagreement noted here is more apparent than real. The poles of the S planes do lie along the trace of the auxiliary plane. They show, however, a peculiar type of scatter which owes its character to the effect of small errors in determining the angle of polarization, ϵ. This becomes evident by considering the effect of these small errors.

It is reasonable to assume that the angles of polarization of S are determined from the particle motion diagrams with probable errors of about plus or minus 10°. Consider, then, the case where, as is shown in Figure 14, the auxiliary plane AA is given. A station at O will have the plane of polarization BB, with its pole at P_B. But if the direction of polarization is allowed to vary $\pm$ 10° the planes B′B′ and B″B″, with poles P_B' and P_B'', result. Scatter is introduced into the data which causes the pole of the plane of polarization to plot along a line transverse to the trace of the auxiliary plane. If a number of stations are located in the vicinity of the point O, the planes of polarization at all of these stations will be closely parallel, and, given errors in determining ϵ, the poles of the S planes will scatter along the line P_B' P_B''. This type of scatter must be expected in strike-slip faulting.

The situation just described is precisely that which maintains in the Alaska earthquakes of October 24, 1927,

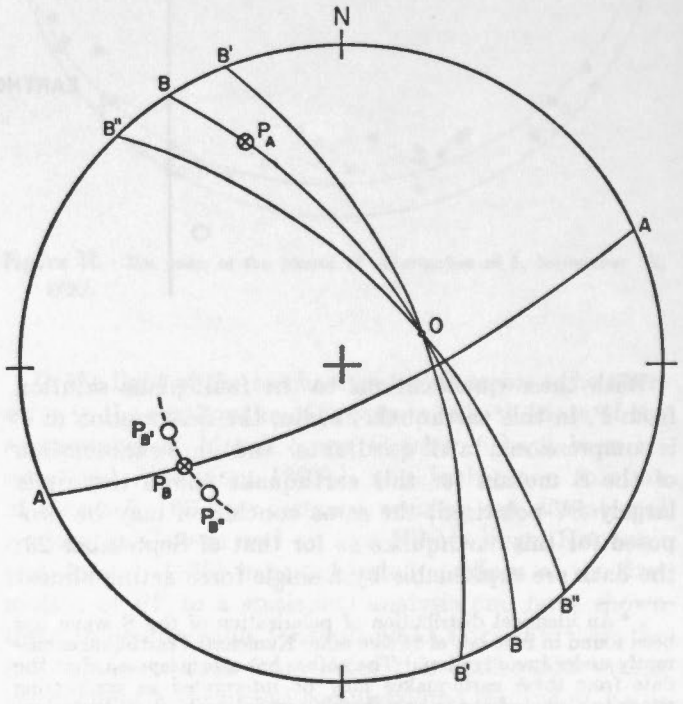

Figure 14. The effect of small errors in determining the angle of polarization of S.

and July 10, 1958. Returning, for example, to Figure 12, the short arcs in the figure represent segments of the planes of polarization of S at the various stations. It is seen that they are closely parallel, and that the positions of the poles of these planes show scatter of the character just mentioned.

Given the scatter of the data, the S planes themselves would be better represented by a mean plane of polarization which would represent the group of stations. Such a plane is indicated in Figure 12 by the dashed line with its pole at the point marked by the solid circle. This point fixes one point on the auxiliary plane. Of necessity, for the case of strike-slip faulting and for the limited range of angles of incidence, i_A, for which data can be available, the poles of the planes of polarization of all stations on the hanging wall side of the fault will plot at or near this point. Unless data are available from a sufficient number of stations on the opposite side of the fault (e.g., points number 30, 31, 32, 33 in Figure 12) there will be no second "mean" point to fix the position of the auxiliary plane.

The precaution just mentioned must especially be borne in mind in using analytic techniques for determining the position of the pole of motion from S wave data. ADAMS (1958), for instance, developed a very direct method of so using S waves, using the relation of Equation (2). But when he applied the method to several earthquakes he found that there was no agreement between the S wave solutions and the previously determined P wave solutions for the same earthquakes. The author has worked closely with ADAMS on this problem. It can be shown (STAUDER and ADAMS, 1960) that the S wave data of ADAMS do agree with the P wave solution, though they show the scatter to be expected for strike-slip faulting. With this correction the earthquakes investigated by ADAMS may be added to the number of those in which agreement is found between P and S wave data and in which the S waves agree with a single dipole source.

CONCLUSIONS

Two conclusions are of particular significance as a result of this study. First, for a certain limited number of earthquakes the direction of polarization of S waves has been found to conform to a single dipole with moment as the mathematical model of the focus, to agree with the previously determined fault-plane solution from P, and to select one of the nodal planes of P as the fault plane. Secondly, for three Kamchatka earthquakes, all of a focal depth of 40-60 kilometers, compressions were recorded in all quadrants at stations corresponding to rays which left the focus downward and the S waves were strongly SV-polarized. This combination of compressions as the first motion of P and SV polarization of the S waves may be explained by a single force type source acting almost vertically downward at the focus. Such a source corresponds, possibly, to a sudden change in volume across a horizontal or nearly horizontal surface.

The methods used in this investigation make use only of the orientation or polarization of the S waves; they do not rely on the sense of initial motion of the S phase. If the single force type mechanism is found in other instances, a new element is hereby introduced into mechanism studies.

References

ADAMS, W. M., 1958. A study of earthquake mechanisms using S wave data: *Seismol. Soc. Am. Bull.*, **48**, 201.

GOTSADZE, O. D., KEYLIS-BOROK, V. I., KIRILLOVA, I. V., KOGAN, S. D., KUKHTIKOVA, T. I., MALINOVSKAYA, L. N. and SURSKY, A. A., 1957, *in* KEYLIS-BOROK, V. I., *Editor*: Investigations of the Mechanism of Earthquakes: *Akad. Nauk SSSR Trudy Geofiz. Inst.*, no. 40, 166.

GUTENBERG, B., 1952. SV and SH: *Am. Geophys. Union Trans.*, **33**, 573.

——— 1955. First motion in longitudinal and transverse wave of the main shock and the direction of slip: *in*, Earthquakes in Kern County, California during 1952; *Calif. Div. Mines*, Bull. **171**, 165.

HODGSON, J. H., 1956. Direction of faulting of the some of the larger earthquakes of the north Pacific, 1950-1953: *Dom. Obs., Pub.* Ottawa, **18**, 219.

——— 1959. (Ed.) The mechanics of faulting (a symposium): *Dom. Obs. Pub.*, Ottawa, **20**, 251.

HODGSON, J. H. and ADAMS, W. M., 1958. A study of inconsistent observations in the fault-plane project: *Seismol. Soc. Am. Bull.*, **48**, 17.

SCHEIDEGGER, A., 1957. The geometrical representation of fault-plane solutions of earthquakes: *Seismol. Soc. Am. Bull.*, **47**, 89.

SOMMER, H., 1931. On the question of dispersion of the first preliminary seismic waves: *Seismol. Soc. Am. Bull.*, **21**, 87.

STAUDER, W., 1959. A mechanism study; the earthquake of October, 1927: *Geofis. Pura e Appl.*, **61**, no. 3, 135.

——— 1960*a*. Seismic studies of the Alaska earthquake of July 10, 1958: *Seismol. Soc. Am. Bull.*, **50**, 293.

——— 1960*b*. Three Kamchatka earthquakes: *Seismol. Soc. Am. Bull.*, **50**, 347.

——— 1960*c*. S waves; Alaska and other earthquakes: *Seismol. Soc. Am. Bull.*, **50**, 581.

STAUDER, W. S. J. and ADAMS, W. M., 1961. A comparison of some S wave studies of earthquake mechanisms: *Seismol. Soc. Am. Bull.*, **51**, 277.

Further Focal Mechanism Studies at De Bilt

A. R. RITSEMA

Royal Netherlands Meteorological Institute, De Bilt, Holland

In the interval between the XIth and XIIth General Assembly of the IUGG, three new series of fault-plane solutions have been determined at de Bilt, viz. the solutions of 16 Sumatran earthquakes (VELDKAMP 1957, 1959), of 48 South East Asian and West Pacific earthquakes (RITSEMA and VELDKAMP 1960), and of 15 earthquakes at different locations which took place in 1950 (RITSEMA 1960). The first two studies were based on P, PKP and S wave data reported by many seismic stations all over the world in reply to questionnaires. The third study is based on the initial motions of P and PKP waves reported in the ISS, together with some additional information provided by stations situated at locations which are important for the determination of the fault-plane solutions.

Wulff's stereographic net has been used throughout to plot the P, PKP and S data. Not the sense of the first motion, but the angle of polarization of the S waves ($\alpha = \tan^{-1}$ SH/SV), has been used to decide which of the two nodal planes for longitudinal waves most probably acted as fault plane.

The new solutions are summarized in Table I in the form of the azimuth and plunge of the A axis (fault movement), the B axis (normal to the plane of action = null vector of HODGSON), and the C axis (normal to the fault plane). The fault motion type is given as a combination of the letters T (normal), P (reversed), L (sinistral) and R (dextral) in such a way that the first character is always dominating. Herewith the solution is completely described.

The earthquakes have been divided into groups a, b, ... i, j according to the scheme of Table II, to give an insight into the reliability of the solutions. The subdivision used here is subjective and therefore provisional.

In the earthquakes of groups a, b, e, f, g, and j the positions of the A and C axes can be interchanged, as the S wave data of these shocks were not decisive. With such a change also the dextral part of the fault motion as given in Table I changes into a sinistral part, and a sinistral part of the fault motion into a dextral part. Also in ambiguous cases the solutions of Table I give the best accordance with the available S data.

The new solutions, quite like those of the former series of southeast Asian shocks, show an important preference for a single couple in the focus as the cause of the investigated shocks. There are 33 single couple shocks and 46 shocks in which the S wave data are insufficient for a decision. In half of these, however, the A- and C-axes can be distinguished if it is assumed that a single couple acted in the focus and not a double couple. These ratios are independent on the depth of the focus and on the magnitude of the shocks. Also in the solutions with thoroughly reliable positions of the nodal planes of longitudinal waves (groups f to g) this preference exists.

DIRECTIONS OF A, B, AND C AXES

General trends in the solutions of these shocks and of those of former series (Ritsema 1957) have been investigated.

To this end the complete solutions, i.e. the positions of the A, B and C axes have been considered together, and not the positions of the B axes or the A axes separately, because otherwise valuable information might be neglected.

Although the mechanisms of the earthquakes generally seem to be determined by local rather than regional influences, some system can be found in the solutions of an individual seismic zone.

Figure 1 shows the directions of A, B and C axes of the earthquakes of the Sunda arc. The general direction of the Sunda arc between Java and the Banda Sea is about west-east. B axes seem to be concentrated between two conic surfaces with an angle of 60° and with a common axis in north-south direction. Most A axes seem to be concentrated inside these conic surfaces, and most C axes outside the double cone with an angle of 30° and with the same direction of the axis. This distribution might point to the fact that the axis of these conic planes, or the normal to the plane that is in best accord with all B axes, represents the direction of the overall tectonic stress.

DIRECTIONS OF MAXIMAL PRESSURE

If only the longitudinal wave data are considered, the solutions might also be represented by the directions of maximal and minimal pressure, bisecting the angles between the normals of the two nodal planes. This is equivalent to Honda's model, in which the initial motions of P and S waves are determined by a double force couple in the focus. The S wave radiation pattern in this model is quadrantal and not two-lobed as in the single couple model.

TABLE I

The New Solutions

Date	Time	Epicenter	Depth	Magn.	A-axis	B-axis	C-axis	Type	Qual.
1933, Jun 24	21 54 38	5°S 104°1/4 E	Shal	7.5	N71E 40°	N290E 42°	N181E 20°	PL	i
1935, Nov 25	10 03 02	5 1/2 N 94 E	Shal	6 1/2	N264E 54	N33E 25	N135E 25	TL	d
1935, Dec 28	02 35 22	1/4 S 98 E	Shal	7.9	N18E 8	N272E 63	N112E 26	LP	i
1936, Aug 23	21 12 13	6 N 95 E	40 km	7.3	N26E 25	N265E 48	N133E 31	LP	i
1937, Jul 1	11 49 49	3 N 96 E	110 km	6.7	N45E 56	N290E 16	N190E 30	PL	d
1937, Aug 4	23 35 22	6 N 94 1/2 E	120 km	6	N68E 7	N320E 69	N161E 20	RT	h
1938, Aug 18	09 30 04	4 S 103 E	100 km	6.9	N90E 30	N197E 26	N320E 48	PR	i
1938, Aug 25	01 28 07	5 S 102 E	70 km	6.9	N10E 12	N132E 68	N276E 18	LT	h
1938, Nov 15	21 00 16	5 S 99 E	Shal	6 1/2	N100E 34	N251E 52	N0E 14	RP	i
1943, Jun 8	20 42 46	1 S 101 E	50 km	7.4	N214E 11	N307E 15	N90E 71	PL	c
1943, Jun 9	03 06 22	1 S 101 E	50 km	7.6	N214E 11	N307E 15	N90E 71	PL	c
1943, Nov 26	21 25 22	2 1/2 S 100 E	130 km	7.1	N14E 22	N264E 40	N125E 42	PL	h
1944, Jan 5	21 12 43	3 1/2 S 102 E	60 km	7.0	N24E 25	N247E 58	N123E 19	LP	e
1946, Mar 26	17 09 03	3 S 102 E	Shal	6.7	N201E 16	N347E 71	N108E 10	RP	i
1946, May 8	05 20 22	1/2 S 99 1/2 E	Shal	7.1	N26E 7	N128E 59	N292E 30	RP	h
1949, May 9	13 36 18	5 N 95 E	Shal	6.7	N125E 57	N286E 32	N21E 9	PR	h
1934, Apr 10	10 23 02	7 S 116 E	Shal	6 3/4	N280E 6	N125E 83	N10E 3	LP	d
1937, Sep 27	08 55 20	8 3/4 S 110 3/4 E	0.005 R	7.2	N211E 6	N318E 71	N119E 18	LT	i
1938, Feb 1	19 04 21	5 S 131 1/2 E	Shal	8.2	N141E 10	N300E 79	N50E 4	RP	g
1940, Mar 21	13 52 51	10 1/2 S 107 1/2 E	Shal	6 3/4	N158E 4	N287E 84	N68E 5	LT	h
1940, Mar 28	15 48 50	14 1/4 N 120 1/2 E	0.02 R	6 3/4	N50E 16	N180E 66	N315E 18	RP	g
1941, Jun 26	11 52 00	12 1/2 N 92 1/2 E	0.005 R	8.1	N146E 5	N56E 0	N326E 85	P	i
1942, Apr 8	15 40 24	13 1/4 N 120 1/2 E	Shal	7.7	N350E 2	N255E 70	N81E 20	LP	i
1942, Jul 29	22 49 13	2 3/4 S 127 3/4 E	Shal	7.0	N180E 40	N90E 0	N0E 50	T	d
1943, Apr 1	14 18 12	6 1/2 S 106 E	Shal	7.0	N186E 25	N84E 24	N315E 54	PL	c
1943, May 25	23 07 36	7 1/2 N 127 1/2 E	Shal	7.9	N128E 15	N271E 71	N35E 11	LT	h
1943, Nov 6	08 31 34	5 3/4 S 134 E.	Shal	7.6	N205E 26	N342E 56	N105E 20	LT	i
1944, Mar 31	02 51 44	5 1/2 S 131 E	0.005 R	7.0	N215E 20	N35E 70	N125E 0	L	d
1944, Apr 26	01 54 11	3/4 S 133 1/2 E	Shal	7.2	N184E 11	N60E 65	N279E 22	LP	g
1944, Apr 27	14 38 03	1 S 133 E	Shal	7.4	N25E 30	N246E 53	N127E 20	LP	c
1944, Nov 15	20 46 57	4 1/2 N 127 1/2 E	Shal	7.2	N35E 5	N125E 0	N215E 85	T	d
1945, Oct 16	16 03 02	0 123 3/4 E	0.005 R	7.1	N160E 26	N288E 52	N56E 26	RP	g
1946, Jan 17	09 39 36	6 1/4 S 147 3/4 E	0.01 R	7.2	N247E 15	N102E 72	N340E 10	RT	b
1947, May 27	05 58 52	1 3/4 S 135 1/2 E	0.01 R	7 1/4	(N199E 20	N342E 65	N104E 14	LT	i
					(N213E 36	N10E 52	N115E 12	LT	i
1948, Jan 24	17 46 43	11 N 122 E	Shal	8.2	N165E 12	N9E 77	N256E 5	RT	h
1948, Mar 1	01 12 24	3 S 127 1/4 E	Shal	7.5	N145E 30	N5E 53	N246E 20	LP	h
1949, Mar 27	06 34 01	3 1/4 N 127 3/4 E	Shal	7.0	N100E 10	N280E 80	N10E 0	L	h
1949, Apr 23	11 15 35	7 1/2 S 120 3/4 E	0.00 R	7.1	N45E 20	N135E 0	N225E 70	P	c
1949, Jun 24	22 38 36	6 1/4 S 105 3/4 E	0.005 R	7	N129E 45	N300E 45	N34E 4	PR	h
1949, Dec 29	03 03 54	18 N 121 E	Shal	7.2	N150E 26	N341E 64	N242E 4	LP	i
1950, Sep 19	20 29 48	2 S 138 1/2 E	Shal	6.9	N308E 34	N98E 52	N208E 15	LT	h
1950, Oct 8	03 23 09	4 S 128 1/2 E	Shal	7.6	N201E 14	N320E 63	N105E 23	LT	h
1950, Nov 2	15 27 56	7 1/2 S 129 E	0.03 R	7.5	N234E 30	N22E 56	N135E 15	LT	i
1950, Nov 8	02 18 12	9 3/4 S 159 1/2 E	Shal	7 1/4	N122E 4	N222E 68	N30E 22	RP	g
1951, Nov 29	04 45 43	1/2 N 120 1/2 E	Shal	6 1/2	(N329E 30	N147E 60	N238E 1	RP	b
					(N144E 35	N328E 55	N235E 2	LP	b
1952, May 8	21 10 40	2 1/2 N 127 E	Shal	6 3/4	N113E 4	N356E 81	N204E 8	LP	i
1952, Nov 6	19 47 20	5 S 145 1/2 E	Shal	7.3	N335E 10	N108E 76	N243E 10	RP	i
1952, Nov 28	21 01 27	6 1/2 S 155 1/2 E	0.01 R	6 3/4	N245E 12	N1E 64	N150E 23	LT	i
1952, Dec 24	18 39 38	5 1/2 S 152 E	Shal	7	N158E 5	N306E 84	N68E 3	LT	h
1953, Apr 23	16 24 17	4 S 154 E	Shal	7.6	N159E 16	N348E 74	N250E 2	RT	i
1954, Jul 2	02 45 09	13 N 124 E	Shal	7	N116E 2	N296E 88	N26E 0	L	i
1955, Mar 31	18 17 12	8 N 124 E	0.005 R	7 1/2	N182E 16	N312E 66	N87E 17	RP	h
1955, May 17	14 49 49	6 1/2 N 94 E	Shal	7 1/4	N116E 14	N304E 76	N207E 2	LP	i
1955, May 29	15 34 04	10 S 110 1/2 E	Shal	6 1/2	N210E 16	N339E 66	N115E 18	LT	i
1955, Sep 15	12 30 27	5 S 134 1/2 E	Shal	6 3/4	N40E 24	N278E 50	N145E 30	RT	i
1956, Feb 12	11 49 20	19 N 119 1/2 E	Shal	6 3/4	N150E 60	N32E 15	N295E 25	TR	i
1956, May 22	12 36 12	4 S 152 1/2 E	0.08 R	6 3/4	(N220E 20	N40E 70	N130E 0	L	i
					(N230E 30	N61E 59	N323E 5	LP	i
1957, Feb 10	22 32 15	10 N 126 E	Shal	6 3/4	(N295E 36	N148E 49	N38E 17	LP	i
					(N165E 12	N14E 77	N256E 6	RT	i
1957, Feb 10	22 50 52	10 1/2 N 126 1/2 E	Shal	6 3/4	N253E 2	N358E 84	N163E 6	LT	h
1957, Feb 11	01 14 44	10 N 126 E	Shal	6 1/2	N68E 0	N338E 87	N158E 3	L	h
1957, Mar 23	05 12 31	5 1/2 S 131 E	0.01 R	7	N24E 28	N252E 52	N128E 24	RT	i
1957, Apr 16	04 04 04	4 1/2 S 107 1/2 E	0.09 R	7 1/2	N48E 36	N298E 25	N182E 43	TR	i
1957, May 2	21 36 25	7 1/2 S 120 E	0.09 R	6 3/4	N43E 30	N288E 36	N161E 40	TR	h
1957, Jun 22	23 50 23	1 1/2 S 137 E	Shal	7.2	N143E 7	N323E 83	N53E 0	L	i
1950, Feb 28	10 20 55	46.0 N 143.8 E	0.04 R	7 3/4	N87E 20	N219E 61	N350E 20	RP	f
1950, Apr 26	07 04 55	33.7 N 135.8 E	0.00 R	6 3/4	N70E 70	N313E 10	N220E 18	TR	f
1950, May 17	11 46 48	39.4 N 130.3 E	0.08 R	6 3/4	N258E 43	N52E 46	N155E 13	RP	f
1950, Jun 7	16 52 34	4.5 S 77.0 W	0.01 R	7	(N65E 18	N312E 50	N168E 34	RT	f
					(N235E 32	N357E 40	N120E 33	LT	f
1950, Jul 9	02 35 29	7.9 N 72.6 W	Shal	-	N90E 5	N347E 70	N182E 20	LP	f
1950, Jul 13	04 03 59	28.0 N 139.6 E	0.08 R	6 3/4	N234E 10	N110E 73	N326E 14	RT	f
1950, Sep 10	03 21 22	35.5 N 140.4 E	Shal	7	N182E 25	N294E 40	N69E 40	PR	f
1950, Sep 16	21 58 17	52.0 N 177.1 E	0.01 R	6 1/2	N186E 30	N41E 54	N286E 17	RT	f
1950, Sep 22	23 53 32	17.6 S 177.1 W	0.06 R	7	N139E 6	N33E 68	N231E 21	LP	f
1950, Sep 29	06 32 13	18.9 N 107.0 W	Shal	7	N44E 0	N314E 88	N134E 2	L	f
1950, Oct 5	16 09 42	10.4 N 85.7 W	0.015 R	7 1/2	N180E 68	N28E 20	N295E 10	PL	a
1950, Oct 21	04 12 59	18.5 S 173.5 W	0.005 R	6 1/2	N170E 5	N274E 70	N78E 20	LT	f
1950, Oct 21	09 42 58	17.8 N 105.5 W	Shal	6 3/4	N312E 16	N75E 62	N215E 22	RP	f
1950, Nov 17	19 28 16	16.8 N 100.7 W	Shal	6 3/4	N185E 30	N95E 0	N5E 60	P	a
1950, Dec 14	01 52 53	19.7 S 175.9 W	0.03 R	8	N240E 8	N336E 39	N140E 50	TL	f

TABLE II

The reliability of the different earthquake groups.

Earthquake group	P and PKP data	S data		Number of shocks
a	sufficient for a solution, but small in number, or with an unfavourable distribution in azimuth and angle of departure from the focus	not used		2
b		not conclusive for a determination of the force system in the focus.	no discrimination of A and C axes possible	3
c			assuming that a single couple acted in the focus A and C axes can be distinguished	4
d		pointing to the single couple model		5
e		pointing to the double couple model		0
f	good	as in group a		13
g		as in group b		5
h		as in group c		19
i		as in group d		28
j		as in group e		0

If these stress directions of the shocks of the Sunda arc are plotted in a single diagram it appears that the maximal pressure component shows a tendency to an azimuth that is in agreement with the north-south direction derived for the direction of tectonic stress from Figure 1.

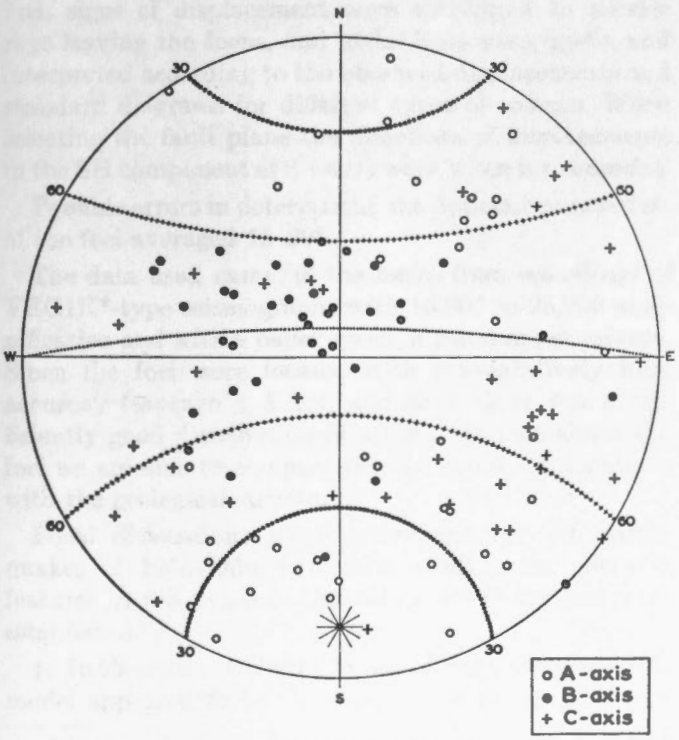

Figure 1. Wulff's stereographic projection of A, B and C axes of Sunda arc earthquakes.

* Scheidegger's catalogues of solutions have been used.

This method of plotting has not only been used for the solutions of southeast Asian and West Pacific shocks, but also to the known solutions of other Circum-Pacific seismic zones*). In most cases a broad azimuth could be selected in which the positions of the maximal pressure preferably are located. These general directions are shown in Figure 2.

In most island arcs the maximal pressure seems to occur in a direction that is about perpendicular to the local trend of the zone. Exceptions are the Tonga-Kermadec zone, the intermediate and deep earthquake zone of the Mariana's, and the shallow and intermediate earthquake zone of the Kuriles, where the maximal pressure has a strong component parallel to the local trend.

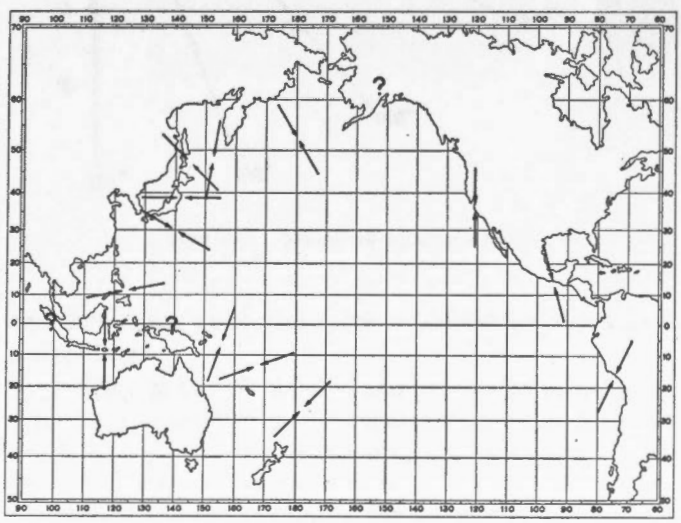

Figure 2. General directions of maximal pressure, provisionally determined from known earthquake fault plane solutions.

In the first region this component is consistent with the direction of motion along the Alpine fault of New Zealand.

In the marginal orogenic systems of the East Pacific maximal pressures in general seem to be directed in an acute angle with the zone, also with a sense that is consistent with geological data (San Andreas fault).

CONCLUSIONS

S wave data of southeast Asian and West Pacific earthquakes show that the majority of the shocks investigated can be considered as being caused by a single force couple in the focus. Some system can be found in the directions of the A, B and C axes of the solutions for various seismic zones.

Most of the fault-plane solutions of the earthquakes of other circum-Pacific seismic zones are only based on longitudinal wave data for which no difference exists between a single and a double force couple in the focus. If the earthquakes of these zones are considered to be caused by a double force couple in the focus or by an equivalent system of maximal and minimal pressures there is some evidence that the directions of maximal pressure are non-random.

It is understood that many more detailed studies should be made before definite conclusions can be reached.

References

RITSEMA, A. R., 1957. On the focal mechanism of southeast Asian earthquakes: *Dom. Obs. Pub.*, Ottawa, **20**, 341.

———, 1960. Focal mechanisms of some earthquakes of the year 1950: *Geophys. J.*, **3**, 307.

RITSEMA, A. R. and VELDKAMP, J., 1960. Fault-plane mechanisms of southeast Asian earthquakes: *Meded. e. Verh.* **76**, *Koninkl. Nederland. Meteor. Inst. De Bilt.*

VELDKAMP, J., 1957. Mechanism of shallow and intermediate earthquakes in Sumatra: *Koninkl. Nederland. Geol. Mijn. Genootschap Verh.* Geol. ser., **18**, 295.

———, 1959. Some Sumatra earthquakes: *Annali Geofis.*, **12**, 249.

Dislocations in Foci of the Tadzhik Depression

T. I. KUKHTIKOVA

Institute of Antiseismic Construction and Seismology, Academy of Sciences of Tashik S.S.R., Stalinabad

ABSTRACT

Focal mechanism was determined for 100 earthquakes which occurred in the Tadzhik depression during the period 1955-59. A dipole with moment was indicated as the appropriate mechanism in 98 cases; in the two remaining cases a single force was found. It was shown that the fault planes determined by seismic means agreed very well with surface faulting. It was also shown that a method which depended on studying the sequence of observations at a single station would have had no success in this area.

GENERAL SUMMARY OF THE STUDY

A study has been made of dislocations in earthquake foci of the most seismically active part of the Tadzhik depression (between 38.0°N and 39.0°N and between 68.5°E and 70.0°E). A few of the epicentres studied were located outside these limits, in southern spurs of the Hissar mountain range which borders the Tadzhik depression in this region.

Determination of dislocations in the foci was carried out after the method of KEYLIS-BOROK (GOTZADZE et al., 1957), using the initial movements of P and S waves of known nature. The displacement field was plotted in a stereographic projection, the centre of which was matched with the focus and the pole with the vertical line, signs of displacement were atrributed to seismic rays leaving the focus, and nodal lines were drawn and interpreted according to the observed displacements and standard diagrams for different types of sources. When selecting the fault plane the directions of displacements in the SH component of S waves were taken into account.

Possible errors in determining the dynamic parameters of the foci averaged 15–20°.

The data used came, in the main, from recordings of VEGIK*-type seismographs with 16,000 to 25,000 magnification and with a paper speed of 240 mm per minute. Since the foci were located with comparatively high accuracy (average ± 5 km) and since there was a sufficiently good distribution of seismic stations about the foci we are able to compare the determined dislocations with the geological structure.

Focal dislocations were determined for 100 earthquakes of 1955-1959, and as a result, some common features in the dynamic characteristics of the foci were established.

1. In 98 cases out of the 100 considered the appropriate model appeared to be the dipole with moment. In the two remaining cases the focus could be identified as a simple force.

2. Fault planes in the foci studied strike in different directions. Distribution of ruptures according to azimuth is shown in the vector diagram of Figure 1. The favoured direction is approximately ENE; a second lesser maximum is oriented close to the meridian.

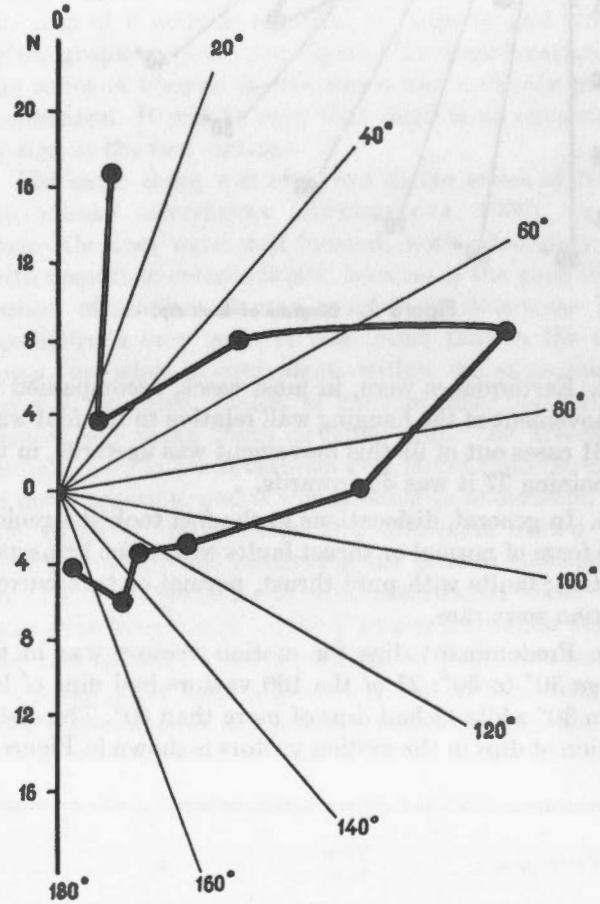

Figure 1. Direction of ruptures in foci.

* Vibrograph Electrodynamic Geophysical Institut Kirnos' design.

3. Fault dips are steep, dips from 40° to 80° dominating. Of 98 planes of rupture, 76 have dip angles > 40°. The distribution of rupture planes with dip is given in Figure 2.

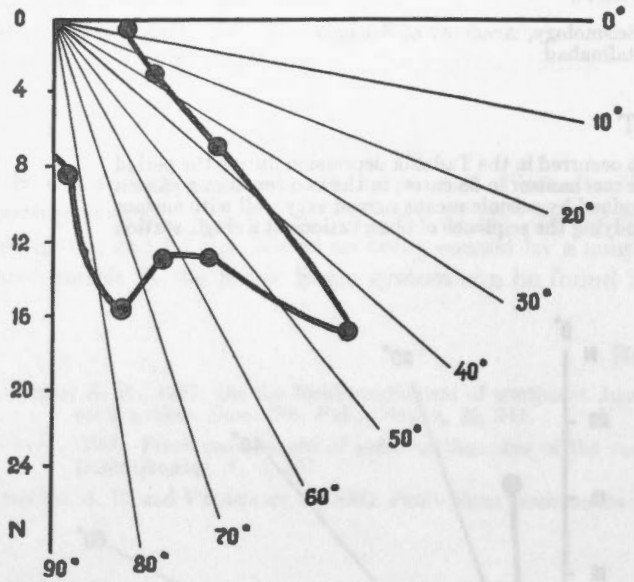

Figure 2. Diagram of fault dip.

4. Earthquakes were, in most cases, accompanied by a movement of the hanging wall relative to the foot wall; in 61 cases out of 98 this movement was upwards, in the remaining 37 it was downwards.

5. In general, dislocations in the foci took the geological form of normal or thrust faults with some transverse motion; faults with pure thrust, normal or transcurrent motion were rare.

6. Predominant dips for motion vectors was in the range 30° to 60°; 27 of the 100 vectors had dips of less than 30° while 14 had dips of more than 60°. The distribution of dips in the motion vectors is shown in Figure 3.

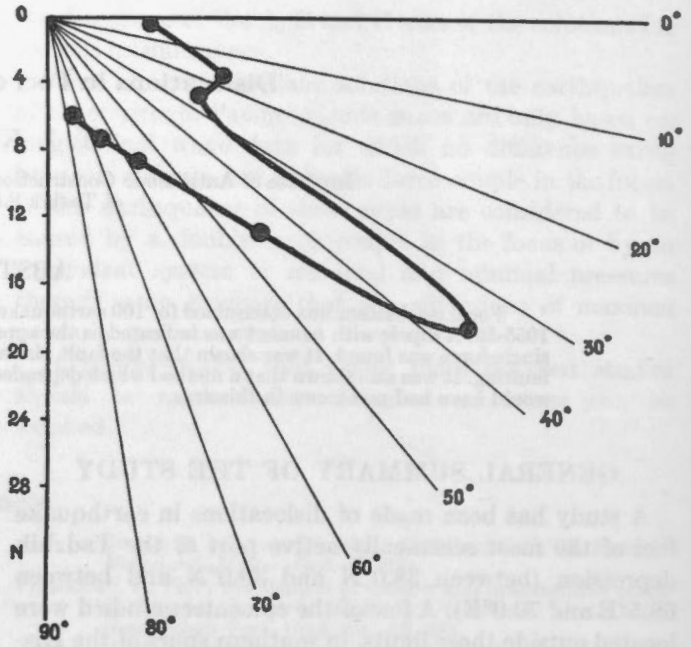

Figure 3. Diagram of vectors movement dip.

7. Different earthquakes connected with the same fault often showed movements of quite different character, ranging from pure transcurrent to pure thrust. However since relatively few foci were associated with any one fault it would be premature to judge whether any one type of motion predominated on a particular fault. Probably a longer period of observation would allow one to draw such a conclusion.

8. A study was made of the two strongest earthquakes of the region and of their aftershock sequences. These earthquakes are known as the Shurab earthquake, which occurred on August 21, 1955, and the Nurek earthquake, of September 22, 1956. Data on the earthquakes are given in the following table.

Earthquakes	Time h. m.	φ	λ	H km.	log Ej.	Number of determined dislocations in aftershocks.
Shurab.....	00.42	38° 36′	69° 40′	20	12–13	12
Nurek.....	15.54	38° 27′	69° 17′	3–4	13	30

For each sequence of earthquakes it was found that the orientation of the rupture plane was maintained throughout the sequence, and that, while the direction of motion varied widely, the relative vertical motion of the two sides of the fault was maintained. This is illustrated in Figure 4, which shows the nodal planes and the zones of compression and dilatation for the Shurab sequence. In the main shock and in 11 of the aftershocks the southeastern block rose, the northwestern block fell; in one aftershock this movement was reversed (Kukhtikova 1960).

9. In the regions of strong earthquakes weak fault movements, which cut the ruptures of the main earthquake at high angles, begin to reveal themselves. Hence,

for the accurate elucidation of the main seismo-genetic lines at depth systematic rather than random determination of focal dislocations should be carried out. This is of particular importance for regions where the seismogenetic ruptures are not expressed on the surface.

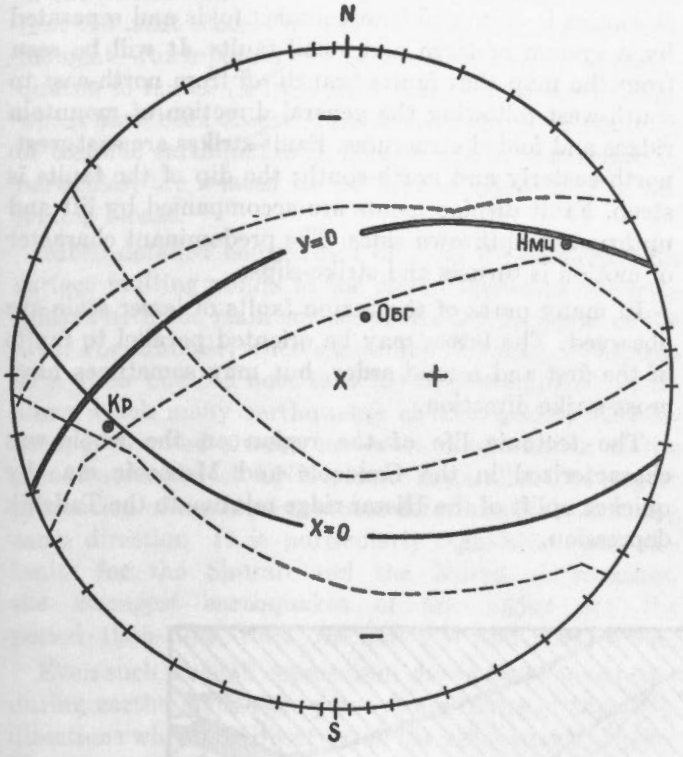

Figure 4. Systems of the main nodal lines in Shurab earthquake series.

P OBSERVATIONS AT A SINGLE STATION

The focal mechanism is determined for a very small percentage of earthquakes because of various reasons, theoretical or practical. Search for more simple ways of estimating if not the actual mechanism at least the direction of the tectonic processes long ago led seismologists to the idea of using observations of the initial P motions at a single station and to study the earthquakes of a particular region in this way. It was supposed that these results would allow one to judge the similarity or difference of focal mechanism and the general tendency of movements in large areas. Such an opinion was expressed in papers by a number of scientists, for example Somville (1925), Gutenberg and Richter (1938), Byerly and Evernden (1950) and Båth (1952).

It was noted that, although the foci in the Tadzhik depression were located within a limited space and were essentially identical in mechanism, the P wave did not always occur with the same sign at any particular seismograph station. This is illustrated in Table I which gives the sign of P arrivals recorded at Kara-Su and Nimich seismograph stations (see Figure 4 for their location) for the series of Shurab shocks which had a closely similar mechanism. It will be seen that there is no consistency of sign at the two stations.

The same thing was observed in the series of Nurek earthquake aftershocks (Kukhtikova, 1960). In this series the foci were well located, both absolutely and with respect to certain faults; because of the good distribution of stations it was possible to determine focal mechanisms very well. It was found that in the same focus (or, what is equivalent, within the same seismogenetic structure) planes of rupture and, particularly, movements along them deviated from one aftershock to the other. These deviations were larger than the errors of determination, and it was possible to understand how the zones of compression and dilatation varied considerably while still preserving the general character of the focal mechanism. It was abundantly clear that change in direction of initial P at any particular station did not indicate a major change in focal mechanism.

On the other hand a great number of essentially different mechanisms can produce waves of the same sign

Table I

No.	Date	Time h.m.	Coordinates of focus			Strike of fault plane	Initial movement in P	
			φ	λ	h, km.		Kara-Su	Nimich
1	21 Aug.	00.42	38°36′	69°40′	20	N70°E	−	+
2	21 Aug.	03.01	38°36′	69°40′	20	N75°E		−
3	21 Aug.	03.21	38°36′	69°40′	20	N68°E	−	+
4	21 Aug.	04.00	38°36′	69°40′	20	N66°E	+	
5	23 Aug.	09.03	38°36′	69°40′	20	N76°E	−	−
6	25 Aug.	13.32	38°36′	69°40′	20	N65°E	+	
7	25 Aug.	14.44	38°36′	69°40′	20	N76°E	−	
8	29 Aug.	19.40	38°37′	69°57′	15	N85°E	+	−
9	30 Aug.	10.49	38°36′	69°36′	35	N85°E	+	
10	2 Sept.	05.09	38°31′	69°46′	10	N66°E	−	−
11	2 Sept.	05.15	38°33′	69°45′	25	N66°E	−	−
12	7 Sept.	00.30	38°34′	69°35′	25	N66°E	+	
13	28 Sept.	09.17	38°34′	69°40′	35	N72°E	+	

at a particular point. In this case directions of initial P at a single station simply mean nothing. It makes sense only to observe them at a group of stations distributed in different azimuths.

CORRELATION WITH GEOLOGICAL FEATURES

Coordination of seismological and geological data is the question of particular interest. Therefore dislocations in the foci are compared with the main geological structures of the Tadzhik depression.

The region may be divided, on the basis of its tectonic structure, into two distinctly different regions, a northern and a southern one (MARKOVSKY, 1959; ZAKHAROV, 1958). The boundary between the northern and southern parts is expressed by a large regional fault which stretches westwards and far eastwards beyond the limits of the region in question. The strike of the fault, on the whole, is east-west, with local deviations. Fault displacements are expressed by thrusts and strike-slips; dips are steep (see Figure 5).

The northern part of the territory consists in general of Palaeozoic structures injected by granitic intrusives. The Palaeozoic complex is broken up by a system of large and small faults. The main directions of the faults are NW and EW.

The south part of the territory is covered by loose sedimentary Mesozoic-Cenozoic rocks. Their average thickness is about 5 to 7 km. All of the Mesozoic-Cenozoic thickness is crumpled into complex folds and separated by a system of large and small faults. It will be seen from the map that faults branch off from north-east to south-west following the general direction of mountain ridges and folded structures. Fault-strikes are east-west, north-easterly and north-south; the dip of the faults is steep. Fault displacements are accompanied by lift and upthrust of upthrown sides. The predominant character of motion is thrusts and strike-slips.

In many parts of the region faults of lesser scale are observed. The latter may be oriented parallel to faults of the first and second order, but may sometimes have cross-strike direction.

The tectonic life of the region on the whole was characterized in the Cenozoic and Mesozoic eras by quicker uplift of the Hissar ridge relative to the Tadzhik depression.

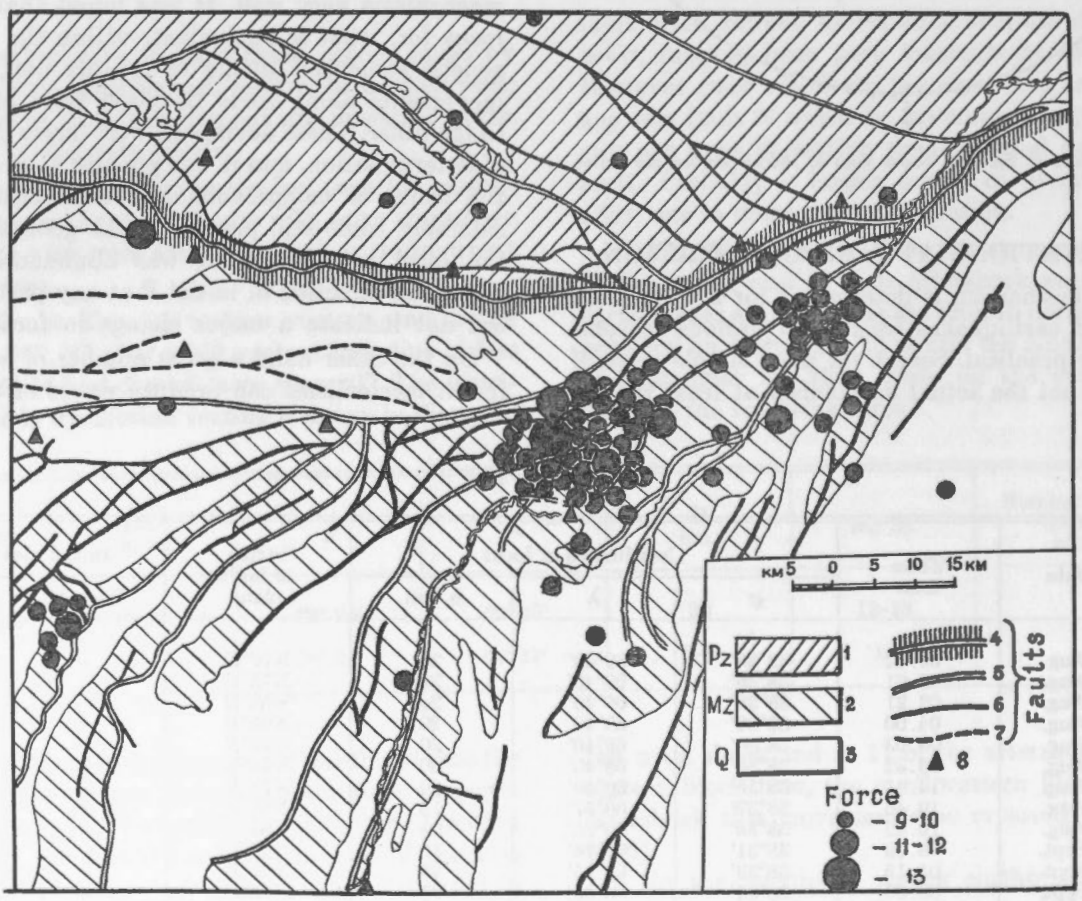

Figure 5. Distribution of the earthquakes analysed.

The epicentral zones of the area were shown by BUNE and REIMAN (1960) to be related to the Alpine faults of the Tadzhik depression. Relationship of earthquakes to folded structures and to recent folding is not as clear as the relationship between earthquakes and faults, at least in the present state of knowledge. It may be significant that the most successful source model is the dipole with moment, which points to a genetic relationship of earthquakes to faults. Sources with this type of mechanism, which have been observed in the overwhelming majority of tectonic earthquakes in general and in our region in particular, are related to the fault displacement of adjoining blocks.

More detailed comparison of focal dislocations with surface faulting points to the close connection of earthquakes with the main surface faults and ruptures of the area. For example, when examining the map of the area as a whole one can note that the largest regional break, along which many earthquakes of the region are distributed, is oriented almost east-west. Some faults of the second order stretch ENE and are in parallel. The largest proportion of the focal ruptures determined strike in the same direction. It is particularly significant that the faults for the Shurab and the Nurek earthquakes, the strongest earthquakes of the region for the period 1955-1959, were oriented EW and ENE-WSW.

Even such a rough comparison shows that movements during earthquakes take place along faults of the same directions which are observed in the main surface faults. However it is difficult to establish any predominant direction of surface faulting for the region as a whole because these directions differ in different parts of the region, and because the same fault can change its strike azimuth. The orientation of focal ruptures is also, at first sight, very irregular. For this reason a differential method was used to compare the predominant directions of surface faults and focal ruptures. The essence of this differential method is that ruptures in specific foci are compared with geological faults in the immediate vicinity.

The results of such a study for the earthquakes of the Tadzhik depression are shown in Figure 6. For this study the region was divided into small sections, in each of which the predominant direction of surface faulting was determined. Then the angle between the mean strike of the focal ruptures and the predominant strike of faulting was measured in degrees. The number of observations within consecutive 20° intervals measured from the observed fault direction (y axis) is plotted in the figure.

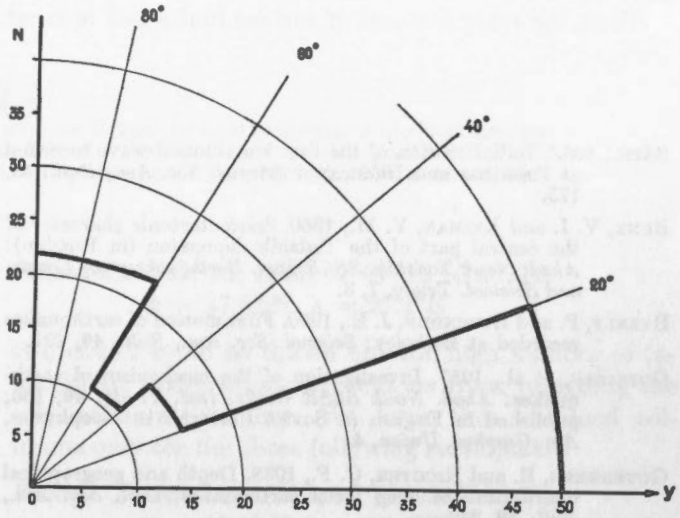

Figure 6. Direction of ruptures in foci relative to faults observed on the surface.

The figure shows:

a. Focal dislocations in the majority of epicentres lie close to the directions of the main geological faults;

b. In some cases focal movements take place in faults at right angles to the main faults. However these almost invariably correspond to the weaker earthquakes.

These conclusions are particularly interesting because they are based on systematic determinations using a high percentage of the earthquakes available. Usually the focal mechanism is determined for a very small percentage, perhaps one percent, of the earthquakes of a particular intensity. Under these circumstances it would be difficult to work out a correlation between focal ruptures and surface faulting (KUKHTIKOVA 1957). In the present example however focal mechanisms have been determined for 76 per cent of the whole number of earthquakes with intensity K9, where K = log Ej, which occurred in the years 1957-1958. The total numbers of earthquakes of the various classes, and the numbers processed, are shown in the following table.

Period	Class according to force											
	Total number						Earthquakes processed					
	9	10	11	12	13	Total	9	10	11	12	13	Total
1955–1956	54	33	7	5	1	100	19	5	1	2	1	28
1957-1958	64	17	8	2		91	46	16	6	1		69
1959								2	1			3

Further points of interest noted in the study included the facts that fault dips, both from geological and seismological evidence, are steep, and that movements in the foci have the same characteristics as the surface faults, i.e., thrusts and strike-slips.

Thus, the main features of surface faults and of focal ruptures were compared. The agreement in the direction of the faults and in the resemblance of the morphological and genetic features determined in this comparison leads to the conclusion that there is a close connection between the earthquakes of the Tadzhik depression and the faults strongly marked on the surface.

References

Båth., 1952. Initial motion of the first longitudinal wave recorded at Pasadena and Huancayo: *Seismol. Soc. Am., Bull.*, **42**, 175.

Bune, V. I. and Reiman, V. M., 1960. Seismotectonic character of the central part of the Tadzhik depression (in Russian): *Akad. Nauk Tadzhik. SSSR Inst. Earthquake-proof Constr. and Seismol. Trudy*, **7**, 3.

Byerly, P. and Evernden, J. E., 1950. First motion of earthquakes recorded at Berkeley: *Seismol. Soc. Am., Bull.*, **40**, 291.

Gotsadze, et al., 1957. Investigation of the mechanism of earthquakes: *Akad. Nauk SSSR Geofiz. Inst. Trudy*, **40**, 166; published in English *in* Soviet Research in Geophysics, *Am. Geophys. Union*, **4**.

Gutenberg, B. and Richter, C. F., 1938. Depth and geographical distribution of deep focus earthquakes: *Geol. Soc. Am., Bull.*, **49**, 249.

Kukhtikova, T. I., 1957. On the coordination of seismic and geological data (in Russian),: *Akad. Nauk Tadzhik SSSR Inst. Seismol., Trudy* **2**, 21.

———, 1960. Dynamic characteristics of the Nurek earthquakes (in Russian): *Akad. Nauk Tadzhik SSSR, Inst. Earthquake-proof Constr. and Seismol. Trudy*, **6**, 141.

Kukhtikova, T. I. and Barinova, A. Ya., 1960. Mechanism of foci in the Shurob earthquakes and their aftershocks (in Russian): *Akad. Nauk Tadzhik SSR Inst. Earthquake-proof Constr. and Seismol. Trudy*, **7**, 97-102.

Markovsky, A. P. (*Editor*), 1959. Geology of the U.S.S.R.: **24**, Tadzhik SSR, Leningrad.

Somville, O., 1925. Sur la nature de l'onde initiale des téléséismes enregistrés à Uccle de 1910 à 1924: *Bur. Central Séismol. Internat., Pubs.* Ser. A, **2**, 65.

Zakharov, S. A., 1958, Meso-Cainozoic structures of Tadzhik depression: *Akad. Nauk. Tadzhik SSR, Inst. Geol. Trudy, v.* 95.

Determination of the Mechanism of Some Anatolian Earthquakes

NEVZAT ÖCAL

Kandilli Observatory, Istanbul, Turkey

ABSTRACT

With the collaboration of J. H. HODGSON, the writer has used the BYERLY method to determine the focal mechanism of three strong Anatolian earthquakes which took place in 1957. For the first of these (in Fethiye, April 24, 1957) movement was vertical on a vertical plane. For the other two earthquakes (in Fethiye, April 25, 1957; in Abant, May 26, 1957) the movement was strike-slip.

INTRODUCTION

The original intention of this research had been to apply the BYERLY method to all the strong Anatolian earthquakes which occurred during the period 1938-1958. We wanted to study the problem of mechanism for the earthquakes in that area as a whole and, especially, to compare the characteristics of the solutions with the known properties of the north Anatolian seismotectonic line on which the foci are located. It was hoped that the results would lead to reliable conclusions on the accuracy of the method. Data were collected for 22 earthquakes but, unfortunately, they were too scanty in 16 cases and too confused in three others. Consequently solutions can be presented in only three cases.

It is assumed that the reader is familiar with the method which has been well described, for example, by BYERLY (1955) and HODGSON (1957). Solutions have made use of the Ottawa tables of extended distance.

PRESENTATION OF THE DATA

We obtained the necessary data on the character of the first P, PP or PKP motions for the 22 strong Anatolian earthquakes which occurred between 1938 and 1958, partly from the *Bulletin Mensuel* of the *B.C.I.S.* and partly from the replies received from several observatories to which questionnaires were sent. The information we obtained for 16 earthquakes out of the 22 was not sufficient to solve the problem. In the following two earthquakes

Kursunlu: Aug. 13, 1951; $18^h33^m36^s$ G.M.T.;
$\phi = 40.6°$N, $\lambda = 33.6°$E

Yenice-Gönen: March 18, 1953; $19^h06^m13^s$ G.M.T.;
$\phi = 40.1°$N, $\lambda = 27.3°$E

the distribution of C and D showed a great confusion in the projection planes so that the construction of the proper circles corresponding to the fault planes and the auxilliary planes was not possible. For the following earthquake

Söke-Balat: July 16, 1955; $07^h07^m12^s$ G.M.T.;
$\phi = 37.9°$ N, $\lambda = 27.1°$E

two circles could be drawn but the high number of inconsistent observations prevent us from regarding the solution as satisfactory. We have thus obtained solutions only for the three following earthquakes

Fethiye (I): April 24, 1957; $19^h10^m05^s$ G.M.T.;
$\phi = 36.0°$ N, $\lambda = 28.5°$E,

Fethiye (II): April 25, 1957; $02^h25^m36^s$ G.M.T.;
$\phi = 36.5°$N, $\lambda = 29.0°$E,

Abant: May 26, 1957; $06^h33^m30^s$ G.M.T.;
$\phi = 40.7°$ N, $\lambda = 31.2°$E.

Table I shows the data which were used for the three earthquakes. In this table there are six main columns. The first three show respectively the name and geographical coordinates of the stations from which the data were obtained. Each of the remaining three main columns, which include the data for the three earthquakes, are divided into three sub-columns. The first sub-column in each case shows the epicentral distances of the stations in degrees of arc, the second sub-column shows the azimuth angle of the stations with respect to the epicentre and the third sub-column shows the character of the first motion of the P, PP or PKP phases. The numbers which are next to the character symbols correspond to those in the diagrams, and one may thus easily find out which point in the projection corresponds to which station. The table gives information from 62 stations for Fethiye (I), from 68 stations for Fethiye (II) and from 70 stations for the Abant earthquake.

ANALYSIS OF THE DATA

Fethiye (I) earthquake, April 24, 1957

The solution for this earthquake is given in Figure 1 in terms of a vertical plane, which separates compressions to the northwest from dilatations to the southeast. There are a number of inconsistent observations; in the

TABLE I

Stations	φ	λ	Fethiye (I) 24.IV.1957			Fethiye (II) 25.IV.1957			Abant 26.V.1957		
			Δ°	Azim.	Obs.	Δ°	Azim.	Obs.	Δ°	Azim.	Obs.
Warszawa	52.2 N	21.0 E	17.1	N 16.0 W	C(1)	16.6	N 17.3 W	D(1)			
Monaco	43.7 N	7.4 E	17.8	N 57.9 W	C(2)	17.9	N 59.8 W	C(2)			
Stutgart	48.8 N	9.2 E	19.2	N 42.0 W	C(3)	19.0	N 43.0 W	C(3)			
Strasbourg	48.6 N	7.8 E	19.9	N 44.0 W	C(4)	19.7	N 45.3 W	C(4)	18.2	N 56.8 W	D(14)
Alger	36.8 N	3.0 E	20.4	N 80.1 W	C(5)	20.9	N 81.6 W	C(5)	22.2	N 91.5 W	D(15)
Clermont	45.8 N	3.1 E	21.5	N 55.0 W	C(6)	21.5	N 56.1 W	C(6)			
Hamburg	53.5 N	9.9 E	21.8	N 30.2 W	C(7)	21.6	N 31.8 W	C(7)	19.6	N 40.7 W	D(66)
Tamanrasset	22.8 N	5.6 E	23.9	N117.5 W	C(8)	24.4	N117.8 W	C(8)	27.9	N122.3 W	D(6)
Kew	51.5 N	0.3 W	25.5	N 43.9 W	C(9)	25.6	N 45.0 W	C(9)	24.1	N 52.8 W	D(16)
Cartuja	37.2 N	3.6 W	25.6	N 77.9 W	D(10)						
Malaga	36.7 N	4.4 W	26.3	N 79.0 W	D(11)	26.5	N 79.8 W	C(10)	27.8	N 87.0 W	D(50)
Quetta	30.2 N	67.0 E	32.4	N 88.8 E	D(12)	32.1	N 90.0 E	C(11)	30.5	N 98.7 E	C(65)
Lwiro	2.3 S	28.8 E	38.4	N179.5 W	D(13)	38.9	N179.7 W	D(12)	43.3	N176.3 W	C(45)
Reykjavik	64.1 N	21.9 W	40.8	N 30.6 W	D(14)	40.6	N 31.0 W	C(13)	38.2	N 34.2 W	D(68)
Tananarive	18.9 S	47.5 E	57.8	N158.7 E	C(15)	58.4	N159.1 E	C(14)			
Pretoria	25.8 S	28.2 E	62.0	N179.8 W	D(16)	62.5	N179.8 W	C(15)			
Kimberley	28.7 S	24.8 E	65.0	N176.7 W	D(17)	65.5	N176.0 W	D(16)			
Brébeuf	45.5 N	73.6 W	72.1	N 45.6 W	C(18)	72.1	N 45.7 W	C(17)			
Weston	42.4 N	71.3 W	72.5	N 49.5 W	C(19)	72.5	N 49.3 W	C(18)	71.0	N 50.0 W	D(18)
College	64.9 N	147.8 W	78.7	N 1.5 W	C(20)	78.3	N 1.2 W	C(19)	73.8	N 0.0 W	C(19)
Seattle	47.6 N	122.3 W	92.1	N 19.3 W	C(29)	91.7	N 18.8 W	C(26)			
Matsushiro	36.5 N	138.2 E	82.2	N 49.8 E	D(21)	81.5	N 49.8 E	D(20)	77.5	N 51.7 E	C(20)
San Juan	18.4 N	66.1 W	82.5	N 72.4 W	C(22)	82.6	N 72.1 W	C(21)	83.0	N 70.8 W	D(23)
Columbia	34.0 N	81.0 W	83.7	N 51.8 W	C(23)	83.8	N 51.6 W	C(22)	82.1	N 50.2 W	D(22)
Sitka	57.1 N	135.3 W	85.6	N 8.7 W	D(24)				81.2	N 7.0 W	D(21)
Rapid City	44.1 N	103.2 W	88.3	N 32.3 W	C(25)	88.1	N 31.9 W	C(23)			
Hungry Horse	48.3 N	114.0 W	89.2	N 23.9 W	C(25)	88.6	N 23.6 W	C(24)	84.9	N 21.9 W	D(24)
Butte	46.0 N	112.6 W	90.3	N 25.8 W	D(27)				87.0	N 21.8 W	D(25)
Bozeman	45.7 N	111.0 W	90.2	N 26.9 W	D(28)	89.9	N 26.5 W	C(25)	87.5	N 25.4 W	D(26)
Salt Lake City	40.8 N	111.8 W	94.5	N 28.9 W	C(30)	94.3	N 28.4 W	C(27)	91.3	N 26.8 W	D(27)
Eureka	39.5 N	116.0 W	97.0	N 26.7 W	C(31)	97.0	N 26.4 W	C(28)			
Boulder City	36.0 N	114.8 W	99.9	N 29.4 W	C(32)	99.7	N 28.9 W	C(29)	96.5	N 26.7 W	D(28)
Riverview	33.8 S	151.2 E	133.4	N104.7 E	C′(33) DD(33)	133.1	N103.8 E	D′(30) CC(30)			
Relizane	35.7 N	0.5 E				23.0	N 84.0 W	C(31)			
Pietermaritzburg	29.6 S	30.4 E				66.2	N178.8 E	D(32)			
Grahamstown	33.3 S	26.6 E				69.9	N177.9 W	C(33)			
St. Lucia	33.4 S	70.6 W				115.7	N113.7 W	C′(34)			
St. Vincent	13.2 N	61.3 W				82.1	N 79.1 W	C(35)			
Djakarta	6.2 S	106.8 E	84.0	N101.9 E	C(34)	83.6	N101.9 E	C(36)	83.0	N104.3 E	D(47)
Ukiah	39.1 N	123.2 W				99.8	N 21.6 W	D(37)			
Tucson	32.2 N	110.8 W				101.2	N 23.8 W	C(38)	98.0	N 31.7 W	D(30)
Fayetteville	34.1 N	94.2 W	91.2	N 44.0 W	C(35)	91.3	N 43.8 W	C(39)			
Witteveen	52.8 N	6.7 E	22.6	N 35.0 W	C(36)	22.5	N 36.5 W	C(40)			
Lisbon	38.7 N	9.2 W							31.0	N 80.2 W	D(51) DD(51)
Shasta	40.7 N	122.5 W	98.1	N 21.8 W	C(37)	98.0	N 21.4 W	C(41)			
Mt. Hamilton	37.3 N	121.6 W				101.0	N 23.5 W	C(42)	97.7	N 21.4 W	C(29)
Halifax	44.6 N	63.6 W	66.8	N 50.7 W	C(38)	64.6	N 51.9 W	C(43)	65.3	N 51.2 W	D(36)
Horseshoe Bay	49.4 N	123.3 W	90.7	N 17.9 W	C(39)	90.4	N 17.6 W	C(44)	86.5	N 16.0 W	D(37)
Kirkland Lake	48.1 N	80.0 W	74.2	N 41.0 W	C(40)	74.1	N 40.9 W	C(45)	72.2	N 40.4 W	D(38)
Ottawa	45.4 N	75.7 W	73.5	N 45.2 W	C(41)	73.5	N 45.1 W	C(46)	71.5	N 44.5 W	D(39)
Resolute	74.7 N	94.9 W	63.0	N 14.2 W	C(42)	62.6	N 14.1 W	C(47)			
Schefferville	54.8 N	66.7 W	63.4	N 39.3 W	C(43)	63.5	N 39.5 W	C(48)	61.5	N 40.2 W	D(54)
Shawinigan Falls	46.6 N	72.8 W	71.2	N 45.3 W	C(44)	71.2	N 45.2 W	C(49)	69.3	N 45.0 W	D(41)
Victoria	48.5 N	123.4 W	91.6	N 18.1 W	C(45)	91.3	N 17.8 W	C(50)	87.6	N 16.4 W	D(42)
Banff	51.2 N	115.6 W				86.7	N 21.3 W	C(51)			
Abuyama	34.9 N	135.6 E	81.9	N 52.3 E	D(46)	81.0	N 52.7 E	C(52)	77.1	N 54.5 E	C(58)
Kφbenhavn	55.7 N	12.4 E	22.5	N 23.8 W	C(77)	22.1	N 25.0 W	C(53)	19.5	N 32.6 W	D(33)
Lamont	41.0 N	73.9 W	74.5	N 49.4 W	C(48)	74.8	N 49.5 W	C(54)	73.5	N 49.3 W	D(43)
Rumangabo	1.3 S	29.4 E	37.5	N178.5 E	D(49)	37.9	N179.4 E	D(55)			
Shillong	25.6 N	91.9 E	54.2	N 82.0 E	D(50)	61.6	N 77.7 E	D(56)	51.7	N 87.1 E	C(62)
Nizamiah Obs.	17.4 N	78.5 E	47.7	N 99.2 E	D(51)	47.4	N100.0 E	D(57)	46.6	N105.7 E	D(64)
Hong Kong	22.3 N	114.2 E	73.3	N 74.0 E	D(52)	72.8	N 74.2 E	D(58)			
De Bilt	52.1 N	5.2 E	23.0	N 37.9 W	C(53)	22.8	N 39.0 W	C(59)	21.0	N 48.2 W	D(32)
Uppsala	59.9 N	17.6 E	24.7	N 12.5 W	C(54)	24.6	N 13.6 W	C(60)	19.2	N 18.8 W	D(3)
Kiruna	67.8 N	20.4 E	32.1	N 5.3 W	C(55)	31.8	N 5.7 W	C(61)			
Skalstugan	63.6 N	12.3 E	29.3	N 14.4 W	C(56)	29.0	N 15.0 W	C(62)			
Paris	48.8 N	2.5 E	22.8	N 47.8 W	C(57)	22.9	N 48.9 W	C(63)	21.8	N 58.5 W	C(2)
Scoresbysund	70.5 N	22.0 W	43.4	N 21.5 W	D(58)	43.1	N 22.0 W	C(64)	39.8	N 24.3 W	D(34)
Aberdeen	57.2 N	2.6 W	29.5	N 34.2 W	C(59)	29.4	N 34.8 W	C(65)			
Melbourne	37.8 S	145.0 E	122.4	N115.3 E	DD(60)	129.8	N112.0 E	D′(66)	129.5	N109.9 E	D′(56) CC(56)

TABLE I—(Concl.)

Stations	φ	λ	Fethiye (I) 24.IV.1957			Fethiye (II) 25.IV.1957			Abant 26.V.1957		
			Δ°	Azim.	Obs.	Δ°	Azim.	Obs.	Δ°	Azim.	Obs.
Rathfarnham	53.3 N	6.3 W	29.4	N 43.5 W	C(61)	29.4	N 44.0 W	C(67)	28.0	N 50.7 W	D(17)
Cleveland	41.5 N	81.5 W	78.9	N 45.5 W	C(62)	79.0	N 45.4 W	C(68)	77.4	N 45.0 W	D(49)
Pavia	45.2 N	9.2 E							16.7	N 68.0 W	D(1)
Jena	50.9 N	11.6 E							17.0	N 47.5 W	D(5)
Neuchâtel	47.0 N	7.0 E							18.4	N 62.0 W	D(7)
Basel	47.5 N	7.6 E							18.1	N 60.2 W	D(8)
Athens	38.0 N	23.7 E							6.4	N112.0 W	C(9)
Belgrade	44.8 N	20.5 E							8.7	N 58 W	D(10)
Jerusalem	31.8 N	35.2 E							9.5	N159 E	D(11)
Messina	38.2 N	15.2 E							12.6	N 96.0 W	D(12)
Roma	41.9 N	12.5 E							14.1	N 79.8 W	D(13)
Ravensburg	47.8 N	9.6 E							17.1	N 58.2 W	D(44)
Morgantown	39.6 N	80.0 W							77.6	N 47.2 W	D(70)
Pasadena	34.1 N	118.2 W							99.7	N 25.4 W	D,DD (31)
Ksara	33.8 N	35.9 E							7.9	N151.0 E	D(46)
Prague	50.1 N	14.4 E							15.3	N 45.6 W	D(48)
Fresno	36.7 N	119.8 W							98.0	N 23.3 W	D(52)
Mineral	40.3 N	121.6 W							95.0	N 20.5 W	C(53)
Saint Louis	38.6 N	90.2 W							83.9	N 41.8 W	D,CC (35)
Seven Falls	47.1 N	70.8 W							67.9	N 45.7 W	D(40)
Toledo	39.9 N	4.0 W							26.6	N 80.1 W	D(55)
Vienna	48.3 N	16.4 E							13.0	N 49.7 W	D(57)
Manila	14.7 N	121.1 E							80.2	N 79.0 E	C(59)
Bogota	4.6 N	74.1 W							98.2	N 76.4 W	C(60)
Poona	18.5 N	73.3 E							42.2	N109.5 E	D(61)
La Paz	16.5 S	68.1 W							107.4	N 97.1 W	DD(63)
Moscow	55.7 N	37.6 E							15.5	N 13.2 E	C(67)

TABLE II

The Solutions of Mechanism of Anatolian Earthquakes

Earthquake			Circle *a*					Circle *b*					Author
Date	φ N	λ E	Strike Direction	Dip Direction	Dip Angle	Strike Component	Dip Component	Strike Direction	Dip Direction	Dip Angle	Strike Component	Dip Component	
13 Aug. 1951	42.0°	33.0°	N70°E	N20°W	80°	0.969	0.246	N17°W	N73°E	76°	0.984	0.179	Karapetyan
20 Oct. 1951	43.0°	32.5°	N11°E	S79°E	84°	0.292	0.956	—	—	18°	—	—	Karapetyan
16 July 1955	37.5°	27.0°	N40°E	N50°W	84°	0.998	0.070	N50°W	N40°E	84°	0.995	0.104	Hodgson & Cock
9 July 1956	37°	26°	N43°E	N47°W	72°	0.798	0.603	N62°W	S28°W	55°	0.921	0.377	Hodgson & Stevens
24 Apr. 1957	36.5°	29.1°	N29°E	N51°W	90°	0	1.000	—	—	—	—	—	Öcal
25 Apr. 1957	36.5°	28.9°	N52.5°E	S37.5°E	87.5°	0.882	0.470	N36.5°W	N53.5°E	62°	0.999	0.044	Öcal
26 May 1957	40.6°	31.2°	N78.5°E	S11.5°E	74.5°	0.999	0.052	N12.5°W	N77.5°E	87°	0.964	0.267	Öcal

northwest sector Cartuja (10) Malaga (11), Reykjavik (4), Sitka (24), Butte (27) and Bozeman (28); in the southeast sector Tananarive (15), Riverview (33) and Djakarta (34). The plane need not, in fact, be exactly vertical. It could be dipping in either sense at a steep angle and may deviate in strike by ±20° from the indicated position which has simply been taken as the best average. There is no control for drawing a second circle, but it is quite clear from the near approach of the observation points to the line that the second circle must be very small, indicating that its normal is approximately vertical.

The "average" plane drawn strikes N 29° ± 20° E. Assuming that it represents the fault, motion on it is

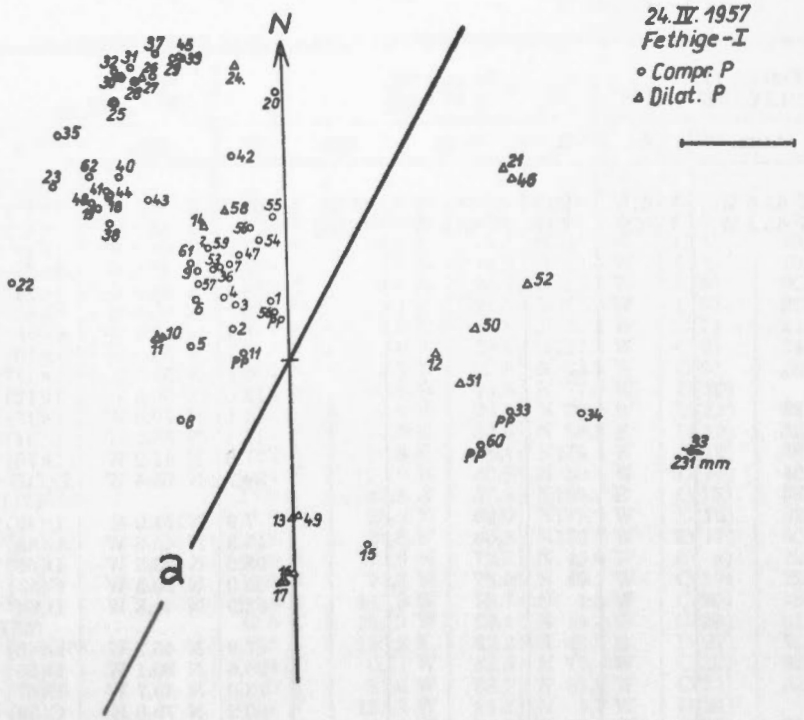

Figure 1.

vertical so that the strike component of motion is zero, the dip component is ± 1.00. The NW block has sunk with respect to the SE block.

Fethiye (II) earthquake, April 25, 1957.

The solution is shown in Figure 2. Circle *a* has been drawn with sufficiently large radius to include the PKP observations of Riverview (30) and Melbourne (66), and circle *b* is drawn to include Warsaw (1) and Quetta (11) in the overlap of the two circles. Inconsistent observations are Matsushiro (20), Tananarive (14), Pretoria (15), Grahamstown (33) and Djakarta (36).

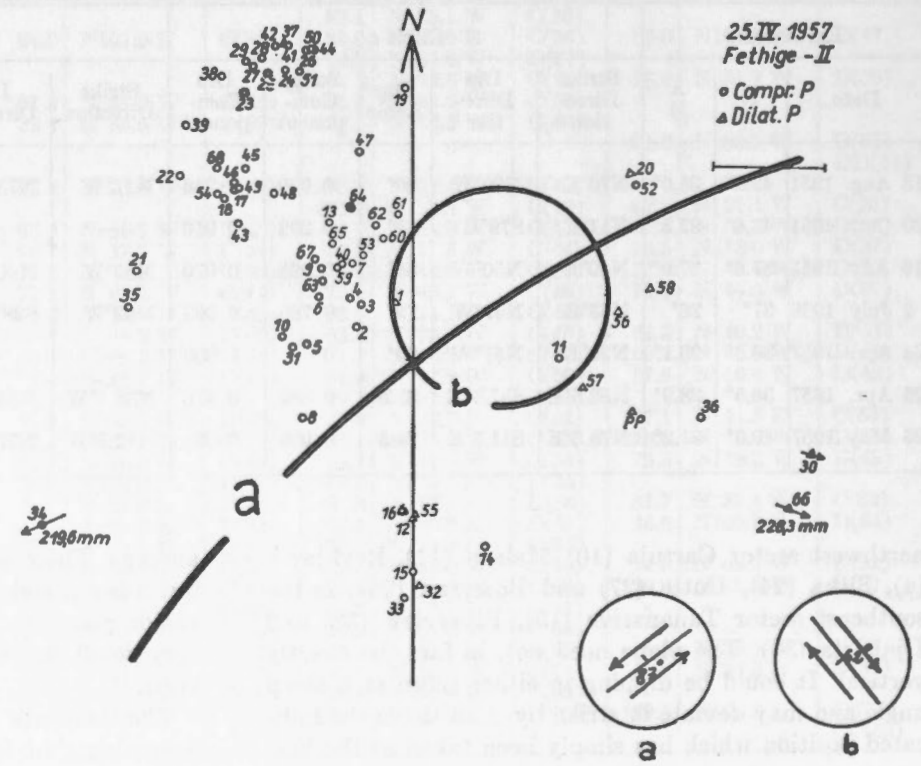

Figure 2.

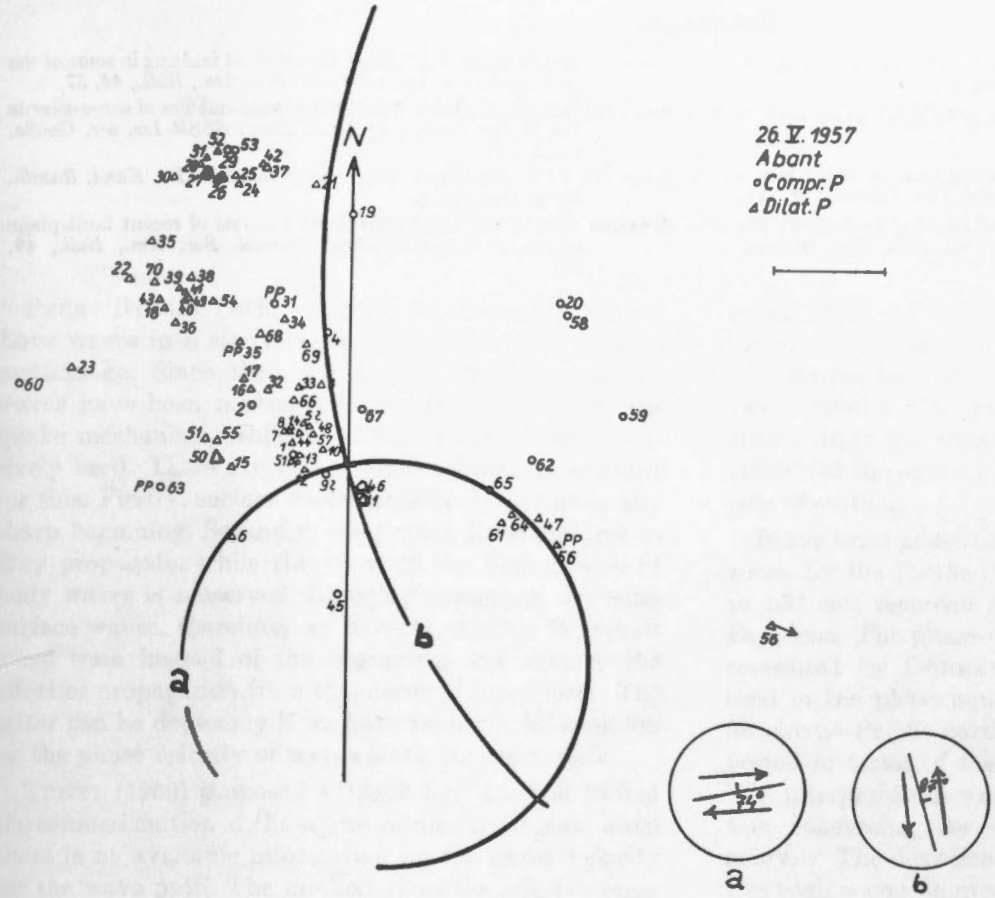

Figure 3.

If circle *a* is taken to represent the fault strikes N 52.5° E and dips at an angle of 87.5° in a direction S 37.5° E. The strike component of a unit vector drawn in the direction of motion is 0.883, the dip component is 0.469. Because the strike component is bigger than the dip component the fault has a strike-slip or transcurrent character. If circle *b* is taken to represent the fault, then the fault strikes N 36.5° W, and dips 62° in a direction N 53.5° E. The strike component of the motion is 0.999, the dip component is 0.044; again the fault has a strike-slip character.

Abant earthquake, May 26, 1957

The solution for this earthquake is shown in Figure 3. Circle *a* is very closely defined by Nizamiah observatory (64) and Quetta (65); circle *b* is equally well defined by Kiruna (4) and Sitka (21). Tamanrasset (6) and Athens (9) lie right on the line, so that their observations can be considered as correct. Paris (2), Mount Hamilton (29), Mineral (53), Melbourne (56) and Bogota (60) are inconsistent with our solution but these do not appear to be serious.

If circle *a* is taken to represent the fault plane, the fault strikes N 78.5° E and dips at an angle of 74.5° in a direction S 11.5° E. The strike component of a unit motion vector is 0.999, the dip component is 0.062. Since the strike component is larger than the dip component the fault is strike-slip. If circle *b* is taken to represent the fault plane, the fault strikes N 12.5° W and dips at an angle of 87° in a direction N 77.5° E. The strike component of motion is 0.964, the dip component is 0.267; again the faulting is strike slip.

DISCUSSION

We do not have any macroseismic observations about the fault for the first two earthquakes, because their centres are under the sea. For the Abant earthquake the azimuth of the fault, from macroseismic observations, is found to be approximately N50° to 60°E (Öcal, 1959). It would appear that circle *a* represents the valid fault plane.

Several seismologists have made studies of Anatolian earthquakes. All available solutions have been summarized in Table II, the data having been taken from the summary of Scheidegger (1959). In addition it should be mentioned that Hodgson and Storey (1954) attempted a solution for the Izmir-Karaburun earthquake of July 23, 1949, but were unable to obtain one because of the conflict of data.

In conclusion, I should like to express my sincere appreciation and gratitude to Dr. J. H. Hodgson, of the Seismological Division of the Dominion Observatory, Ottawa, who helped me a great deal in making the solution diagrams while I was working on this project.

References

Byerly, P., 1955. Nature of faulting as deduced from seismograms: *Geol. Soc. Am.* Spec. Paper No. 62, 75.

Hodgson, J. H., 1957. Nature of faulting in large earthquakes: *Geol. Soc. Am., Bull.*, **68**, 611.

——— and Cock, J. I., Direction of faulting in some of the larger earthquakes of 1954-1955: *Pub. Dom. Obs.*, Ottawa, **19**, 221.

——— and Stevens, A. E. Direction of faulting in some of the larger earthquakes of 1955-1956: *Pub. Dom. Obs.*, Ottawa, **19**, 281.

——— and Storey, R. S., 1954. Direction of faulting in some of the earthquakes of 1949: *Seismol. Soc. Am., Bull.*, **44**, 57.

Karapetyan, N. K., 1958. The dynamic parameters of some seismic foci in the Caucasus: *Akad. Nauk SSSR Izv.* ser. Geofiz, no. 2, 260.

Öcal, N., 1959. 26. Mayis. 1957 Abant zelzelesi: *Ist. Kand. Rasath. Sism. Yay*, no. 4.

Scheidegger, A. E., 1959. Statistical analysis of recent fault-plane solutions of earthquakes: *Seismol. Soc. Am., Bull.*, **49**, 337.

The Use of Long-Period Surface Waves in the Study of Earthquake Mechanism*

KEIITI AKI**
Seismological Laboratory, California Institute of Technology, Pasadena, California

PERRY BYERLY (1930) tried to use the first motion of Love waves in a study of the mechanism of a Chilean earthquake. Since then, for almost 30 years, surface waves have been neglected in the study of the earthquake mechanism, while body waves have been extensively used. There are two obvious reasons to account for this. Firstly, surface waves usually do not have any sharp beginning. Secondly, their wave form changes as they propagate, while the sense of the first motion of body waves is conserved through propagation. In using surface waves, therefore, we have to observe the whole wave train instead of the beginning, and remove the effect of propagation from the observed wave form. The latter can be done only if we have accurate information on the phase velocity of waves along the wave path.

TUKEY (1959) proposed a 'black box' method to find the sense of motion at the source of an earthquake, when there is no available information on the phase velocity for the wave path. The method gives the relative sense of motion to that of a standard earthquake which has the epicentre close to that of the earthquake in question. This method is effective for earthquake swarms or aftershocks, and is successfully applied by AKI (1960a) to Love waves of California and Nevada shocks.

With the rapid progress in the study of propagation of surface waves in theory and practice, we are now able to remove the effect of propagation from the individual record of Rayleigh and Love waves of a certain period range for a certain wave path. The method is simply to subtract the amount of theoretical phase delay of a certain Fourier component, due to propagation from the actual phase delay of that component. Various techniques are devised; a Fourier method by SATÔ (1955, 1956), a stationary phase method by BRUNE, NAFE and OLIVER (1960), and a cross-correlation method by AKI (1960b).

We applied our method to Love waves (period 10 to 50 sec) of the North American paths, and showed that the earthquake source is a double couple rather than a single couple (AKI, 1960b). Rayleigh waves in the period range 15 to 60 sec were also studied, and the source motions found from Rayleigh waves were in agreement with the fault-plane solutions obtained from P wave data (AKI, 1960b). The phase-velocity curves used in the above study are those obtained by EWING and PRESS (1959) for the entire United States from many tripartite nets of stations.

In the third paper (AKI, in press), we studied Rayleigh waves for the Pacific Ocean paths in the period range 35 to 150 sec, recorded at the Seismological Laboratory, Pasadena. The phase-velocity curve for the model 8099 computed by DORMAN, EWING and OLIVER (1960) is used in the phase equalization. The source function of 53 circum-Pacific earthquakes are obtained, and interpreted in terms of the direction of force at the source. The interpretation was checked by additional information concerning the earthquake as well as an error analysis. The direction of horizontal force deduced from Rayleigh waves showed a systematic, geographic distribution, which favors BENIOFF'S (1957) and ST. AMAND'S (1957) hypothesis that right hand strike-slip prevails throughout the circum-Pacific earthquake belt. The vertical forces are found to be mostly directed upward on the oceanic side.

In interpreting the source function, we adopted the following assumptions:

(1) Since equalization removes the phase delay due to the dispersive medium and yields the source function, the theory of Rayleigh wave generation in the homogeneous half space can be used to interpret the source function.
(2) The force exerted at the source is a step function in time.
(3) The source is not a singlet, but a single couple or a double couple.
(4) The earthquake focus is shallow.
(5) The effect of the finiteness of the fault at the source is neglected.

In our latest paper (AKI, in preparation), we obtained the source functions from the records of many IGY stations for three Pacific earthquakes, and found a force pattern at the source of each earthquake which is consistent with the third assumption given above. The pattern is quadrant and represents right hand strike-slip

* Publications of the Division of the Geological Sciences, California Institute of Technology, Pasadena, California, Contribution No. 990.
** On leave from the Earthquake Research Institute, Tokyo, Japan.

with the strike parallel to the trend of seismic zone for all of the earthquakes.

In analyzing the records of IGY stations, we made extensive use of a program written by AKI and NORDQUIST (in press). The program computes an impulse response seismogram of Rayleigh waves for a given epicentre and a given station entirely automatically on the Bendix G-15D electronic computer at the Seismological Laboratory, Pasadena.

The earth's surface is divided into three regions; the Atlantic Ocean (includes the Indian and other oceans, excludes the Pacific), the Pacific Ocean, and the continents.

For the Pacific Ocean, we use the phase-velocity curve for the model 8099; for the Atlantic Ocean, we used the curve which may correspond to a slightly modified model 8099; and for the continents, we used the one corresponding to Lehmann's model mantle computed by DORMAN and others (1960) for the long-period branch, combined with PRESS' curve (1960) for the short-period branch.

References

AKI, K., 1960a. The use of Love waves for the study of earthquake mechanism: *J. Geophys. Res.*, **65**, 323.

AKI, K., 1960b. Study of earthquake mechanism by a method of phase equalization applied to Rayleigh and Love waves: *J. Geophys. Res.*, **65**, 729.

AKI, K., 1960. Interpretation of source functions of circum-Pacific earthquakes obtained from long-period Rayleigh waves: *J. Geophys. Res.*, **65**, 2405.

AKI, K., and NORDQUIST, J. M. 1960. Automatic computation of impulse response seismograms of Rayleigh waves for mixed paths: *Seismol. Soc. Am. Bull.*, **51**, 29.

AKI, K., 1961. The pattern of the force at some earthquake sources obtained from long-period Rayleigh waves: (in preparation).

BENIOFF, H., 1959. Circum-Pacific tectonics: *Dom. Obs. Pub.*, Ottawa, **20**, 395.

BRUNE, J., NAFE, J. and OLIVER, J., 1960. A simplified method for the analysis and synthesis of dispersed wave trains: *J. Geophys. Res.*, **65**, 287.

BYERLY, P., 1930. Love waves and the nature of the motion at the origin of the Chilean earthquake of November 11, 1922: *Am. J. Sci.*, **19**, 274.

DORMAN, J., EWING, M., and OLIVER, J., 1960. Study of shear-velocity distribution in the upper mantle by mantle Rayleigh waves: *Seismol. Soc. Am. Bull.*, v. **50**, 87.

EWING, M. and PRESS, F., 1959. Determination of crustal structure from phase velocity of Rayleigh waves Part III; the United States: *Geol. Soc. Am. Bull.*, **70**, 229.

PRESS, F., 1960. Crustal structure in California-Nevada region: *J. Geophys. Res.*, v. **65**, 1039.

SATÔ, Y., 1955-56. Analsyis of dispersed surface waves by means of Fourier transform I, II and III: *Earthquake Res. Inst. Bull.*, Tokyo, **33**, 33, 1955; **34**, 9 and 131, 1956.

ST. AMAND, P. 1959. Circum-Pacific orogeny: *Dom. Obs. Pub.*, Ottawa, **20**, 403.

TUKEY, J. Equalization and pulse shaping techniques applied to the determination of initial sense of Rayleigh waves: *in* L. W. Berkner, *Chairman*, Report on a Panel of Seismic Improvement, Appx. 7, 1959.

Radiation Pattern of Rayleigh Waves from the Southeast Alaska Earthquake of July 10, 1958*

JAMES N. BRUNE

Lamont Geological Observatory, Columbia University, Palisades, N.Y., U.S.A.

Long-period Rayleigh wave data obtained during the IGY are used in this paper to measure the initial phases and amplitudes of Rayleigh waves as a function of azimuth for the Southeast Alaska earthquake of July 10, 1958. This study indicates that the radiation pattern bears a simple relation to the fault motion, showing four sectors of initial phase and a four-lobed pattern of amplitudes. The symmetry of the radiation pattern is in agreement with the motion on the fault as determined by a fault-plane solution and by field observation of the direction of faulting. The symmetry differs radically from that expected from explosions. It is concluded that this simple technique can be used to study focal mechanism from surface wave data for most of the larger earthquakes when instrumentation is improved and regional variations in phase velocity for shorter periods are known.

INTRODUCTION

In this paper phase velocity measurements are reported and are used to study initial phase as a function of azimuth for Rayleigh waves radiated from the Southeast Alaska earthquake of July 10, 1958. Amplitudes are also determined as a function of azimuth. The error in initial phase determination is estimated to vary from $\pi/5$ at distances less than 40,000 km to $\pi/2$ at distances greater than 60,000 km. The study indicates that the radiation pattern of Rayleigh waves is closely related to the motion of the fault, and that study of the radiation patterns of numerous earthquakes to obtain information about earthquake mechanism is feasible.

It has been shown by several authors that information about the source motion may be obtained from a train of surface waves provided the phase velocities of the waves are known (SATÔ, 1955, 1956; BRUNE, NAFE and OLIVER, 1960; AKI, 1960b, 1960c). Knowledge of phase velocity is implied in the equalization method of TUKEY (1959). The use of surface waves in studies of earthquake mechanism will be an important supplement to similar studies based on body waves and in addition will make many smaller earthquakes amenable to mechanism studies. The method of BYERLY (cf. BYERLY, 1955) is based on the observed quadrant distribution of initial motion of P waves. The value of this method has been confirmed by actual field observation which showed that the direction of motion was generally in agreement with that indicated by the fault-plane solution. STAUDER (1960) has recently made use of the plane of polarization of S waves to study earthquake mechanism. He has shown that it is possible to eliminate the ambiguity between the fault plane and the auxiliary plane using S waves and also that it may be possible to decide whether the double couple or the single couple is the more appropriate model for the majority of earthquakes as far as symmetry is concerned. Love waves will also be important in deciding which of these two models is more appropriate (AKI, 1960a, 1960b).

The method used in this paper may be applied without the use of electronic computing machines. The simple algebraic operations necessary may easily be performed on a hand calculator. Thus it is possible for investigators at seismograph stations which do not have electronic computers available to study the initial phases of surface waves. This should lead to a greatly increased knowledge of earthquake mechanism and tectonic forces in various parts of the world.

METHOD

The object of this paper is to measure initial phase, ϕ_a of Rayleigh waves at the origin ($x = 0$) from observations of phase ϕ_b, period T and time t obtained from seismograms. This is done by the method presented in an earlier paper (BRUNE, NAFE, and OLIVER, 1960). The method is briefly summarized in the following paragraph. For a more detailed description of the method the reader is referred to the original paper.

Ground motion resulting from the passage of a Rayleigh wave is regarded as a superposition of spectral components. Phase velocity is the velocity of propagation of a spectral or Fourier component of a given frequency. Points of like phase (peaks, for example) on an infinite sinusoidal Fourier component are separated in space by an integral number of wavelengths at any given time and separated in time by an integral multiple of the period at any given distance. If at two stations along the path of propagation at distances X_a and X_b we select certain phases ϕ_a and ϕ_b at times t_a and t_b on an infinite sinusoidal Fourier component of period T the following relation may be written:

$$C = X/(t - nT) \qquad n = \frac{\phi_b - \phi_a}{2\pi} + N \text{.....(1)}$$

where C is the phase velocity, X the distance $X_b - X_a$, t

*Lamont Geological Observatory Contribution No. 478.

the difference in time $t_b - t_a$ and N is an integer which must be determined. The phase ϕ_a at a given distance X_a and time t_a is defined so that the displacement is of the form $\cos[\omega(t-t_a) + \phi_a]$. Thus at a given distance the phase is zero at times t_a when the displacement is a maximum and is postive if the maximum displacement occurs slightly earlier.

When the wave train involved is sufficiently dispersed, the stationary phase approximation may be used to determine the phase at a given time and distance without resorting to direct Fourier analysis provided the $\pi/4$ phase correction, or the $T/8$ time correction due to dispersion, is made. The sign of this correction depends on whether the dispersion is normal or inverse (*see* BRUNE, et al., 1960).

To determine the initial phases of surface waves the station a is considered to be the epicenter at zero distance. The initial phase is to be determined from observations of T_b, t_b and ϕ_b at a given distance, the phase velocity being known. The relation (1) is also used to measure phase velocity. In this case the station a is not the epicenter but one of two stations along a path of propagation. In order to determine phase velocity observations of ϕ_a and ϕ_b at times t_a and t_b and distances X_a and X_b are made. The integer N is determined by using pairs of stations with different spacing (*see* NAFE and BRUNE, 1960).

COMPARISON WITH FOURIER ANALYSIS

As a check on the stationary phase approximation, results from it were compared with those obtained by Fourier analysis on an IBM 650 computer. The Rayleigh wave train R_4 recorded at Honolulu from the Southeast Alaska earthquake of July 10, 1958 (Figure 1) was digitalized by reading amplitudes at 1-second intervals for 45 minutes following an arbitrary time t_0 indicated on the record. A Fourier analysis was performed using a program for the IBM 650 prepared by M. LANDISMAN. The results of both the Fourier analysis and stationary phase analysis are shown in Figure 2. Amplitudes determined by Fourier analysis are shown at the top of the figure. The Fourier analysis yielded the phase angle of each spectral component with respect to t_0. The quantity, $-\phi T/2\pi$, the time after t_0 when a crest of the Fourier component with period T arrives at the station, (column 3, Table IV), is plotted in Figure 2 as a function of T. A stationary value of $-\phi T/2\pi$ means that the Fourier components of period near T will be in phase as peaks at the station at time $\phi T/2\pi$ after t_0 , and thus the group of energy of period T will arrive at this time (see NAFE and BRUNE, 1960, Figures 1 and 2).

Any multiple of 2π could be added to all the values listed for ϕ, giving other curves such as the solid curve

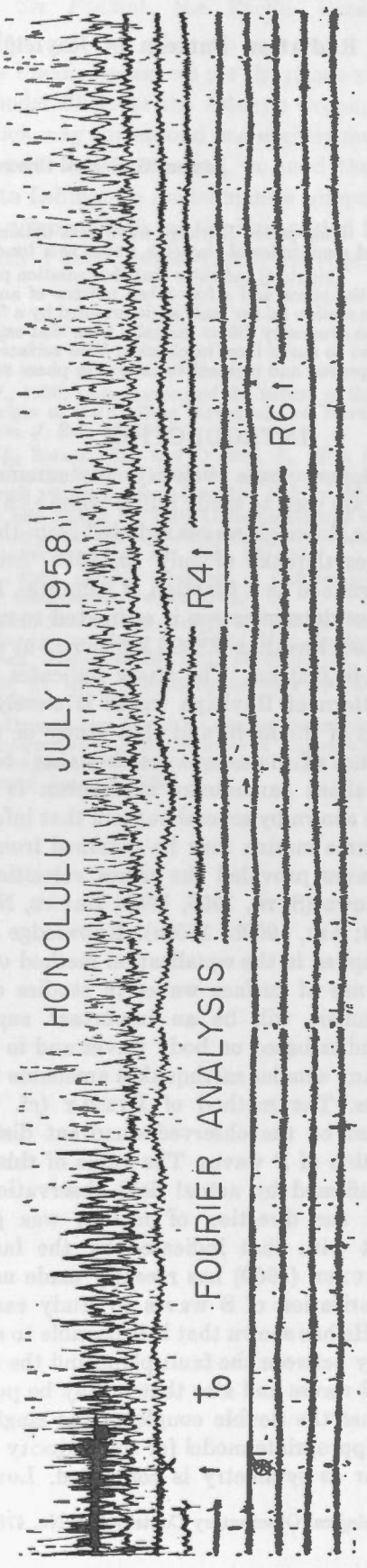

Figure 1. Honolulu vertical seismogram for July 10, 1958, t_0 = 11:50:00 GMT. See Table I.

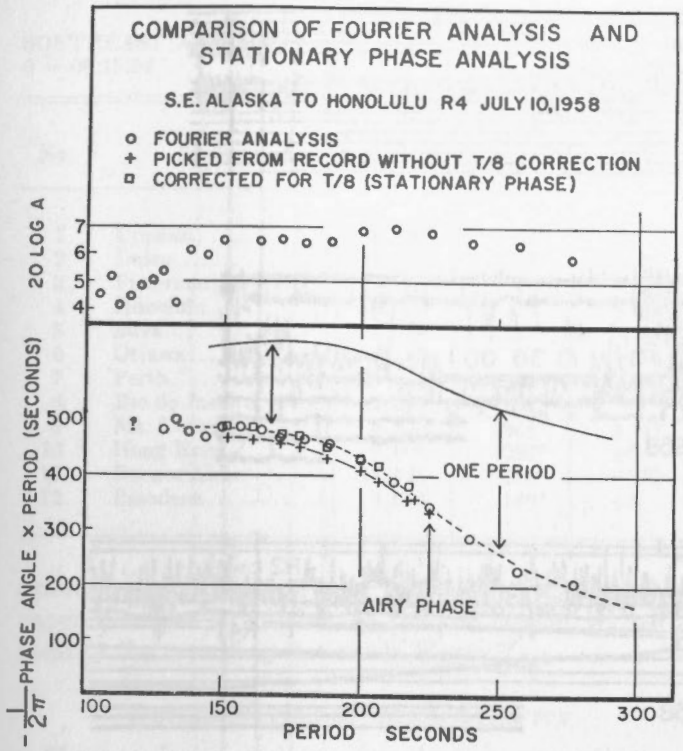

Figure 2. Comparison of stationary phase analysis and Fourier analysis of the Honolulu record shown in Figure 1.

in Figure 2, indicated at one period above the dashed line, which would have been obtained by decreasing all ϕ by 2π. It indicates the times after t_0 at which the next crest of each period will arrive. The stationary value of $-\phi T/2\pi$ on it occurs at a higher value of T and a later time. The actual arrival times of peaks of the total displacement on the record, minus an integer times the period, are indicated by the crosses. For each successive peak in time one more multiple of the period is subtracted. It is seen that the crosses lie earlier than the circles for the period range corresponding to the main part of the train, and agree more closely with the Fourier analysis points near the Airy phase. This is in agreement with the theory given by PEKERIS (1948, p. 61–64). If the crosses from the main part of the train are corrected by adding $T/8$ seconds, the points indicated by the squares result. These agree very closely with the results of Fourier analysis.

If the motion is not sufficiently dispersed for the stationary phase approximation to be valid, one must resort to Fourier analysis as was done by SATÔ (1958) in the study of the G wave. In the present paper an example of determination of initial phase using Fourier analysis as well as stationary phase analysis will be given.

For the wave trains analyzed in this paper the dispersion is such that the stationary phase approximation is valid, but a possible source of error occurs near the Airy phase. Near the Airy phase, the total motion is made up of a superposition of a normally dispersed train and an inversely dispersed train having nearly equal periods. For the case where the two trains have equal amplitudes the theory of the Airy phase given by PEKERIS (1948, p. 61-64) applies. In this case the $T/8$ correction on one train is cancelled by the $-T/8$ correction from the other train so that at the Airy phase there is no phase shift of the total motion with respect to the Fourier component of the same period. But when the amplitude is changing as a function of period near the Airy phase, differential phase shifts of the total motion occur due to the predominance of one train over the other. Thus for points at the Airy phase we may expect some uncertainty when using the theories of stationary phase and Airy phase. Most of this uncertainty may be eliminated by taking into account the relative amplitudes of the two branches or by considering only those parts of the wave train not too near the Airy phase.

Effect of Error in Measuring Period

In general, small errors in the measurement of the period of a given peak or trough do not critically affect the accuracy of initial phase computed by this method, that is, small errors in measurement of period are self correcting in the computation. This results from the principle of stationary phase which states that when motion of a given period arrives on a record, the phases of all of the spectral components with periods near that of the motion on the record are nearly the same. This can be seen from the Fourier analysis results shown in Figure 2. At 483 seconds after t_0 (ordinate) and a period of 160 seconds (abscissa) the dashed line of constant phase becomes horizontal, that is the phase becomes stationary. Thus energy of approximately 160 seconds period arrives at this time on the record. Clearly, since the line is nearly horizontal, the phase of all the Fourier components of period near 160 seconds is the same. Similarly, the phase will be stationary for any period at the time when energy of that period arrives.

APPLICATION TO THE SOUTHEAST ALASKA EARTHQUAKE, JULY 10, 1958

Data

The Southeast Alaska earthquake of July 10, 1958 generated long-period mantle waves which were recorded on most of the long-period intruments of the seismograph network operated during the IGY. The instruments used are described by SUTTON and OLIVER (1959). In general the inverse branch of mantle Rayleigh waves of period 90-225 seconds predominated although at some stations the normal branch with periods 225-380 seconds was recorded. Typical records are shown in Figures 1 and 3. Table I shows the epicentral distance,

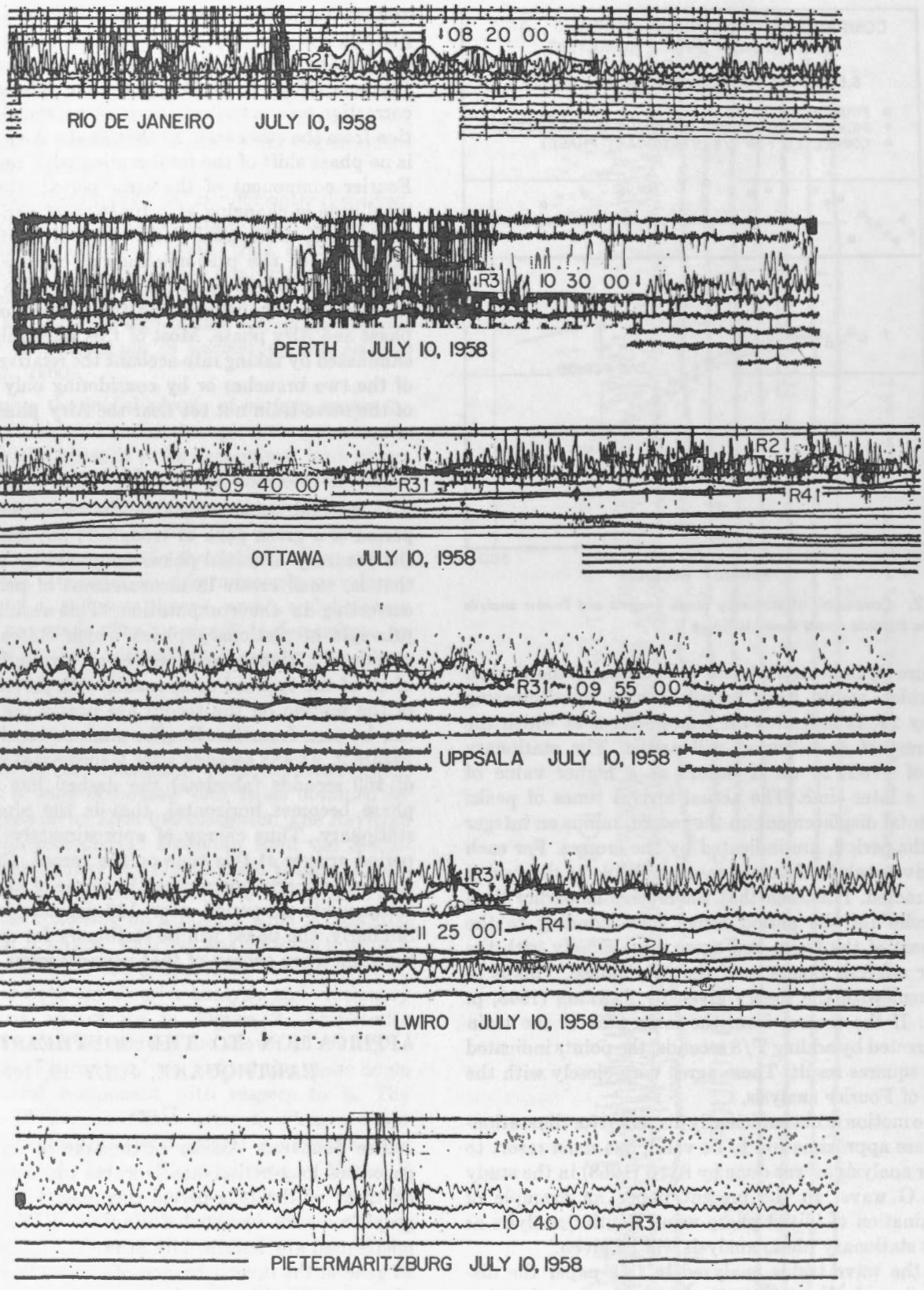

Figure 3. Typical IGY long-period records of the Southeast Alaska earthquake of July 10, 1958. Phase corrections are indicated in Figure 10. All of the instruments except Rio de Janeiro in this figure are the type 15-80A. Rio de Janeiro is the type 15-80B (see Brune, et al. 1960, and Sutton and Oliver, 1959). All of the records except that from Lwiro are from vertical component seismographs. The Lwiro record is for the N–S component of motion and is reversed in polarity.

TABLE I

SOUTHEAST ALASKA JULY 10, 1958
0 = 06:15:54 58½° N 136° W

No.	Station	X	Azimuth	Time Correction
1	Uppsala	6,691	15°	−9
2	Lwiro	13,639	18°	+67
3	Pietermaritzburg	16,641	24°	+8
4	Honolulu	4,490	212°	±0
5	Suva	9,460	223°	+10
6	Ottawa	4,233	83°	±0
7	Perth	14,008	226½°	±0
8	Rio de Janeiro	12,304	100°	±0
9	Mt. Tsukuba	6,330	286½°	+147
10	Hong Kong	9,009	298°	±0
11	Buenos Aires	12,541	119°	−377
12	Pasadena	3,016	146°	+5

azimuth and time correction for stations used in this paper. The station numbers in the first column serve to identify the recording stations in Figure 7.

DETERMINATION OF PHASE VELOCITY

Phase velocity was measured over several great circle paths using equation (1). A sample calculation of phase velocity is shown in Table II. Observation of phase was made for two successive passes of a given wave train circling the earth and arriving at the same station. In this way instrumental phase shift and unknown initial phases were eliminated (SATÔ, 1958, NAFE and BRUNE, 1960). The polar phase advance of $\pi/2$ at each polar or antipodal crossing was taken into account (BRUNE, NAFE and ALSOP, 1960). Ambiguity in choice of the integer N was eliminated by correlation between stations located on nearly the same azimuth from a given earthquake. It was found that phase velocity was nearly independent of path for periods between 130 and 400 seconds. However, certain variations in observed phase velocity in this period range were greater than the experimental error. For instance, phase velocities over the great circle paths including the epicenter of the Southeast Alaska earthquake of July 10, 1958 and the seismograph stations Perth and Ottawa (very nearly at the same azimuth from the earthquake) are significantly higher than the phase velocities over most of the other great circle paths considered. These higher phase velocities apparently correlate to the fact that these great circle paths lie with approximately 270° of their length in deep oceanic areas, primarily the Indian and Atlantic oceans. Over the particular great circles used in this study the phase velocities are known to an accuracy of better than ½ per cent.

The mean phase-velocity curve in the period range 130 to 230 seconds for six measurements of phase velocity

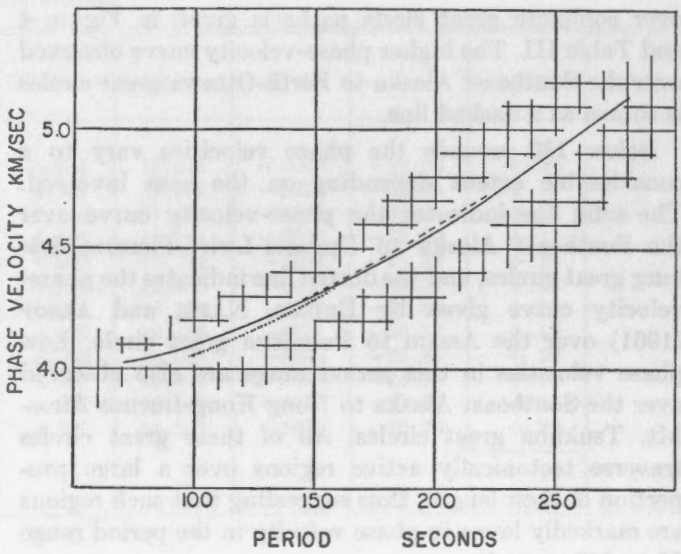

Figure 4. Phase velocity as a function of period as assumed for calculation of initial phase.

TABLE II

SAMPLE CALCULATION OF PHASE VELOCITY

X = 40,020 km

Rio R4			Rio R2			Δt	$\overline{T}$	$(n-\frac{1}{2})$	$(n-\frac{1}{2})\overline{T}$	$\Delta T(n-\frac{1}{2})\overline{T}$	C km/sec
Phase	T	t^*_1	Phase	T	t^*_1						
p	180	18564	p	151	7534	11030	167	11.5	1921	9109	4.393
t	190	18658	t	190	7618	11040	190	11.5	2185	8855	4.519
p	215	18760	p	220	7721	11039	217	11.5	2496	8543	4.685
t	220	18868	p	220	7721	11147	220	12.0	2640	8507	4.704
p	225	18976	t	225	7828	11148	225	12.0	2700	8448	4.737

*The symbol t_1 is used to designate travel times associated with phases of the total motion to distinguish these times from travel times of phases of the Fourier components.

TABLE III

ASSUMED PHASE VELOCITY AS A FUNCTION PERIOD FOR THE COMPUTATION OF INITIAL PHASES

T sec	C km/sec
130	4.217
140	4.258
150	4.302
160	4.352
170	4.404
180	4.459
190	4.513
200	4.570
210	4.632
220	4.703
225	4.737
230	4.770
240	4.838

over complete great circle paths is given in Figure 4 and Table III. The higher phase-velocity curve observed over the Southeast Alaska to Perth-Ottawa great circles is shown as a dashed line.

Below 130 seconds the phase velocities vary to a considerable extent depending on the area involved. The solid line indicates the phase-velocity curve over the Southeast Alaska to Uppsala-Lwiro-Pietermaritzburg great circles, and the dotted line indicates the phase-velocity curve given by BRUNE, NAFE, and ALSOP (1961) over the Assam to Pasadena great circle. Low phase velocities in this period range are also observed over the Southeast Alaska to Hong Kong-Buenos Aires-Mt. Tsukuba great circles. All of these great circles traverse tectonically active regions over a large proportion of their length, thus suggesting that such regions are markedly lower in phase velocity in the period range 80 to 120 seconds.

DETERMINATION OF INITIAL PHASE

Once phase velocity is known, the calculation of initial phase is straightforward. We solve equation (1) for ϕ_e

$$\phi_e = 2\pi\,(X/CT - t/T + \phi_b/2\pi - N) \quad \ldots\ldots(2)$$

where, as before, t is the arrival time of a phase of a particular Fourier component; t may be determined by Fourier analysis, or more simply by the stationary phase approximation provided the train is sufficiently dispersed. Equation 2 applies when the waves are plane waves and always sinusoidal. When dealing with surface waves on the earth we must define initial phase in a slightly different manner because the actual solutions of the equations of motion are not plane waves but spherical harmonic surface waves which are not perfectly sinusoidal in space near the epicenter or antipode

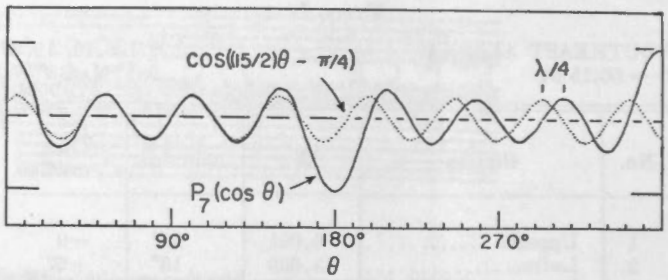

Figure 5. Illustration of phase shifts due to the non-sinusoidal shape of spherical harmonic wave functions. From Brune, Nafe, and Alsop, 1960.

(BRUNE, NAFE, and ALSOP, 1960). In effect the phase of the motion is advanced $\pi/2$ in a polar or antipodal passage and is advanced $\pi/4$ in leaving the source. This may be seen from Figure 5 which compares P_7 (cos θ) with a sinusoidal wave of the same wavelength. To correct for these advances of phase, which are not related to the phase of motion at the origin, we retard the measured phase of motion by $\pi/4 + m\,\pi/2$ where m is the number of polar or antipodal passages which the waves have made. Thus on the earth we define initial phase as follows:

$$\phi_0 = 2\pi(X/CT - t/T + \phi_b/2\pi - N) - \pi/4 - m\pi/2 \ldots.(3)$$

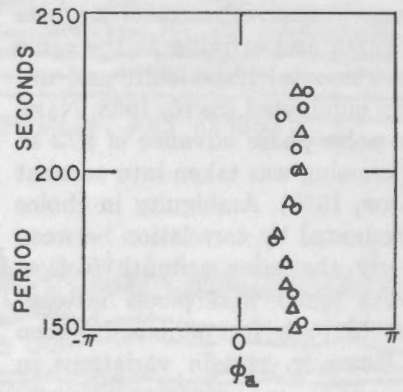

Figure 6.

Initial phase ϕ_e as a function of period for the Rayleigh wave train R4 at Honolulu. The circles were obtained by stationary phase analysis and the triangles by Fourier analysis. The phases have not been corrected for the $\pi/4$ phase advance in leaving the source (see column 11 of Table IV)

Eleven of the IGY seismograph stations as well as Pasadena recorded long-period mantle Rayleigh waves for which it is possible to determine the initial phase of the vertical component of Rayleigh waves (positive upward) for 23 azimuths from the epicenter. A sample calculation of initial phase using both Fourier analysis and stationary phase analysis is shown in Table IV. The initial phase is determined from equation (2) for various spectral components in the period range 130 to 300 seconds. A convenient way to display initial phase as a function of period is shown in Figure 6. This method of display is much simpler to interpret than a source function which is a complicated superposition of many spectral components and usually the points scatter very little. The mean of the values for initial phase

TABLE IV

SAMPLE COMPUTATION OF INITIAL PHASE

Honolulu R4 Z X = 75, 550 km

Fourier Analysis t_0 = 20, 046 sec

T seconds	$-\phi$ radians	$-\phi T/2\pi$	t_1	Inst. Corr.	t	C	X/C	X/C-t	$+\phi_e/2\pi$	$\phi_e^*/2\pi$	$\phi_0^*/2\pi$
150.0	20.420	487.5	20,534	+1	20,535	4.302	17,562	−2973	−19.82	+.18	
156.5	19.534	486.6	20,533	+2	20,535	4.334	17,431	−3104	−19.83	+.17	
163.6	18.540	482.7	20,529	+2	20,531	4.371	17,284	−3247	−19.85	+.15	
171.4	17.278	471.3	20,517	+5	20,522	4.413	17,120	−3402	−19.85	+.15	
180.0	16.291	466.7	20,513	+8	20,521	4.459	16,943	−3578	−19.88	+.12	
189.5	15.223	459.1	20,505	+10	20,515	4.509	16,755	−3760	−19.84	+.16	
200.0	13,527	430.6	20,477	+14	20,491	4,570	16,532	−3959	−19.80	+.20	
211.8	11.560	389.7	20,436	+15	20,451	4.647	16,258	−4193	−19.80	+.20	
225.0	9.600	343.8	20,390	+18	20,408	4.737	15,949	−4459	−19.82	+.18	
										+.17	+.29

Stationary Phase Analysis

T	Phase	t_1	T/8	Inst. Corr.	t	C	X/C	X/C-t	$-n$	$\phi_e^*/2\pi$	$\phi_0^*/2\pi$
152	p	20,514	+19	+1	20,534	4.311	17,525	−3009	−19.80	+.20	
161	t	20,591	+20	+2	20,613	4.357	17,340	−3273	−20.33	+.17	
171	p	20,671	+21	+5	20,697	4.410	17,132	−3565	−20.85	+.15	
178	t	20,763	+22	+8	20,793	4.448	16,985	−3808	−21.39	+.11	
188	p	20,850	+23	+10	20,883	4.502	16,781	−4102	−21.82	+.18	
200	t	20,956	+25	+14	20,995	4.570	16,532	−4463	−22.32	+.18	
207	p	21,056	+26	+15	21,097	4.614	16,374	−4723	−22.82	+.18	
217	t	21,164	+27	+16	21,207	4.682	16,136	−5071	−23.37	+.13	
220	p	21,283	+0†	+17	21,300	4.703	16,064	−5236	−23.80	+.20	
225	t	21,393	+0†	+18	21,411	4.737	15,949	−5462	−24.28	+.22	
225	p	21,506	+0†	+18	21,524	4.737	15,949	−5575	−24.78	+.22	
225	t	21,620	+0†	+18	21,638	4,737	15,949	−5689	−25.28	+.22	
										+.18	+.30

†Indicates this phase was assumed to be part of the Airy phase.
*An integral multiple of 2π radians has been added to ϕ_e to give these figures.

computed for various periods is then determined for each station and wave train as shown in Table IV. Corrections are made for the polar phase advance. This mean initial phase, ϕ_0, is plotted in Figure 7 as a function of the azimuth along which the waves radiated from the epicenter. The initial phases were first determined using the mean phase velocities given in Table II —(open symbols)—then the initial phases for the three stations, Ottawa, Perth and Rio, were recalculated using the higher phase velocities indicated by the dashed line in Figure 4. Points computed with the higher phase velocity are indicated by solid symbols. When possible the initial phase was checked by using two successive passes of a given train, such as R2 and R4 or R3 and R5. The accuracy of the determinations appears to be better than one-tenth of a period, that is, better than $\pi/5$ for observations at distances less than 40,000 km (indicated by squares) and better than $\pi/3$ for observations at distances between 40,000 and 60,000 km (indicated by circles). For distances greater than 60,000 km the accuracy is probably about $\pi/2$ (triangles).

AMPLITUDES

The amplitudes were read from the record and corrected for relative instrument amplification, dispersion, spreading on a sphere, and attenuation ($1/Q = 665 \times 10^{-5}$) (EWING and PRESS, 1954). The amplitude was read as the maximum trace deflection in the period range 190–225 seconds, and hence the amplitude pattern is only for a relatively narrow band-width.

Although the IGY instruments were not all accurately calibrated at the time of this earthquake, conclusions

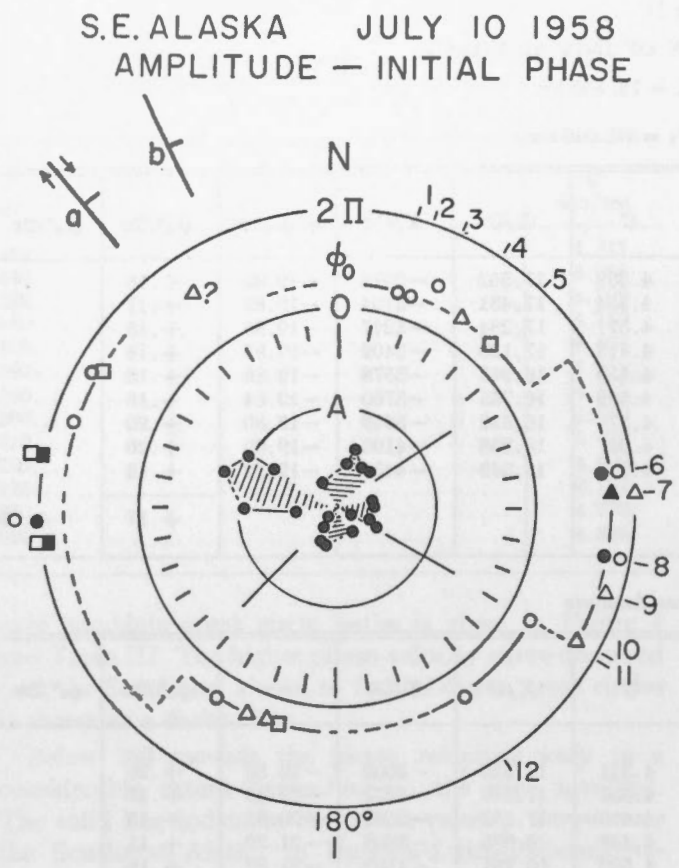

Figure 7 Radiation pattern of Rayleigh waves from the Southeast Alaska earthquake of July 10, 1958. Initial phase ϕ_0 and amplitude A are plotted as a function of azimuth from the epicenter. The USCGS preliminary epicenter (see Table I) was used in the calculation. If the revised epicenter of Stauder (1960) is used, a small correction (less than $\pi/5$) will be necessary for stations to the E and W. The amplitudes are subject to an error of approximately 20 per cent since Fourier analysis was not used. See Table 1 for the names of the stations.

based on amplitude and phase may be made since the instruments were all very similar in period response. However, if the method is to be developed to its full usefulness it will be necessary that the stations be accurately calibrated for phase and amplitude response.

Radiation Pattern

Although data are lacking in certain regions it is possible to recognize several important features of the radiation pattern:

1. The initial phase is not significantly different from either $\pi/2$ or $3\pi/2$ except for the determinations near 270°.

2. The initial phases appear to be divided into four sectors with the phases in each sector being either $\pi/2$ or $3\pi/2$ with the exceptions noted above.

An initial phase of $\pi/2$ along a given azimuth indicates that at the epicenter at the origin time a surface particle was displaced away from the receiving station and was moving downward through zero vertical displacement.

3. The amplitudes in the period range 190-225 seconds tend to form a four-lobed pattern with one lobe in each sector, one of the lobes (290°) having significantly higher amplitudes than the other three. The amplitudes are low near boundaries between adjacent sectors where there are data (Buenos Aires R3, 121°; Suva R1, 224°).

4. Nodes appear to exist in the amplitude pattern for these long waves. The station Suva (224°) did not record any definite long-period Rayleigh waves from the southwest side of the fault, whereas it recorded remarkably large Love waves and S waves in this direction. The P wave had a node near this azimuth (Stauder, 1960).

5. The pattern is not perfectly quadrant, nor do opposing nodal lines lie exactly 180° apart. This is certain since Suva R1 (224°) was near a node and Suva R2 (44°) recorded normal amplitudes. This indicates that the northeast nodal line does not lie along the same azimuth as the southwest nodal line, being displaced more to the east. The station Buenos Aires R3, although recording very low amplitudes, indicated the opposite phase from Hong Kong R4 which is at only a slightly different azimuth. This indicates that one of the nodal lines is between 118° and 121°, whereas the northwest nodal line strikes more northerly than 301°.

6. The symmetry of the radiation pattern is approximately in agreement with the observed ground displacement at the epicenter (Tocher, 1960, indicated by dip symbol *a* at upper left) and the fault-plane solution by Stauder (1960, dip symbol *b*) both of which indicated right-lateral strike-slip motion along a steeply dipping fault striking NW-SE. For a vertical fault striking NW-SE with a pure strike-slip right-lateral motion, the Rayleigh wave radiation pattern would be quadrant with opposing quadrants showing the same phase.

According to the theory of Lamb (1904) as generalized by Aki (1960c), a right lateral force couple which is a step (Heaviside) function in time would have initial phases of π (E–W) and zero (N–S). The phases measured in this paper do not agree with this model, differing by $+\pi/2$, even though the symmetry is approximately the same. The explanation for this difference awaits further studies. It is possible that the equivalent force system at the origin is not a step function in time.

In the above discussion the effects of a finite fault length and a finite rupture velocity have been neglected. These effects will be important if the fault length is an appreciable fraction of the wave-length and the total duration of rupture and energy release is an appreciable fraction of the period. Dr. Frank Press has suggested

that the observed asymmetry of amplitudes in Figure 7 is caused in this way. The finiteness of the source could explain the difference in amplitude between the direct and indirect paths to stations 8, 9 and 10 and to stations 4 and 5, but would also predict such a difference at stations 1 and 2, although no definite difference is observed at these stations (*see* BEN MANAHEM, in press). The theory of finite length of fault and finite rupture velocity also predicts a phase shift as a function of period. The wave trains analyzed in this study show no definite shift of initial phase as a function of frequency, thus suggesting that the source may have been effectively a point source for the long wave-lengths used to determine initial phase. The simplicity of the initial phase pattern obtained without correcting for an effect of finiteness of fault also suggests that the source may have effectively been a point source. The simple pattern of the plane of polarization of S for this earthquake (STAUDER, 1960) further suggests a point source.

Even though as pointed out above, several features of the waves generated by this earthquake suggest a point source, it cannot be concluded that the effect of finiteness of the source is not important. Therefore, for the sake of completeness, the following discussion of the possible effects of a finite source are included, and the final evaluation of the importance of the finiteness of the source is left for further studies.

An upper limit for the difference of initial phase between $T = 150$ sec and $T = 230$ sec for the stations Uppsala, Suva and Honolulu is less than $\pi/3$. If we assume a rupture velocity of 3 km/sec this implies that the length of rupture is less than 330 km. On the basis of field evidence and aftershocks, the probable length of rupture is approximately 200 km (TOCHER, 1960). If it is assumed that the fault motion is purely strike-slip, that the rupture proceeds from the epicenter in one direction along the fault with velocity of rupture v and that the amount of energy release is distributed evenly along the length of rupture, the phase shift introduced according to BEN MANAHEM is:

$$\phi^1 = \frac{-\pi b}{CT}(C/v - \cos\theta_0)$$

where θ_0 is the azimuth to the recording station from the epicenter with $\theta_0 = 0$ along the fault in the direction of rupture, and b is the length of the fault. If we assume $b = 200$ km and $v = 3$ km/sec, then at $T = 220$ sec:

$$\phi^1 = -\pi/5(1.5 - \cos\theta_0)$$

which introduces a phase shift of -0.3π perpendicular to the fault and a phase shift of $-\pi/2$ in the direction along the fault opposite to the direction of rupture. A phase shift of $-\pi/10$ is introduced in the direction of rupture. Thus if the assumptions made above apply to this earthquake, the phases measured must be corrected by these amounts before interpreting the radiation pattern in terms of a point source. The source mechanism implied would differ accordingly. Other mechanisms which might explain the observed asymmetry of amplitudes are being investigated.

STAUDER has also presented the theoretical P wave amplitudes expected from the fault-plane solution (Figure 8). The similarities of the two patterns are striking. The P wave amplitudes are largest in the west-northwest direction and the observed Rayleigh wave amplitudes are also largest in this direction. The initial motion of P changes phase along approximately the same azimuths as those along which the initial motion of Rayleigh waves changes phase.

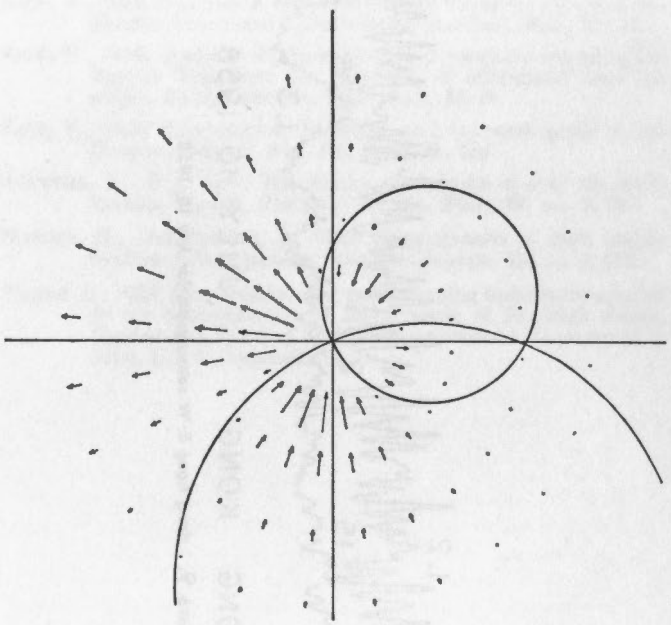

Figure 8. Theoretical amplitudes for P waves for the Southeast Alaska earthquake of July 10, 1958 (from Stauder, 1960).

There are limited data which suggest that the symmetry of the earthquake may be more like that expected for a single couple than for a double couple. The paths Hong Kong R2 and Buenos Aires R3 lie near the southeast Rayleigh wave node and should lie along a Love wave node if the single couple were the appropriate mechanism or along an antinode if the double couple were the appropriate mechanism. The recorded amplitudes of Love waves in this direction are very low compared to those generated in other directions and thus indicate symmetry similar to that expected from a single couple source (compare Hong Kong L2 and L3 in Figure 9). More definite conclusions await determination of the radiation pattern of Love waves from this and other earthquakes. The phase-velocity curve for long-period Love waves is expected to be available in the near future.

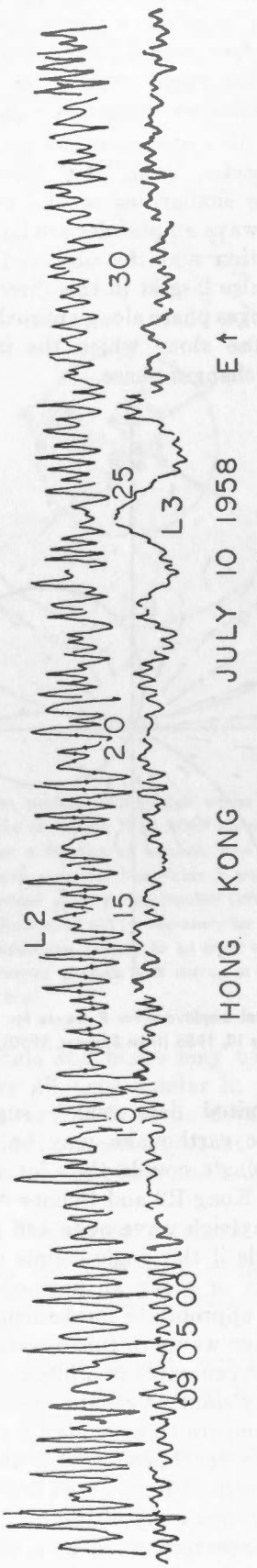

Figure 9. Hong Kong E–W seismogram for July 10, 1958.

The radiation pattern obtained in this paper may be regarded as verification that the radiation pattern of Rayleigh waves from a typical strike-slip earthquake possesses radically different symmetry from the symmetry expected from an explosion. A similar contrast may be expected for earthquakes with a large dip-slip component. It is probable that this result will hold for shorter periods than those used in this study.

It is difficult to draw any further conclusions on the basis of one radiation pattern. However, this study indicates that the use of surface waves may yield valuable information concerning earthquake mechanism and that large-scale use of this technique is feasible. A few simple algebraic operations on a hand calculator yield the initial phases, the phase velocity being known. It is expected that in the near future numerous other determinations will be made and it may then be possible to draw more definite conclusions regarding the surface wave radiation pattern to be expected for various types of earthquakes. Certainly the use of surface waves makes a much greater number of earthquakes amenable to mechanism studies.

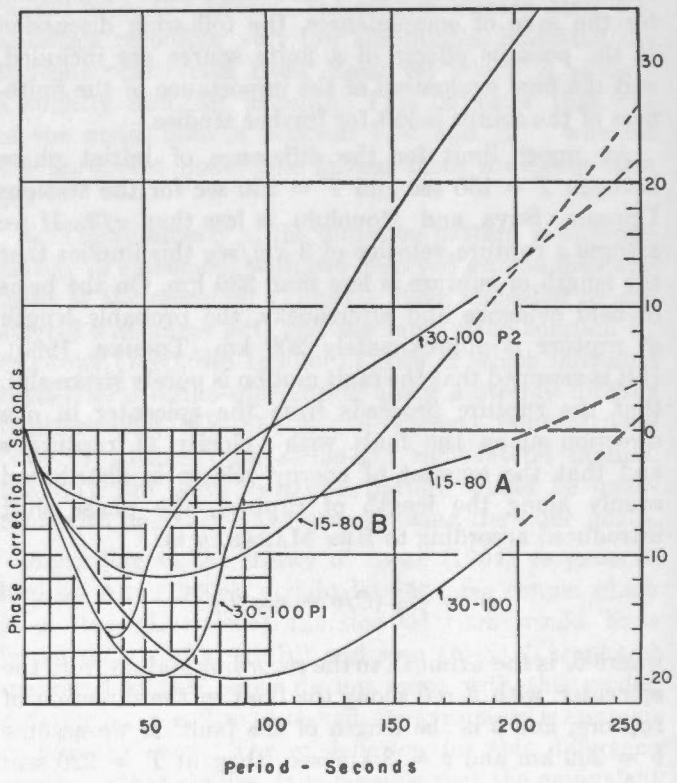

Figure 10. Phase-correction curves for the instruments used in this paper (from Brune, et al., 1960).

ACKNOWLEDGMENTS

The author wishes to thank Drs. Maurice Ewing, John E. Nafe, Jack Oliver and George Sutton of Lamont Geological Observatory for valuable help and

advice in carrying out this study. The author especially wishes to thank those who cooperated in sending the records used in this study. Accumulation of the data under the IGY program was supported by National Science Foundation Grant Y/11. 12/54. This work was supported in part by the Office of Ordnance Research under Contract DA 30-069-Ord-2431, the Office of Naval Research under Contract Nonr 266(53) and the Air Force Cambridge Research Center under Contract AF 19 (604) 4144. Use of an IBM 650 computer was provided by the IBM Watson Scientific Computing Laboratory.

References

Aki, K., 1960a. The use of Love waves for the study of earthquake mechanism; *J. Geophys. Res.*, **65**, 323.

1960b. Study of earthquake mechanism by a method of phase equalization applied to Rayleigh and Love waves; *J. Geophys. Res.*, **65**, 729.

1960c. Source functions of circum-Pacific earthquakes; *J. Geophys. Res.*, **65**, no. 8, 2405.

Ben Manahem, A., (in press) Radiation of seismic surface waves from simple models of fault planes Part I: Rayleigh waves. *Seismol. Soc. Am. Bull.*

Brune, J. N., Nafe, J. E. and Alsop, L. F., 1960. The polar phase shift of surface waves on a sphere; (in press) *Seismol. Soc. Am. Bull.*

Brune, J., Nafe, J. E. and Oliver, J., 1960. A simplified method for the analysis and synthesis of dispersed wave trains; *J. Geophys. Res.*, **65**, 287.

Byerly, P., 1955. Nature of faulting as deduced from seismograms, in crust of the earth; *Geol. Soc. Am.* Spec. Paper 62, 75.

Ewing, M., Jardetzky, W. S. and Press, F., 1957. Elastic waves in layered media; McGraw-Hill Book Co., New York.

Ewing, M., and Press, F., 1954. Mantle Rayleigh waves from the Kamchatka earthquake of November 4, 1952; *Seismol. Soc. Am. Bull.* **44**, 3, 471.

Hodgson, J. H., 1957. Current status of fault-plane studies; *Publ. Dom. Obs.* Ottawa, **20**, 413.

Lamb, H., 1904. On the propagation of tremors over the surface of an elastic solid; *Roy. Soc. London, Phil. Trans*, ser. A, 203.

Nafe, J., and Brune, J., 1960. Observations of phase velocity for Rayleigh waves in the period range 100-400 seconds; *Seismol. Soc. Am. Bull.*, **50**, 427.

Peckeris, C. L., 1948. Theory of propagation of explosive sound in shallow water; *Geol. Soc. Am.*, Mem. 27.

Press, F., 1960. Crustal structure in the California-Nevada region; *J. Geophys. Res.*, **65**, no. 3, 1039.

Satô, Y., 1955. Analysis of dispersed surface waves by means of the Fourier Transform I; *Earthquake Res. Inst. Bull.*, **33**, 33.

Satô, Y., 1956. Analysis of dispersed surface waves by means of the Fourier Transform II: Synthesis of movement near the origin; *Earthquake Res. Inst., Bull.*, **34**, 9.

Satô, Y., 1958. Attenuation, dispersion and the wave guide of the G wave; *Seismol. Soc. Am. Bull.*, **48**, 231.

Stauder, W., S. J. 1960. The Alaska earthquake of July 10, 1958; Seismic Studies, *Seismol. Soc. Am. Bull.*, **50**, no. 2, 293.

Sutton, G., and Oliver, J., 1959. Seismographs of high amplification at long periods; *Annales Géophys.*, **15**, no. 4, 423.

Tukey, J., 1959. Equalization and pulse shaping techniques applied to the determination of initial sense of Rayleigh waves, Papers on a Panel of Seismic Improvement, *Department of State*, U.S.A. Appendix 9.

The Tectonics of Asia in The Light of Earthquake Fault-Plane Solutions

ADRIAN E. SCHEIDEGGER
University of Alberta, Calgary, Canada

ABSTRACT

It may be argued that a correlation must exist between the tectonics of a region and the fault-planes of the earthquakes of this region. This correlation exists but it is not possible to determine it readily. It is found that one must consider the nodal direction in these earthquakes and it is observed that nodal directions are, in general, normal to the direction of tectonic displacement. Consequently, it is possible to determine the direction of tectonic displacement by a least-squares method. This method has been applied to some Asiatic earthquakes for which numerous observations have been published in the Russian geophysical literature. A remarkable uniformity of tectonic displacement has been found in continental Asia, extending from Sakhalin to the Pamirs and the mountains of Kopet Dagh. This result indicates a large scale uniformity of tectonic forces in the Earth's crust.

Earthquakes are commonly thought to be due to tectonic stresses. These stresses are present in the upper parts of the earth and may increase until a breaking point is reached. The break, a fault, finds its expression as an earthquake shock.

It would therefore be expected that there should be a connection between the faulting present in earthquakes and the regional tectonic motion direction. It has recently become possible, owing to methods originated by BYERLY, RITSEMA and KEYLIS-BOROK, to determine the plane of faulting which is active in an earthquake, and it seems obvious that fault-plane solutions so obtained should have some connection with the regional tectonic stresses. However, if the fault-plane solutions of earthquakes available in any one area are plotted on a map, a rather irregular arrangement results which must be regarded as a random pattern (for a discussion of this, *see* e.g. SCHEIDEGGER, 1958a).

Most fault-plane solutions of earthquakes available in the literature are ambiguous to the extent that either one of the two orthogonal, "nodal", planes may be the fault plane. However, there is one axis in these fault-plane solutions which is uniquely defined: the line of intersection of the two nodal planes. Whichever plane represents the fault, this is a line of no motion, a null axis. It has been suggested by WILLMORE that any tectonophysical inferences ought to be based only upon this unique axis, rather than on the complete fault-plane solution. The writer, during the period since the last general assembly of the International Union of Geodesy and Geophysics, has made studies with regard to the tectonophysical significance of the null axis. The present paper represents a review and synthesis of the results obtained in these studies together with a new interpretation in terms of the tectonics of Asia.

THE METHOD

As noted in the introduction, a connection between earthquake fault-plane solutions and tectonophysics must be sought on the basis of the one uniquely defined direction in such solutions, the null axis.

The basic concept in utilizing these null axes is as follows. It is assumed that earthquakes are due to the stresses created by the relative motion of blocks adjacent to an earthquake belt. The actual faults represented by the earthquakes may be quite randomly oriented. However, it seems apparent that the null axis, being the intersection of two nodal lines, is in general orthogonal to the axis of greatest differential motion. This, then, would be the axis of relative tectonic motion for the two blocks adjacent to the earthquake belt under consideration.

Although the basic concept is very simple, the null axes in a series of earthquakes will never exactly be orthogonal to one exactly defined tectonic motion axis. The latter, therefore, has to be calculated by a least-squares procedure. The method has been outlined in an earlier paper of the writer's (SCHEIDEGGER, 1958b), and therefore is not reported here in detail.

It has been pointed out to the writer by Dr. RITSEMA of De Bilt that the original least-squares formulae used may, in fact, introduce a bias in the weighting of the data which depends on the choice of the co-ordinate system, because the variation of the sought-after vector is taken along a plane. It would be better to vary the vector along a sphere, in which case one ought to introduce polar co-ordinates

$$x = R \sin\theta \cos\varphi$$

$$y = R \sin\theta \sin\varphi$$

$$z = R \cos\theta.$$

96705-9—7

If n_{xi}, n_{yi}, n_{zi} denote the direction cosines of the null axis of the i-th fault-plane solution in an area, the minimization condition becomes (for constant R)

$$\delta \sum_i (\sin\theta \cos\varphi\, n_{xi} + \sin\theta \sin\varphi\, n_{yi} + \cos\theta\, n_{zi})^2 = 0\,,$$

which leads to the following two normal equations:

$$-\sin^2\theta \cos\varphi \sin\varphi\, \Sigma n^2_{xi} + (\cos^2\varphi - \sin^2\varphi) \sin^2\theta\, \Sigma n_{xi} n_{yi}$$

$$-\cos\theta \sin\theta \sin\varphi\, \Sigma n_{xi} n_{zi} + \sin^2\theta \cos\varphi \sin\varphi\, \Sigma n^2_{yi}$$

$$+\cos\theta \sin\theta \cos\varphi\, \Sigma n_{yi} n_{zi} = 0$$

and

$$\sin\theta \cos\theta \cos^2\varphi\, \Sigma n^2_{xi} + 2\sin\theta \cos\theta \sin\varphi \cos\varphi\, \Sigma n_{xi} n_{yi}$$

$$+ (\cos^2\theta - \sin^2\theta) \cos\varphi\, \Sigma n_{xi} n_{zi} + \cos\theta \sin\theta \sin^2\varphi\, \Sigma n^2_{yi}$$

$$+ (\cos^2\theta - \sin^2\theta) \sin\varphi\, \Sigma n_{yi} n_{zi} - \cos\theta \sin\theta\, \Sigma n_{zi}^2 = 0.$$

It is relatively easy to eliminate θ from these equations (by introducing tan 2θ into the second and tan θ into the first equation), but then one ends up with a transcendental equation for φ for which no easy solutions seem to exist. It can be shown, however, that the simplified original method will give correct (i.e. *exact*) results under a wide range of conditions, particularly if the null axes do not scatter too much about the plane. These conditions can be arrived at by comparing the variation of the function to be minimized in the case where the vector *xyz* varies along a plane with the case where it varies along a sphere. The consequences regarding large scale tectonics about which we shall talk here, will scarcely be altered by the use of the new formulae given above, although the applicability of the simplified formulae ought really to be tested in each case and the new formulae ought to be used if the simplified formulae do not apply.

TECTONIC MOTIONS IN ASIA

Sufficient data have now been analyzed so that it is possible to investigate some of the tectonic features of Asia in the light of fault-plane solutions of earthquakes. Taking the tectonic motion directions that have been determined by the author (SCHEIDEGGER, 1958c, 1959), and averaging the results for any one "larger" area, leads to the result shown in Table 1. These results have been plotted in Figure 1.

Examination of the last figure indicates that there is a considerable difference between the tectonic motion directions found in the outer island areas of Eastern Asia and the tectonic motions on what might properly be called continental Eurasia. We have shown earlier

TABLE I

	No. of Earthquakes	Strike	Dip (up)
Kuriles	16	N13½W	−10
Sakhalin	7	N36½E	9
Honshu	42	N14W	2
Philippines	8	N05W	−7
Pamir	156	N05W	−16
Hindu Kush	9	N20E	22
Tien Shan	23	N06E	−8
Kopet Dagh	22	N14E	3
Caucasus	46	N10E	−1

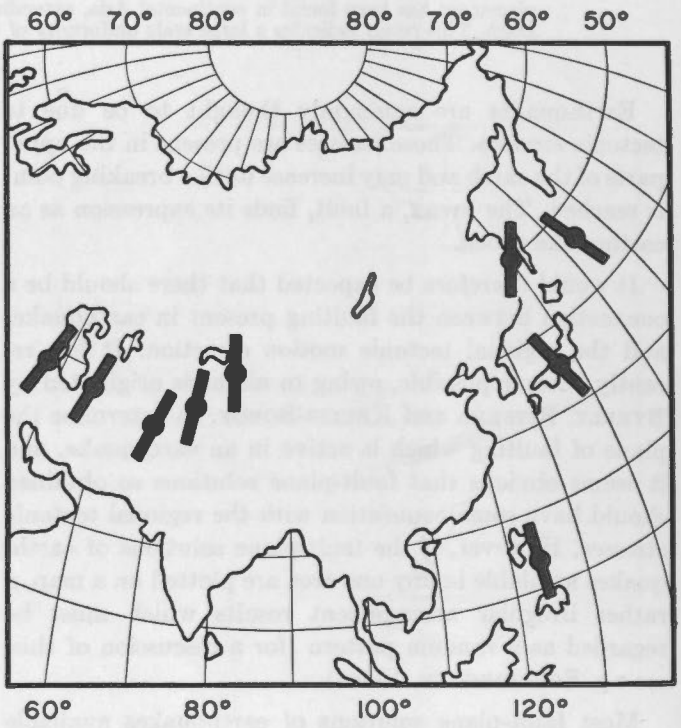

Figure 1.

(SCHEIDEGGER, 1959) that there is a remarkable consistency in tectonic motion directions as found in the island area adjacent to the northwest Pacific Ocean. Except for the motion found for Sakhalin, the motion at the edge of the Pacific lies considerably west of north which might be interpreted as a thrust of that part of a Pacific block against the rim of Asia.

The anomalous motion found for Sakhalin, however, ties in remarkably well with the motion found in other parts of continental Eurasia. Thus allowing for the difference in longitude, there is almost complete parallelism between the tectonic motion found for Sakhalin and that found for the Pamir Knot.

A correspondence of the tectonic motion over such a large distance (from Sakhalin practically to the Caucasus) would seem to indicate an almost incredible

uniformity of the stresses in the Earth's crust. Unfortunately, it is impossible at the present time to test this correlation further because not enough faultplane solutions of earthquakes within the area of Tibet and the upper reaches of the Hwang Ho are available.

Nevertheless, there are in fact other indications that the correlation between the tectonic motion of Sakhalin and the Pamirs found from fault-plane solutions is not just a coincidence. For, if we assume that the correlation is real, the relative motion of the various crustal blocks involved must be as indicated in Figure 2. We have assumed a thrust motion everywhere because this seems to fit with the tectonics of the areas involved, although of course the seismic method gives no indication as to the sign of the relative motion. It will now be noted that the general strike of the Alpide orogenic belt fits very well into the postulated motion of the blocks; in particular, the very pronounced bend of the mountains north of Burma, where the general east-west strike of the mountain ranges changes into a north-south one, agrees very well with what the assumed motion of the crustal blocks would be expected to generate.

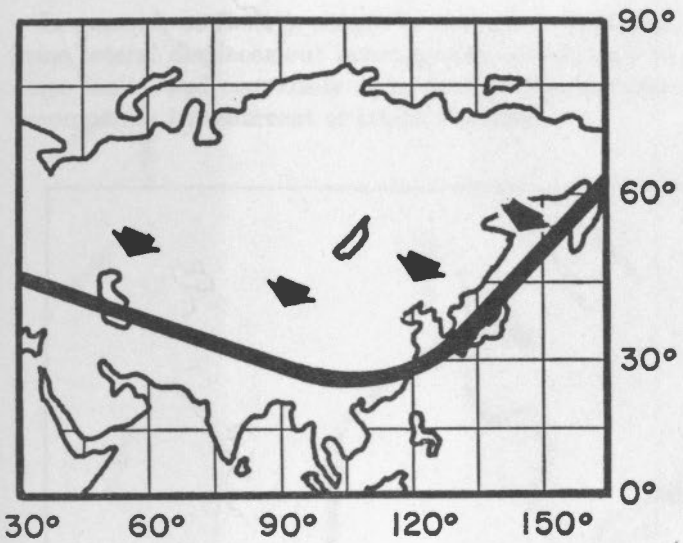

Figure 2.

It thus appears that the tectonics of Asia is not inconsistent with the above outlined interpretation of the seismically defined tectonic motion direction. However, it should be kept in mind that, as long as no further data are available for western China, the above remarks must be regarded as speculative.

The relative motion between the Asian block and India has been described above as a thrust from the north. However, since all motions are relative, it also could be described as a thrust from the south. It then would be in accord with the view of India moving northward as has been postulated in some versions of the continental drift theory (see e.g. SCHEIDEGGER, 1958a).

All in all, it can be said that evidence is accumulating that crustal stresses may be uniform over very large areas and that various parts of the earth's crust may be in motion with regard to each other, acting as large coherent blocks.

References

SCHEIDEGGER, A. E., 1958a). Principles of geodynamics: (in English), *Springer Verlag*, Berlin.

——— 1958b. Tectonophysical significance of fault-plane solutions of earthquakes: *Geofis. Pura e Appl.* **39**, 19.

——— 1958c. Seismological evidence for the tectonics of the northwest Pacific ocean: *Seismol. Soc. Am. Bull.*, **48**, 369.

——— 1959. Seismic evidence for the tectonics of central and western Asia: *Seismol. Soc. Am. Bull.* **49**, 369.

Principal Horizontal Stress Directions as an Aid to the Study of Crustal Deformation

G. J. LENSEN

New Zealand Geological Survey

INTRODUCTION

Diastrophism is the result of stresses acting upon the crust of the earth and it is only after finding the properties of these stresses that a mechanism causing the diastrophism can be postulated.

Faults are controlled by stress in the earth's crust. ANDERSON (1942, p. 12) defined types of faulting in relation to one of the three stress components, the Principal Horizontal Stress (PHS).

In general, no fault is simple in character. Typically, some lateral displacement accompanies normal and reverse faults, and conversely some vertical displacement accompanies transcurrent or lateral faulting.

Along any particular fault the ratio of horizontal (measured along the strike of the fault) to vertical displacement (H/V) can be used to determine the direction of the PHS and the character of the fault.

By definition, for purely normal or reverse faults, the H/V ratio is zero, and for purely transcurrent faults this ratio is infinite. The strike directions of normal and reverse faults intersect at right angles and the transcurrent faults strike within this angle. In any quadrant between the two the H/V ratio progresses from zero to infinity to zero. This relationship can be expressed (method 1) by the equation:

$$H/V = \tan 2\alpha$$

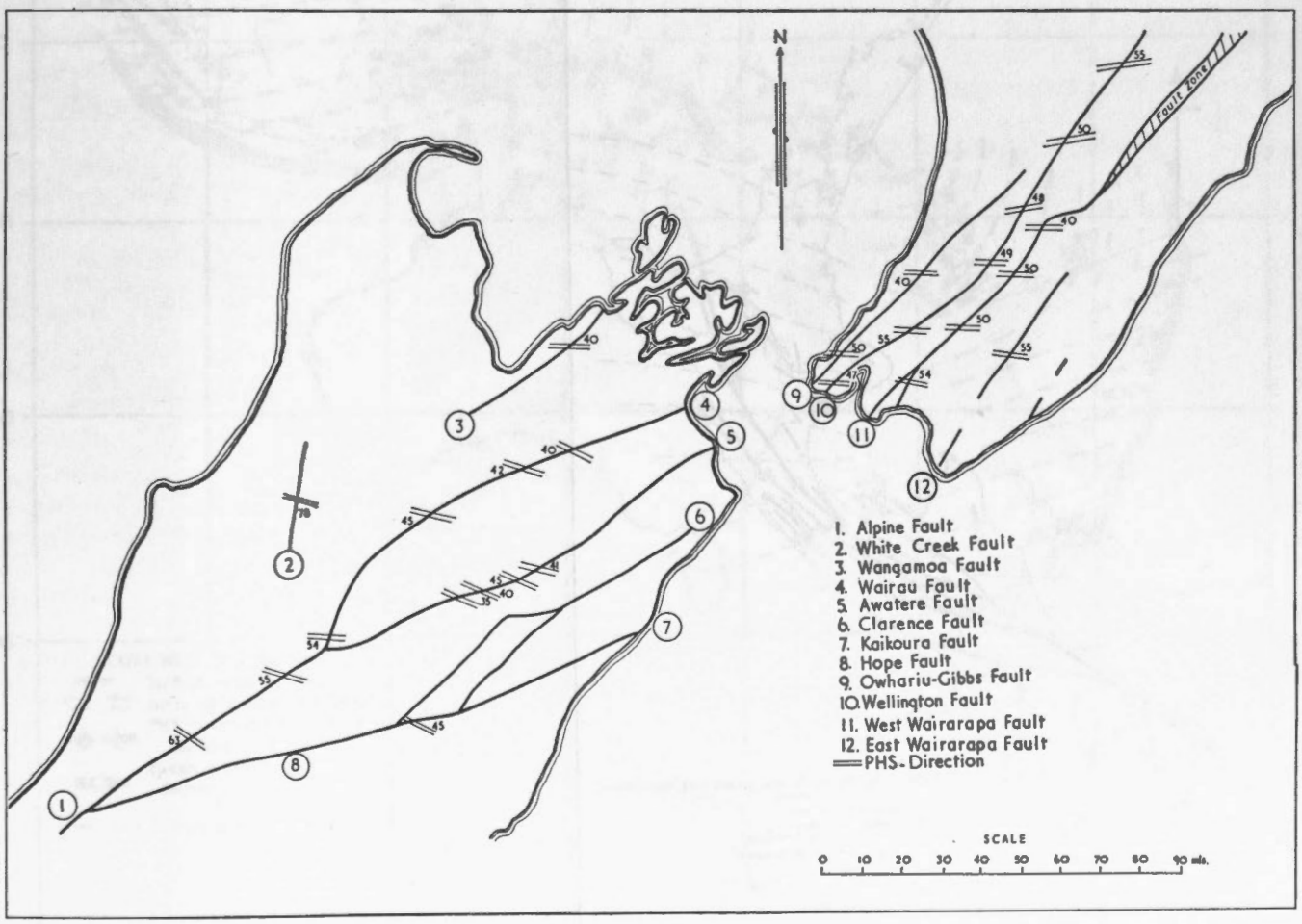

Figure 1.

where α or its complement is the angle between the strike of the fault and the PHS direction (PHS angle).*

The value of α for a purely transcurrent fault, where $H/V = \infty$, is 45°. This angle corresponds to the angle between the PHS direction and ANDERSON'S (1942, p. 14) plane of maximum tangential stress. This approach has already been published in detail and a classification of faults, based on the H/V ratio and the PHS angle, follows logically from this (LENSEN, 1958a).

It has further been shown that the compressional angle between the surface strike of transcurrent clockwise and anti-clockwise faults is acute in tensional regions and obtuse in compressional regions (LENSEN, 1958b). Following this the author (1958c) shows that the PHS direction coincides with the bisector of the compressional angle between intersecting transcurrent clockwise and anticlockwise faults (method 2). Where it is possible to measure the horizontal and vertical components of displacement along recent faults the first method to find the PHS angle is applicable. Where such measurements are not possible, or where these are not recorded in publications, and where faults of both lateral senses intersect, the second method is applicable. The latter method also applies to fault-plane solutions.

The PHS directions over a large region can be expected to show a consistent pattern. This uniformity in PHS directions is illustrated in Figure 1, which takes in the northern part of the South Island and the southern part of the North Island of New Zealand, and demonstrates that in the area examined the application of the first method reveals a consistent pattern.

NEW ZEALAND

Figure 2

Figure 2 shows the major active faults in New Zealand and the PHS direction pattern deduced from those

* The equation $H/V = \tan 2\alpha$ is a particular instance of $H/V = \tan x\alpha$, where x is a chosen integer, to take account of the fact that normal and reverse faults intersect at right angles. Further, if x had a value other than 2, other types of faults with different properties should exist; so far none have been found.

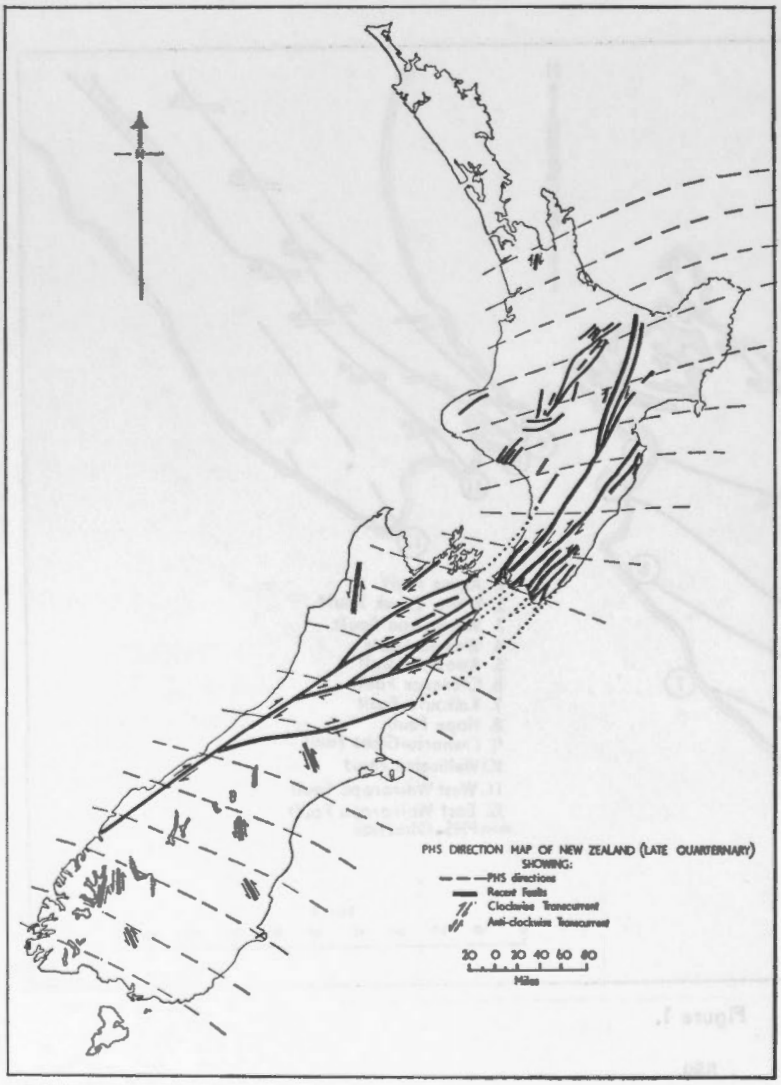

Figure 2.

faults. The dominant faults are the northeasterly striking clockwise transcurrent faults, minor anticlockwise transcurrent faults occur also and strike in a northwesterly direction.

The fact that the strike of the major clockwise transcurrent belt is roughly parallel to the general trend of the Pacific coast and to the Hikurangi trench, is regarded as important.

The PHS direction is again consistent and shows a gradual swing from slightly south of east in the South Island to north of east in the North Island.

SOUTHWEST PACIFIC

Figure 3

Extending this analysis of PHS directions into the southwest Pacific, fault-plane studies by several authors (*see* † in references) of shallow earthquakes* of magnitudes 6 and over have been used by applying method 2. Fault-plane solutions are rather scarce in some regions, and the PHS direction pattern for this part of the Pacific must be regarded as provisional only.

Tonga-Kermadec Region

The New Zealand trend can be followed into the Tonga-Kermadec region and a very consistent crustal stress pattern for the Tonga-New Zealand region becomes apparent.

* As the available evidence indicates that the PHS directions change with the depth of the hypocentres only fault-plane solutions of shallow shocks have been used.

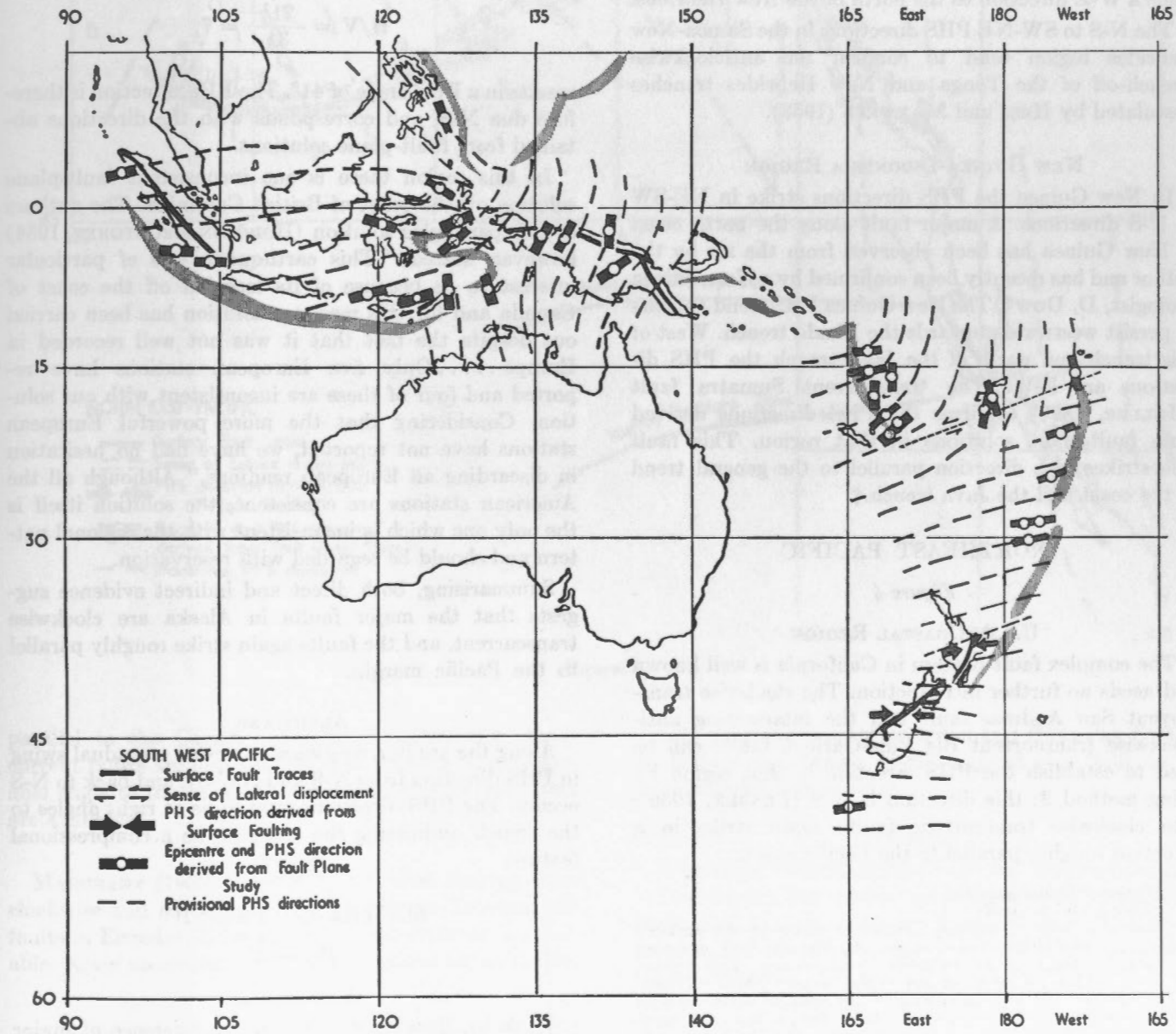

Figure 3.

In New Zealand we have seen that the direction of major surface faulting is roughly parallel to the trench and is clockwise transcurrent in character.

Fault-plane solutions in the Tonga-Kermadec region also show clockwise transcurrent faults striking nearly parallel to the trench, and it is therefore very likely that these are the actual faults while the others represent the auxiliary plane. The Tonga-New Zealand region can therefore be regarded as a region of clockwise transcurrent shear.

Samoa-New Hebrides Region

South of Samoa and Fiji there appears to be a sudden N-S swing in the PHS directions, while towards the New Hebrides this trend veers to a SW-NE direction, to become a W-E direction to the north of the New Hebrides.

The N-S to SW-NE PHS directions in the Samoa-New Hebrides region tend to confirm the anticlockwise wrench-off of the Tonga and New Hebrides trenches postulated by Hess and Maxwell (1953).

New Guinea-Indonesia Region

In New Guinea the PHS directions strike in NE-SW to N-S directions. A major fault along the north coast of New Guinea has been observed from the air by the author and has recently been confirmed by a New Guinea geologist, D. Dow*. The New Guinea PHS trend appears to persist westwards towards the Banda trench. West of this trench and north of the Java trench the PHS directions are E-W. The transcurrent Sumatra fault (Muller, 1895) confirms the PHS directions derived from fault-plane solutions in that region. This fault also strikes in a direction parallel to the general trend of the coast and the Java trench.†

NORTHEAST PACIFIC

Figure 4

U.S.A. Coastal Region

The complex fault pattern in California is well known and needs no further introduction. The clockwise transcurrent San Andreas fault and the intersecting anticlockwise transcurrent Big Pine-Garlock faults can be used to establish the PHS direction in that region by using method 2; this direction is N-S (Lensen, 1959). The clockwise transcurrent faults again strike in a direction roughly parallel to the Pacific coast.

PHS directions derived from fault-plane solutions show similar strikes.

Most of the faults in Alaska are shown on a map published by St. Amand in 1957. The major faults are considered to be transcurrent, from the indirect evidence. The Holitna fault is a major thrust fault striking O15° E. The PHS direction will be approximately at right angles to this fault and the sense of the transcurrent Denali fault striking 050° E, which strikes at 35° to the thrust, should therefore be clockwise. Direct evidence has recently been supplied by Tocher (1959) who observed the displacements on the recently active Fairweather fault. This fault strikes at N41° W and is clockwise transcurrent with a normal component. The displacement ratio

$$H/V = \frac{21\frac{1}{2}}{3\frac{1}{2}} = 7,$$

results in a PHS angle of 41°. The PHS direction is therefore due N-S, and corresponds with the directions obtained from fault-plane solutions.

In this region there is one inconsistent fault-plane solution off the coast of British Columbia. The authors of this particular solution (Hodgson and Storey, 1954) however, stated: "This earthquake was of particular interest to us because of its location off the coast of Canada and for this reason a solution has been carried out despite the fact that it was not well recorded in Europe . . . . . Only five European stations have reported and four of these are inconsistent with our solution. Considering that the more powerful European stations have not reported, we have had no hesitation in discarding all European readings." Although all the American stations are consistent, the solution itself is the only one which is inconsistent with the regional pattern and should be regarded with reservation.

Summarising, both direct and indirect evidence suggests that the major faults in Alaska are clockwise transcurrent, and the faults again strike roughly parallel to the Pacific margin.

Aleutians

Along the arc in a westward direction a gradual swing in PHS direction from N-S and NW-SE and back to N-S occurs. The PHS directions tend to be at right angles to the trench, indicating the latter to be a compressional feature.

SOUTHEAST PACIFIC

Figure 5

Venezuela

Work by Rod (1956) showed the existence of major clockwise transcurrent faults that strike approximately

*Personal Communication.

†Note added in proof:

Richter's book *Elementary seismology* came to the author's notice after completion of this paper. Richter (p. 606) describes the Sumatra Fault to be clockwise transcurrent. The present writer based his information on the original paper by Muller (1895). The figures in this paper are missing in the copies available in New Zealand and appear to have been omitted. Reid's findings suggest that the NW-SE PHS directions prevailing in the Philippines continue across to Sumatra.

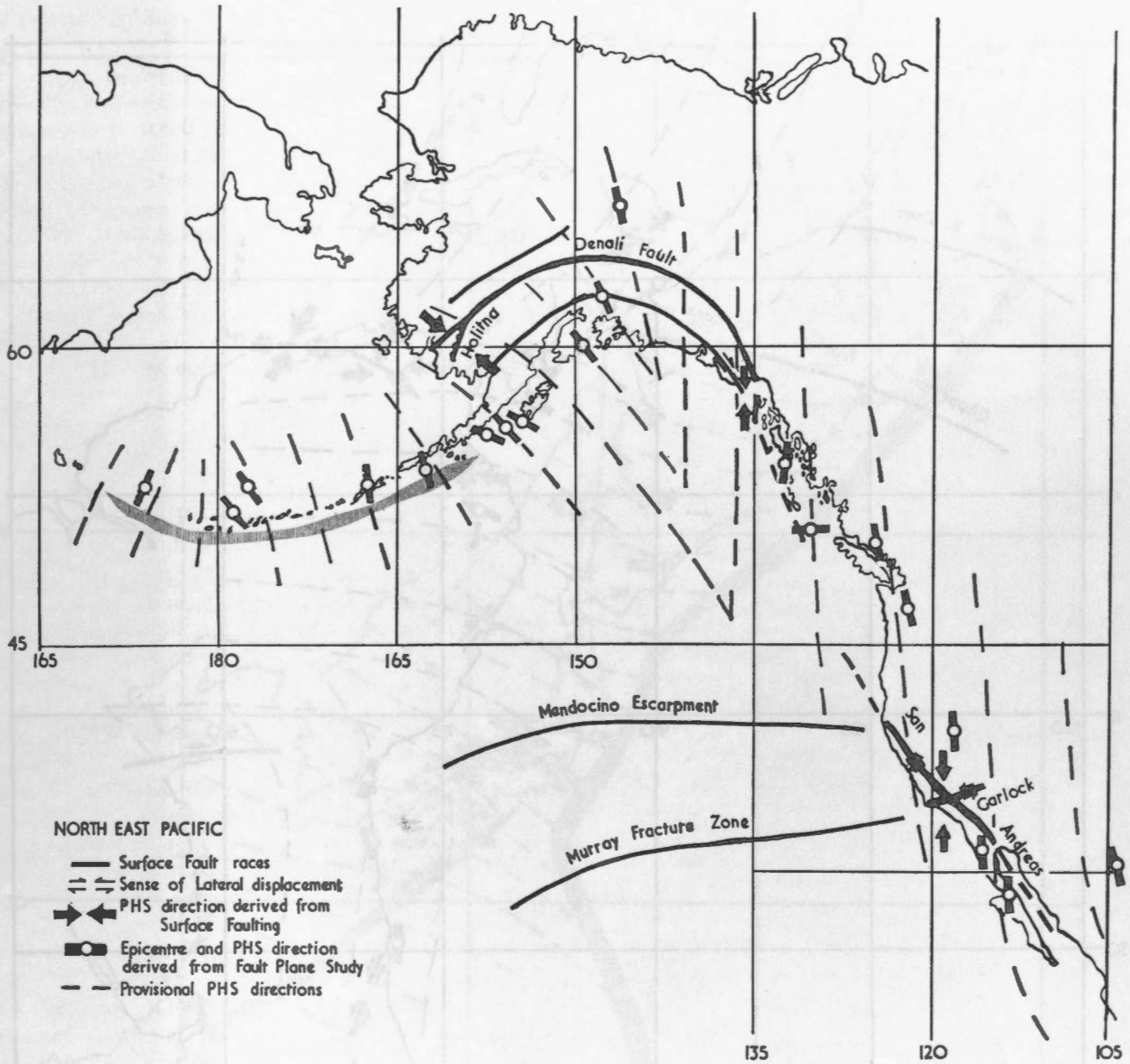

Figure 4.

parallel to the Caribbean coast. Anticlockwise transcurrent faults are also present, and strike at a considerable angle to the coast. No crustal fault-plane solutions are available.

Ecuador

Marchant (1959) described northwest striking anticlockwise and northeast striking clockwise transcurrent faults in Ecuador. No map or detailed evidence is available. Again no crustal fault-plane solutions are available.

Peru

Silgado (1951) mentioned a set of nearly parallel active faults striking in a northwesterly direction. Using a fault-plane solution by Hodgson and Bremner (1953), de Ridder and Lensen (1960) suggest this fault to be anticlockwise transcurrent.

Chile

A personal communication from St. Amand in regard to faulting in Chile states that: "Gigantic N-S strike-slip faults which seem to be right handed based on offset streams, antithetic structures etc. . . . . Several of these faults are several hundred kilometers long and some have tectonic breccias as much as 6 km in width". The few available fault-plane solutions suggest a N-S to NE-SW orientation of the PHS directions.

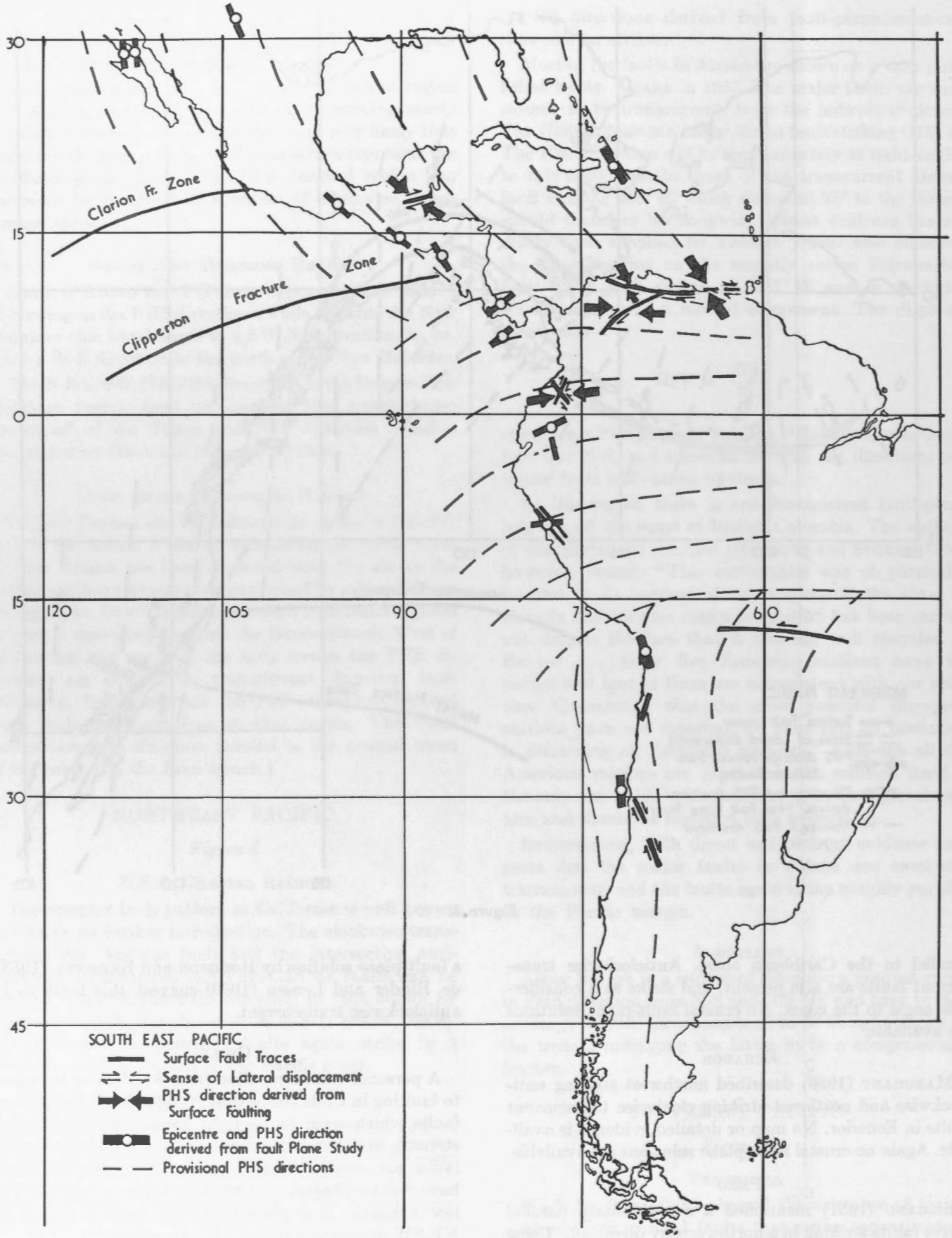
30
15
0
15
30
45
120
105
90
75
60
Clarion Fr. Zone
Clipperton Fracture Zone
SOUTH EAST PACIFIC
Surface Fault Traces
Sense of Lateral displacement
PHS direction derived from Surface Faulting
Epicentre and PHS direction derived from Fault Plane Study
Provisional PHS directions

Figure 5.

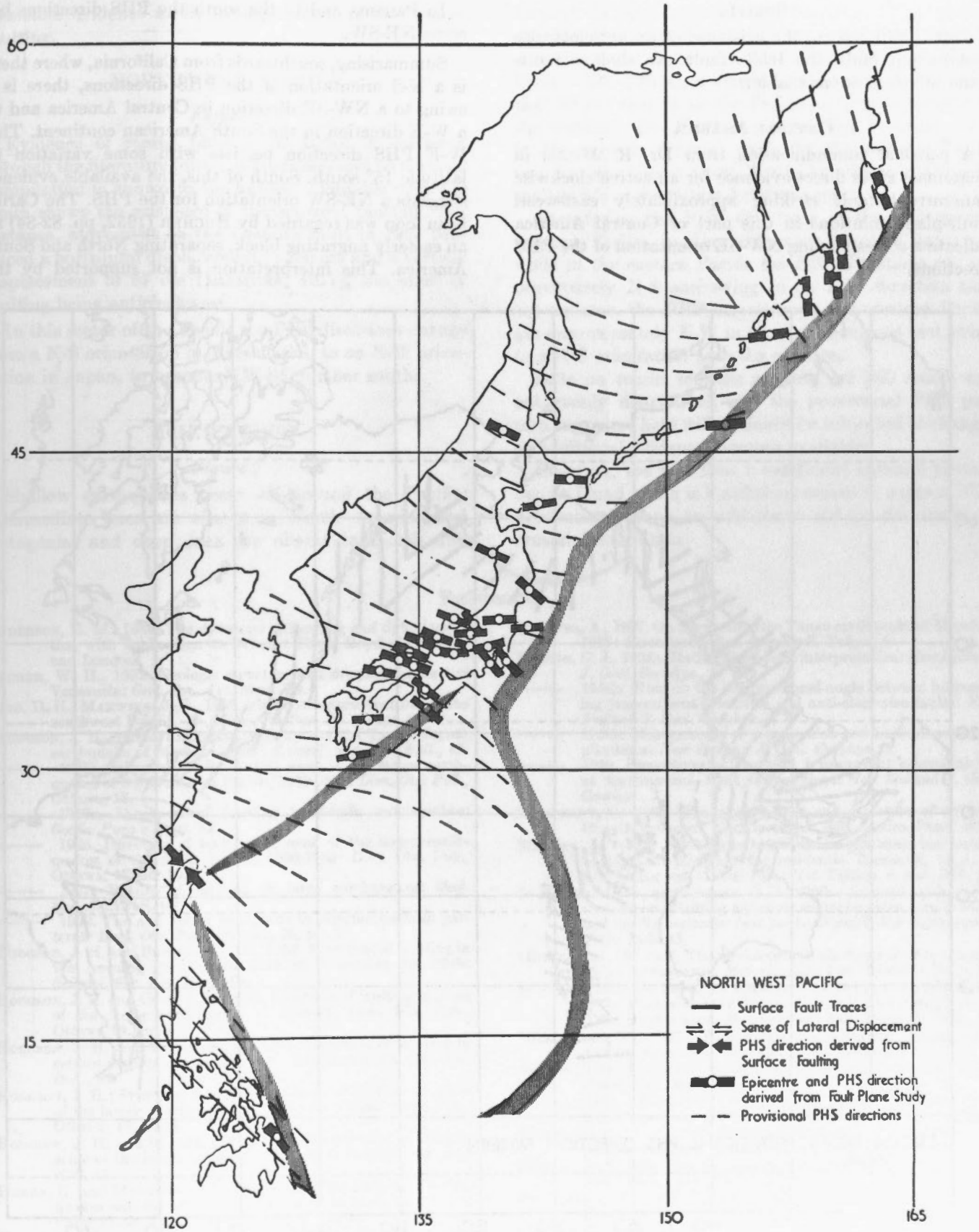
60
45
30
15
120
135
150
165
NORTH WEST PACIFIC
Surface Fault Traces
Sense of Lateral Displacement
PHS direction derived from Surface Faulting
Epicentre and PHS direction derived from Fault Plane Study
Provisional PHS directions

Figure 6.

Bolivia

Rod (1960) reports the existence of an anticlockwise transcurrent fault, the Ichilo fault. No shallow fault-plane solutions are available.

Central America

A personal communication from Dr. R. Jäckli in Guatemala gives direct evidence for an active clockwise transcurrent fault striking approximately east-west. Fault-plane solutions in this part of Central America indicate a corresponding NW-SE orientation of the PHS directions.

In Panama and to the south the PHS directions become NE-SW.

Summarising, southwards from California, where there is a N-S orientation of the PHS directions, there is a swing to a NW-SE direction in Central America and to a W-E direction in the South American continent. This W-E PHS direction persists with some variation to latitude 15° south. South of this, the available evidence suggests a NE-SW orientation for the PHS. The Caribbean loop was regarded by Bucher (1952, pp. 82-84) as an easterly migrating block, separating North and South America. This interpretation is not supported by the

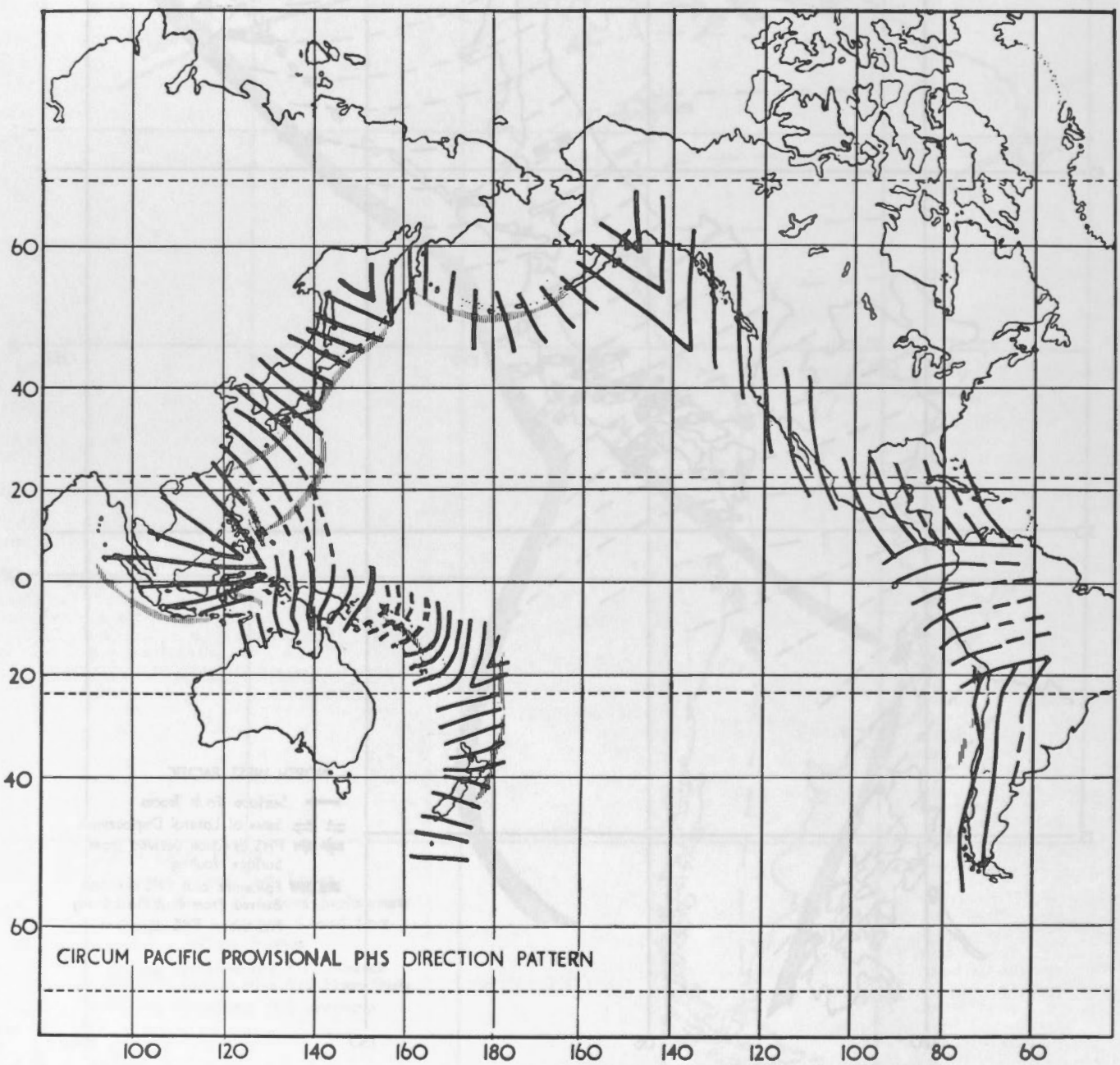

Figure 7.

available evidence of fault-plane solutions and recent faulting.

NORTHWEST PACIFIC

Figure 6

Evidence of recent faulting in Japan is scattered through the literature (often in Japanese) and no regional compilation is known to the author. Available evidence again shows the existence of transcurrent faulting. For instance, movement on the Gomura fault in 1927 produced a horizontal displacement of 250 cm and a vertical displacement of 57 cm (IMAMURA, 1927), the sense of faulting being anticlockwise.

In this sector of the Pacific the PHS directions change from a N-S orientation in Kamchatka, to an E-W orientation in Japan, to become NW-SE further south.

THE PACIFIC

Figure 7

Shallow earthquakes occur all around the Pacific; intermediate ones are absent in North America and Patagonia, and deep ones are absent in North and Central America and also in Patagonia. This relative absence of intermediate and deep earthquakes in the eastern Pacific makes this part differ from the western Pacific. The difference increases if we take into account that 70 per cent of all the Pacific earthquakes occur in the western part. Further, all the deep trenches occur in the western Pacific, while in the eastern Pacific trenches are absent along North America and are only shallow along the South American coast.

Considering the PHS directions in the eastern and western Pacific, another difference becomes apparent: while in the eastern Pacific the PHS directions are approximately N-S and swing to an E-W direction near the equator, the PHS directions in the western Pacific are approximately E-W in temperate regions and swing to a N-S orientation near the equator.

Data on recent tectonic activity are still scarce and not evenly distributed, and the provisional PHS pattern suggested here will no doubt be subjected to changes as additional evidence becomes available.

However, the fact that a consistent regional pattern can be found at all, is a sufficient reason to suggest PHS determinations as an additional aid in the study of crustal deformation.

References

ANDERSON, E. M., 1942. The dynamics of faulting and dyke formation with application to Britain: Oliver Boyd, Edinburgh and London.

BUCHER, W. H., 1952. Geologic structure and orogenic history of Venezuela: *Geol. Soc. Am.* Mem. 49.

HESS, D. H., MAXWELL, J. C., 1953. Major structural features of the southwest Pacific, etc.: *Proc. 7th Pac. Sci. Congr. 2.*

†HODGSON, J. H., 1955a. Fault-plane solutions of the Tango, Japan, earthquake of March 7, 1927: *Seismol. Soc. Am. Bull.*, **45.**

†——— 1955b. Direction of faulting in some of the larger earthquakes of the southwest Pacific, 1950-1954: *Dom. Obs. Pub.*, Ottawa, **18,**

†——— 1955c. Direction of faulting in Pacific earthquakes: *Geofis. Pura e Appl.* **32.**

†——— 1956. Direction of faulting in some of the larger earthquakes of the north Pacific, 1950-1953: *Dom. Obs. Pub.*, Ottawa, **18,** no. 10.

†——— 1957. Nature of faulting in large earthquakes: *Geol. Soc. Am. Bull.* **68.**

†——— 1959. The null vector as a guide to regional tectonic patterns: *Dom. Obs. Pub.*, Ottawa, **20,** no. 2.

†HODGSON, J. H. and BREMNER, P.C ., 1953. Direction of faulting in the Ancash, Peru, earthquake of November 10, 1946: *Seismol. Soc. Am. Bull.*, **43.**

†HODGSON, J. H. and COCK, J. L., 1958. Direction of faulting in some of the larger earthquakes of 1954-55: *Dom. Obs. Pub.*, Ottawa **19,** no. 5.

†HODGSON, J. H. and MILNE, W. G., 1951. Direction of faulting in certain earthquakes of the North Pacific: *Seismol. Soc. Am. Bull.*, **41.**

†HODGSON, J. H.; STEVENS, A., 1958. Direction of faulting in some of the larger earthquakes of 1955-56: *Dom. Obs. Pub.*, Ottawa, **19,** no. 8.

†HODGSON, J. H. and STOREY, R. S., 1954. Direction of faulting in some of the larger earthquakes of 1949: *Seismol. Soc. Am. Bull.* **44.**

†HONDA, H. and MASATSUKA, A. 1952. On the mechanism of earthquakes and the stresses producing them in Japan and its vicinity: *Sci. Rept. Tohôku Univ.*, ser. 5, **4.**

†HONDA, H., MASATSUKA, A. and EMURA, K., 1957. On the mechanism of the earthquakes and the stresses producing them in Japan and its vicinity: *Sci. Rept. Tohôku Univ.*, ser. 5, **8.**

IMAMURA, A., 1927. On the destructive Tango earthquake of March 7, 1927: *Earthquakes Res. Inst. Bull.* Tokyo, **4.**

LENSEN, G. J., 1958a. Rationalized fault interpretation: *New Zealand J. Geol. Geophys.*, **1.**

——— 1958b. Note on the compressional angle between intersecting transcurrent clockwise and anti-clockwise faults: *New Zealand J. Geol. Geophys.*, **7.**

——— 1958c. Measurement of compression and tension; some applications: *New Zealand J. Geol. Geophys.*, **1.**

——— 1959. Secondary faulting and transcurrent splay-faulting at transcurrent fault intersections: *New Zealand J. Geol. Geophys.*, **2.**

MARCHANT, S., 1959. The stratigraphy and structure of western Guayas province, Ecuador: *Geol. Soc. London Proc.*, 1570.

MULLER, J., 1895. Nota betreffende de verplaatsing van eenige Triangulatie-pilaren in de residentie Tapanoeli, t.g.v. de aardbeving van 17 Mei 1892: *Nat. Tijdsch. v. Ned. Ind.*, **54.**

de RIDDER, N. A., and LENSEN, G. J., 1960. Indirect evidence for transcurrent faulting and some examples from New Zealand and the Netherlands: *Inst. for Land and Water Management*, Tech. Bull. **15.**

†RITSEMA, A. R., 1956. The mechanism in the focus of 28 south-east Asian earthquakes: *Met. Geophys. Inst. Djarkata Verh.*, **50.**

†———, 1957. On the use of transverse waves in earthquake mechanism studies and the direction of fault displacement in SE Asian earthquakes: *Met. Geophys. Inst. Djakarta Verh.*, **52.**

†RITSEMA, A. R., 1957. Fault-plane solutions for southeast Asian Earthquakes: *Met. Geophys. Inst. Djakarta Verh.*, **54.**

ROD, E., 1956. Strike-slip faults in northern Venezuela: *Am. Assoc. Petrol. Geol. Bull.*, **40.**

——— 1959. West end of Serrania Del Interior, Eastern Venezuela: *Am. Assoc. Petrol. Geol. Bull.*, **43.**

†SCHEIDEGGER, A. E., 1959. Statistical analysis of recent fault-plane solutions of earthquakes: *Seismol. Soc. Am. Bull.*, **49.**

SILGADO, F. E., 1951. The Ancash, Peru, earthquake of November 10, 1946: *Seism. Soc. Am. Bull.*, **41.**

ST. AMAND, P., 1957. Circum-Pacific orogeny: *Dom. Obs. Pub.*, Ottawa, **20,** no. 2.

TOCHER, D., 1959. Field observations on the effects of the Alaska earthquake of July 10, 1958: *Geol. Soc. Am. Bull.*, **70.** (abstr. only.)